NTNU

Norwegian University of
Science and Technology

Sensitivity in the dynamic response estimation of pantograph-catenary interaction, due to time step and cut-off frequency

A numerical study

Kristine Ristad

Master of Science in Mechanical Engineering
Submission date: February 2017
Supervisor: Anders Rönnquist, KT

Norwegian University of Science and Technology
Department of Structural Engineering

Abstract

This thesis investigates the sensitivity in the dynamic response when simulating the pantograph-catenary interaction due to time step and cut-off frequency. In addition, the contact formulation stated in standard EN50318 is addressed.

Catenary systems involve major investments, thus reducing wear and damage of the contact wire and the pantograph is crucial. This thesis considers previous work on the subject, which argues that when studying wear, higher frequencies than stated in the standards for simulations of the catenary system, are of interest.

This thesis suggest a minimum sampling frequency that should be used when simulating the catenary, if the response with higher frequencies are of interest.

The simulations ability to detect elasticity variations along the span, and the wave propagation are addressed.

The simulations were performed using a numerical model derived by Petter Naavik, and the results were analysed using Python and Matlab. Important output with regards to wear is presented, and used to evaluate the results.

Contents

1 Introduction

The railway catenary system is a system of connected wires that supplies electrical power to trains. With modernizing of the railway infrastructure and increasing train speeds, minimizing wear of the contact wire is crucial, as it represents substantial investments.

In light of this, it is important to improve the understanding of wear caused by arcing and excessively high contact forces on the contact wire. These are effects that is often related to elasticity variations along the catenary system, and the wave propagation in the contact wire. To aid this, virtual testing methods that gives accurate descriptions of the railway catenary system are invaluable.

In the literature it is suggested that frequencies up to 100 Hz are important when simulating wear in a catenary section. This is significantly higher than 20 Hz, which is the frequency that the simulation models are validated for according to standards.

This project aims to suggest a minimum requirement of the sampling frequency, when the frequency range of interest is increased, by attaining the following objectives:

How an increase in sampling frequency (i.e. decrease in time step) influences the simulations ability to...

1. *produce correct contact forces*: Looking at the time series and statistical values of the contact force.
2. *detect elasticity variations along the span*: Looking at where the maximum and minimum contact forces appear in the span
3. *describe the dynamic response of the catenary*: Looking at the acceleration of the dropper and contact wire of critical points in the span.

How filtering affect the dynamic response...

I *by increasing Cut-off frequency*: Looking at time series and statistical data of filtered contact forces

II *filtering according to standard*: Looking at the time response of the contact force.

In addition, a study of the contact formulation stated in EN50318, by using the suggested minimum sampling frequency will be performed.

Chapter 2 presents the most important system characteristics. This is to gain an understanding of the different components of the system, and the difficulties with simulations of these components. Chapter 3 outlines the challenges when solving a contact problem with finite element method. Chapter 4 states some important theory on analysis in the frequency domain. Chapter 5 outline the simulation method used in this thesis. Finally the results from the simulations are presented in Chapter 6 and Chapter 7.

2 Description of the Catenary System

The railway catenary system is a wire system that supplies electrical power to trains. The pantograph is mounted to the top of the train, and is in continuous contact with the contact wire. With the increasing train speed, maintaining this contact becomes more challenging.

Catenary systems have been under constant development since 1881, to accommodate the demand for higher train speeds. The first electrical railway in Norway where built in 1908.

In this section the railway contact line system will be described. Firstly the catenary components, excluding the droppers. Secondly, the pantograph and finally the droppers.

2.1 The Catenary System

Figure 1: The catenary system, and the train [8]

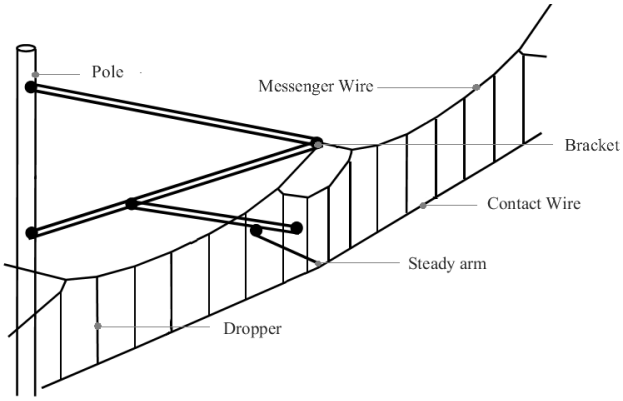

Figure 2: Catenary system [7]

The section between two supporting poles is defined as the *span*. The catenary is divided into multiple spans. For cost reasons the span length should be long as possible. As shown later in section 2.4, there are dynamic criteria for the system that limit the maximum span lengths. The most common span lengths are from 40 m to 60 m, depending on the catenary system's design.

The main purpose of the *contact wire* is to supply uninterrupted electrical energy to the train, through continuous contact with the pantograph. It is a pre-tensioned copper wire. It is a pre-tensioned copper wire, the cross section is shown in Figure 3. The two notches in the contact wire are for the clamps that connect the contact wire to the dropper, in that way keeping the contact surface free of discontinuities.

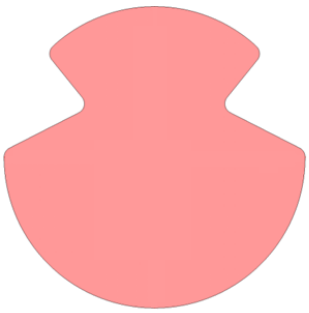

Figure 3: Contact wire cross section [8]

The poles holds the system by connection to the messenger wire by the brackets. The *messenger wire* contributes to a more uniformly distributed elasticity in the catenary system. It is coupled to the contact wire through the droppers. The messenger wire is pre-tensioned. This is important for the stiffness of the system, and is an important design parameter. The tension forces in the contact wire and messenger wire are illustrated in Figure 4. The choice of tension forces will be discussed in Chapter 2.4. Figure 5 shows how the contact wire and messenger wire are pre-tensioned.

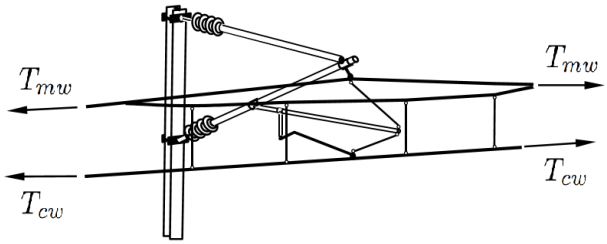

Figure 4: Tension forces in the contact wire and the messenger wire with weights, T_{mw} [7]

For cost reasons the contact wire and messenger wire cross section should be kept to a minimum [16]. However, other factors must be considered when choosing the cross section. This will be be discussed in chapter 2.4.

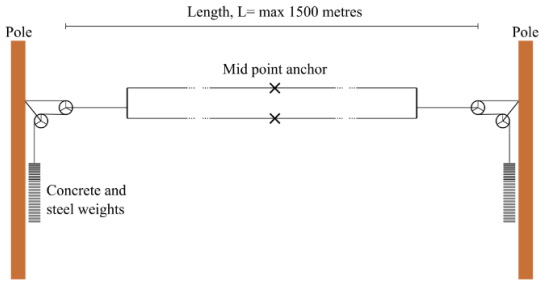

Figure 5: Pre-tensioning of the contact wire and the messenger wire [8]

The *stitch wire*, see Figure 2, produces a spring effect that results in a better match between the elasticity at the support and at the middle of the span. They are tensioned in such a way that elasticity variations along the span are reduced. The stitch wires also contribute to a more uniform contact wire height, which is of importance for maintaining the contact. Including stitch wires in a catenary section allows for longer span lengths [16].

The catenary system is arranged in such a way that it has an initial sag, which is called *pre sag*. The assumption is, that since the elasticity at the middle of the span is higher than at the support, the pantograph will lift the contact wire higher there. By lowering the contact wire at the middle of the span the point of contact between the contact wire and the pantograph will become more uniform.

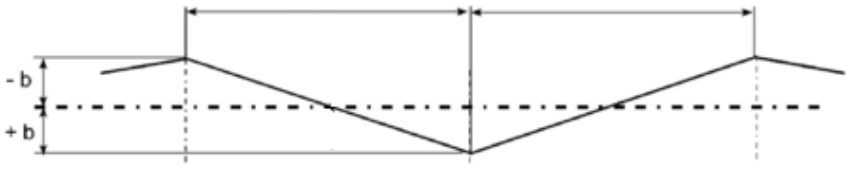

Figure 6: Contact line seen from above

The contact between the contact wire and the pantograph causes wear on both components. In order to reduce the wear of the on the pantograph, the contact wire is arranged in such a way that the point of contact on the pantograph varies. Seen from the top, the contact wire is forms a zig-zag shape.

2.2 The Pantograph

The pantograph components are shown in figure 7. The *arm* lets the *pantograph head* move in a vertical direction, with respect to the *main frame*. The main frame is mounted on the insulators on the train roof. The *drive* is a device that keeps the pantograph height constant. The *collector strips* are the component in direct contact with the contact wire, and are connected to the pantograph head.

Since the collector strip is in direct contact with the contact wire, this is the pantograph component that experiences the most wear. The contact wire is placed in a zig-zag formation, in that way changing the contact point on the collector strip, the aim is that the wear of the collector strip is evenly disturbed. The collector strip are an easily replaceable part of the pantograph [**?**].

The force exerted on the contact wire by the pantograph is called the *contact force*, F_c. This is a vertical force that is the sum of all forces at the point of contact[10]. The contact force has both a static, dynamic and a aerodynamic component [16]

$$F_c = F_{static} + F_{aerodynamic} + F_{dynamic} \tag{1}$$

The aerodynamic component is a result of the air flow around the pantograph components[10], it is estimated by the manufacturer of the pantograph, see equation 2. The dynamic force component is a result of the dynamic properties of the contact line, the pantograph, the track geometry and the trains speed and running behavior [16].

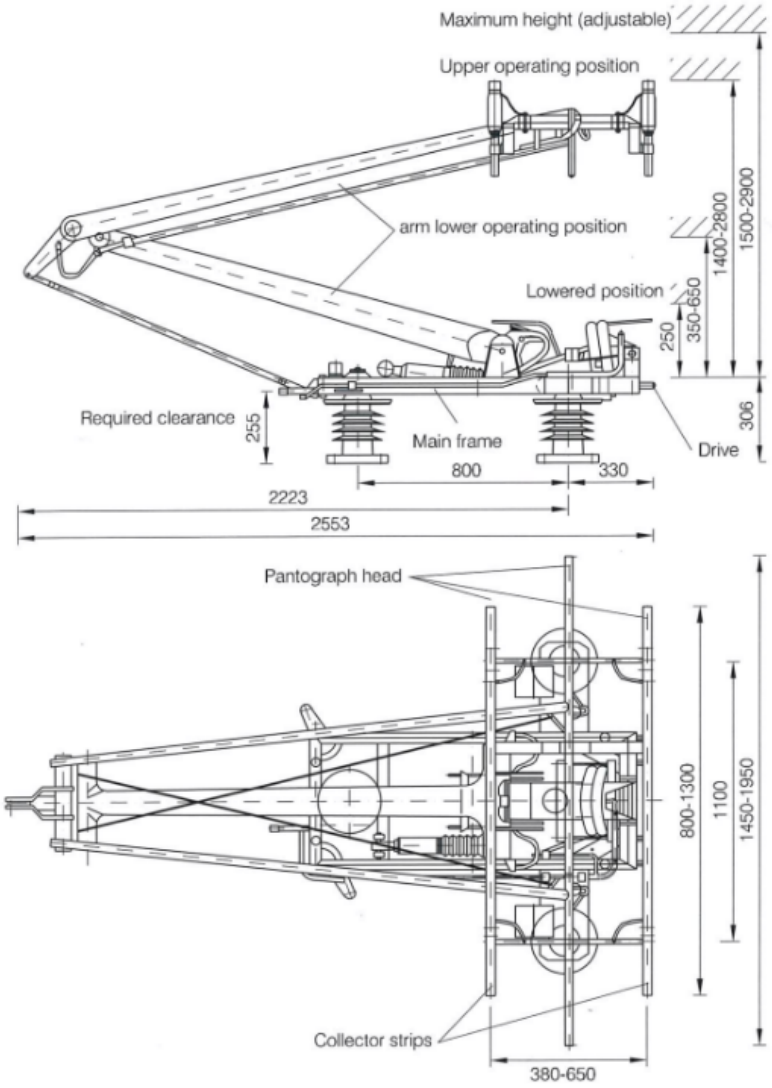

Figure 7: Pantograph [16]

For the WBL88, the sum of aerodynamic and static component is given by

$$F_{static} + F_{aerodynamic} = 55 + 0.0068v^2 \tag{2}$$

where v is the train speed.

There are several different methods used to describe the pantograph in simulations. A *pantograph model* is defined as a mathematical model that describes the dynamic characteristics of a pantograph [10]. The most used method is a *lumped-mass-model* also referred to as a *mass-spring-damper-model*. A *multy-body-model* is also used.

In Figure 8 a lumped mass model of a pantograph is shown. As seen, the pantograph is divided into three rigid masses, connected by springs and dampers. All the parameters in figure 8 have to be found experimentally. The lumped mass model in 8 describe the pantograph with three degrees of freedom, the three masses represent the lower arm, upper arm, and the pantograph head. Some use a lumped mass model with only two degrees of freedom, i.e. a pantograph model with two rigid bodies.

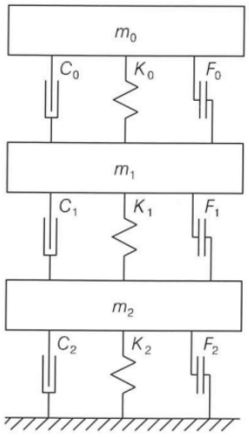

Figure 8: Lumped mass model [16]

In a multi-body model, dynamic constraints between the masses are introduced.

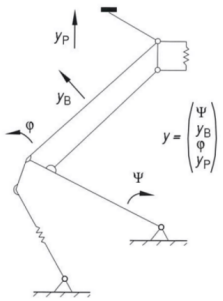

Figure 9: Analytical pantograph model [16]

The pantograph is of great importance for the energy transmission in the system. Article [4] studies how the contact depends on the pantograph components, simulations of the system are done using a combination of a multi-body model and a lumped-mass-model.

The most important pantograph model components, see Figure 8, are varied in the range $+/-$ 10%. Maximum, minimum, mean, standard deviation and statistical minimum of the contact force is measured to see how it is affected by the change of the parameter. All of the parameters in figure 8 are varied. The simulations are done at three different train speeds; 200 km/h, 250

km/h and 300 km/h. Changing the different parameters only affect the max/min contact force value, while the average force is more or less constant. The mean, the standard deviation and the statistical minimum are nearly non-sensitive to the variation. This simulation results is filtered using a low pass filter, with a cut-off frequency of 20 Hz (according to standard EN50318). With a higher cut off frequency the variations could be larger.

2.3 The Droppers

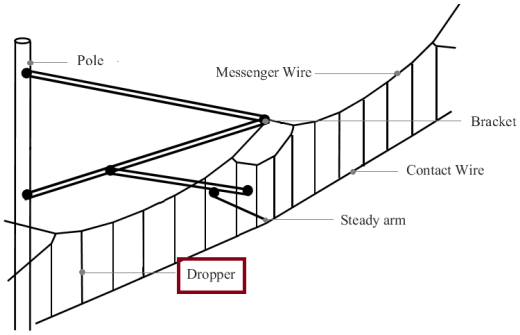

Figure 10: Catenary system [7]

As described earlier the dropper is a wire that connects the contact wire to the messenger wire and the stitch wire. The messenger wire contributes to a more uniform elasticity of the system, and a constant system height. Both properties are important for the interaction between the contact wire and the pantograph. The spacing between the droppers, together with the tensile force in the contact wire, decide the sag between the droppers, this should be kept to a minimum [16].

The dropper introduces a nonlinearity in the system, in the sense that it has no resistance to compressive forces. Hence, when the dropper is under compression it no longer connects the contact wire to the messenger wire. This cause a rapid changes in the stiffness of the system when the pantograph passes a dropper.

This nonlinearity caused by the slacking of the dropper causes problems when simulating the system. Some authors do not include the slacking of the dropper, some state that is included, but does not state how as in [2]. In [1] Cho develop and validate a numerical model including the nonlinear effect of the dropper. Here the dropper is described as a mass spring damper system, as seen in figure 11.

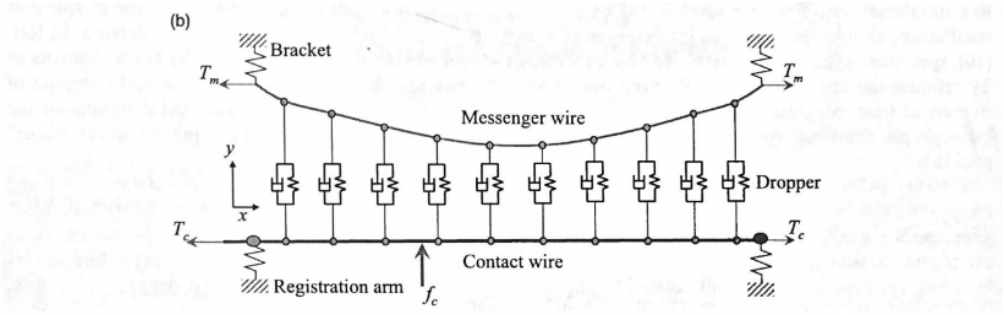

Figure 11: Dynamic simulation model of the pantograph and the overhead contact lines [1]

With stiffness $k_d = 10000N/m$, and damping $c_d = 5Ns/m$. There are no stitch wires this

catenary system. The non-linear effect is included in Cho's model by removing the contribution of a dropper when it is slackened. This is done by calculating the internal forces in the dropper, when the internal forces are negative the dropper is under compression, and the effect of that dropper must be taken out of the global stiffness matrix. The internal forces in all the droppers, f_{drop}, need to be checked in every iteration in the simulations. f_{drop} is calculated as following:

$$f_{drop} = f_0 + k_d(v_m - v_c) + c_d(\dot{v}_m - \dot{v}_c) \tag{3}$$

Cho validates the dropper formulation by comparing the forces in a dropper measured in the field with those measured in the same dropper in the simulation model. The dropper placed closest to the brackets are chosen, since this undergoes the highest variation of forces (when there are no stitch wires in the catenary). A sampling frequency of 1000 Hz is used. The result from the validation is shown in figure 12.

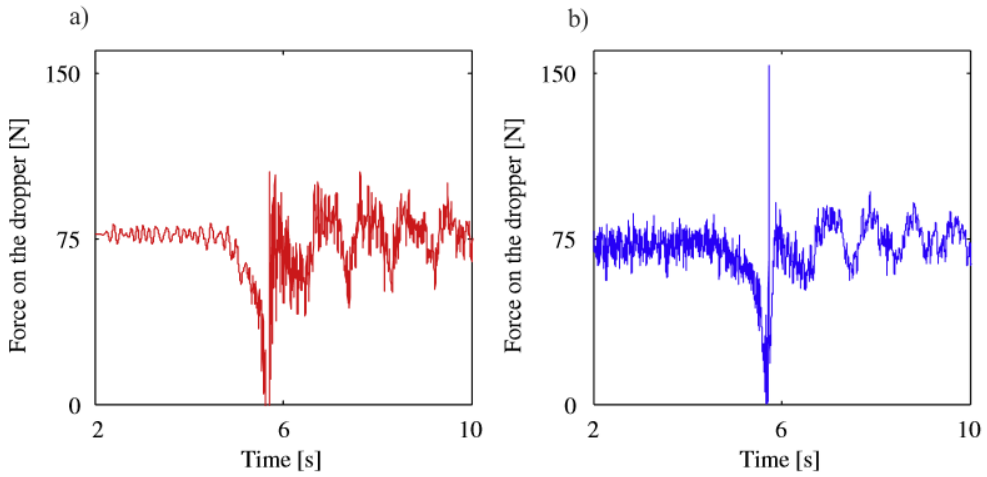

Figure 12: Forces in the dropper used in Chos model

Figure 12 a) show that when the pantograph is approaching the dropper, the forces on that dropper are gradually reduced. When the pantograph passes, the dropper is slackened for a short period. When the tension in the dropper return, an impulse is applied to the dropper. Figure b) show that the simulations are able to include the slacking of the dropper. Even though the modelling of the dropper in [1] describes the slacking well, this a very time consuming method. The internal forces in each dropper must be calculated for every iteration.

In [7] the droppers are included in the global stiffness matrix as bar elements. In [7] this is solved by adding a force equal to the bar compression force to the force vector.

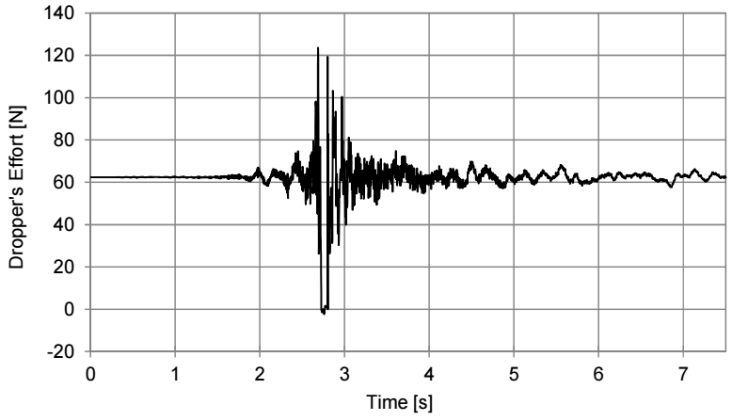

Figure 13: Forces in the dropper used in [7]

In [7] the results are not compared with measured field values. However, figure 13 shows that the forces in the droppers are zero when the pantograph hits the dropper. But when comparing with the measured values in [1], the forces in the dropper should be gradually reduced when the pantograph is approaching the dropper. At least six iterations were needed in order to find the right compensation forces to add to the force vector, so this is also an time consuming method.

In Naaviks numerical model, used for simulations in this theses, the slacking of the dropper is included by pre bending beam elements in the dropper wire, thus making it more effected by compressive forces. This will described in details chapter 5.2. This is much more time efficient method.

2.4 Dynamic characteristics

Theoretical studies of the interaction between the pantograph and the contact line have led to numerous criteria for the railway catenary system. Some of them will discussed in this section. All of the equations and figures in this section are taken from [16], and full derivations of the functions can be found there.

When the pantograph hits the contact wire at high speeds, this results in a vertical displacement of the contact wire, called the *contact wire uplift*. If the contact wire uplift is too large, a gap between the pantograph and the contact wire will occur. This is called a *contact loss*. It is critical to keep the contact loss at a minimum, to ensure no interruption in the energy transmission.

The *wave propagation speed* is the speed of the transverse wave that runs along the contact wire. The wave is a result of the impulse caused by the contact force exerted by the pantograph. The wave propagation speed c_p is defined as

$$c_p = \sqrt{\frac{\sigma_{cw}}{\rho_{cw}}} = \sqrt{\frac{T_{cw}}{m'_{cw}}} \tag{4}$$

where σ_{cw} is the tensile stress in the contact wire, ρ_{cw} is the contact wire density. T_{cw} is the tensile force in the contact wire, and m'_{cw} the mass per unit length $[kg/m]$. As identified in section **??**, when the train speed v approaches the wave propagation speed, the contact wire uplift goes towards infinity, making contact between the pantograph and contact wire impossible. The maximum train speed should be less than 70 % of the wave propagation speed according to standard EN50119 [12]. From Equation 4, high tensile forces and low density would increase the wave propagation speed.

The transverse wave in the contact wire will partly be reflected by discontinuities in the catenary system. For instance, the dropper connecting the contact wire to the messenger wire, as shown in Figure 14

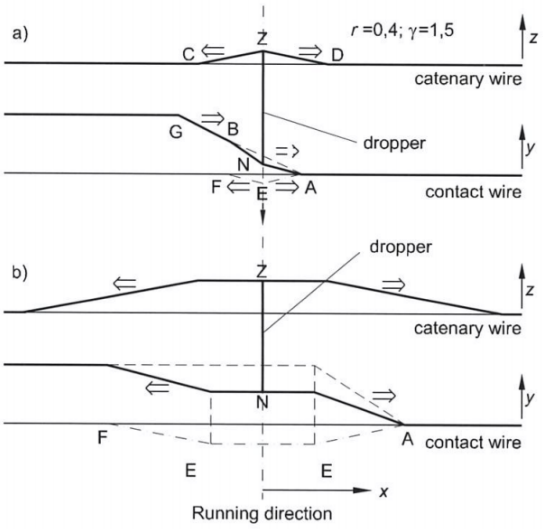

Figure 14: The reflection of a mechanical wave at a dropper [16]

Figure 14 a) shows the condition just before the wavefront meets the dropper, and Figure 14 b) shows the condition just after the wave has passed the dropper. The figure illustrates that a wave travelling along the contact wire that passes a dropper, will be reflected to the messenger wire by the dropper. The result is a wave front travelling in both directions in the messenger wire. A transmitted wave will travel in the running direction in the contact wire, in addition a reflected wavefront will travel in the opposite direction of the original wave. The *reflection factor* r, for the reflection of a wave passing a dropper is described by

$$r = \frac{1}{1 + \sqrt{\frac{T_{mw} m'_{cw}}{T_{cw} m'_{mw}}}} \tag{5}$$

where T_{mw} and m'_{mw} is the tensile force and specific mass in the messenger wire.

When a pantograph is moving towards a wave propagation, the amplitude of the wave can increase. A simple example is shown in [16] , where a pantograph is travelling along a contact wire with a discontinuity at point x_r, without exerting any forces. At the point x_0 the pantograph suddenly exerts a vertical contact force. This force causes a lift in the contact wire, and a transverse wave traveling with speed c_p. This wave will be reflected by the discontinuity at x_r, and travel back towards the pantograph, where it will be reflected again. This will be repeated until the pantograph reaches the discontinuity point x_r. This is shown in Figure 15

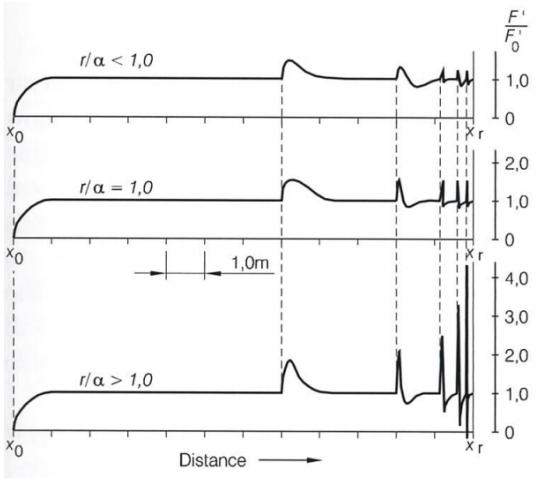

Figure 15: Amplification of reflected wave [16]

where γ is the *amplification coefficient*

$$\gamma = \frac{r}{\alpha} \tag{6}$$

where r is the reflection factor shown in equation 5, and α is the *Doppler factor*

$$\alpha = \frac{c_p - v}{c_p + v} \tag{7}$$

where c_p is the wave propagation speed, and v is the train's running speed.

Figure 15 shows that when $\gamma > 1$ the amplitudes of the wave increase until the pantograph reaches x_r. While if $\gamma < 1$ the amplitudes will decrease. In order to achieve constant current transmission between the contact wire and the messenger wire, the amplification coefficient γ must be less than or equal to zero. From equation 6 and 7, it can be seen that this leads to another limitation of the train speed v.

The *elasticity* of the system is also important for the current transmission. The contact wire uplift must be kept small, in order to achieve constant contact between the pantograph and the wire. Thus, the elasticity of the system should be low, and evenly distributed. An approximation of the elasticity in the middle of a span can be calculated by

$$e \approx \frac{L}{k_E \times (T_{cw} + T_{mw})} \tag{8}$$

where k_E is a constant dependent on contact line design data, and L is the span length. Equation 9 show that the need for low elasticity limits the maximum span length in a system. For a system with stitch wires $k_E = 3.5$, and for a system without $k_E = 4$. The *degree of elasticity* can be measured by

$$u = 100 \cdot \frac{e_{max} - e_{min}}{e_{max} + e_{min}} \% \tag{9}$$

this value should be lower than 15%

In a railway catenary system the stiffness variations, together with the wave propagation, are the main source of contact loss between the contact wire ant the pantograph [9]

2.5 The Equation of Motion

The dynamic interaction between the pantograph and the contact wire is a typical wave propagation problem [1]. In [16] some simplified dynamic equations of the contact between the pantograph and the contact wire are derived. Two are shown here with the motivation of understanding which parameters that are important for the contact. Firstly, looking at a contact wire that is deflected transversely, with no external forces applied. Secondly, a simplified contact force is exerted on the contact wire.

With assumed negligible stiffness, the contact wire can be viewed as a tensioned string. The wire is pre-tensioned with stress σ, and has a specific mass γ. Figure 16 show the contact wire element.

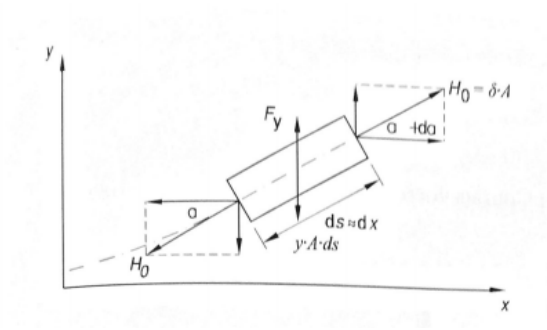

Figure 16: Contact wire element

The contact wire element, with length dx is rotated with an angle α. The element has a cross section area A, and mass $m = dxA\rho$. Newton's second law in y-direction gives,

$$H_0 sin(\alpha + \mathrm{d}\alpha) - H_0 sin(\alpha) = ma_y \tag{10}$$

where $a_y = \frac{\partial^2 y}{\partial^2 t}$ is the acceleration in the y-direction, and $H_0 = \sigma A$. When assuming small deflections, $\alpha \sim \tan(\alpha) = \frac{\partial y}{\partial x}$, and $\mathrm{d}\alpha = \mathrm{d}x\left(\frac{\partial^2 y}{\partial^2 x}\right)$. Combining this with equation 10, and rearranging the equation results in

$$\frac{\partial^2 y}{\partial^2 x} - \frac{\gamma}{\sigma} \cdot \frac{\partial^2 y}{\partial^2 t} = 0 \tag{11}$$

where $\frac{\sigma}{\gamma} = c_p^2$, where c_p is the wave propagation speed. This is known as the *wave equation*. The result of this equation gives the contact wire deflection in the y-direction. The general solution to the equation is all functions having the format $y = f(x \pm c_p t)$, i.e. a function with a period of $c_p t$. In conclusion, the movement of the contact wire is highly effected by the wave propagation speed of the contact wire.

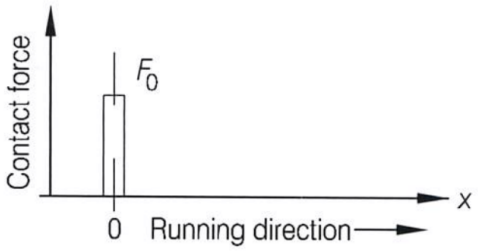

Figure 17: Contact force exterted by a running pantograph [16]

Now applying a contact force to the contact wire. The contact force is not constant, and is dependent on numerous parameters, as seen in 2.2. Then again, some important factors of the contact wire pantograph interaction can be achieved by looking at the constant contact force, which acts on a time dependent position $x_t = vt$, where v is the train speed. This force can be described by

$$F_x = F_0 \cdot \delta(x - x_t) = F_0 \cdot \delta(x - vt) \tag{12}$$

where $\delta(x)$ is the dirac delta function, where $\delta(0) = 1$ and $\delta(x \neq 0) = 0$. Adding this term to equation 11 results in the equation

$$\frac{\partial^2 y}{\partial^2 t} = c_p^2 \frac{\partial^2 y}{\partial^2 x} + \frac{F_0}{c_p^2} \cdot \delta(x - x_t) \tag{13}$$

The arithmetic will not be shown, but the solution is

$$y(x,t) = \frac{2F_0 l}{c_p^2 \pi^2 (c_p^2 - v^2)} \sum_{n=1}^{\infty} \frac{1}{n^2} sin\frac{n\pi x}{l} \left(sin\frac{n\pi vt}{l} - \frac{v}{c_p} sin\frac{n\pi c_p t}{l} \right) \tag{14}$$

Even though this is a simplification of the contact force, the fundamental resonance characteristics are visualized by the solution of the equation. That is, when the train speed goes towards the wave propagation speed, $v \to c_p$, the contact wire uplift goes towards infinity. Thus, showing that the wave propagation speed is a physical limit for the energy transmission.

3 Solving the Contact Problem using FEM

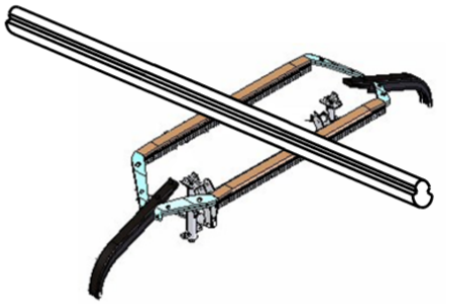

Figure 18: Interaction between a contact wire a the pantograph [7]

The contact between the pantograph and the contact wire determines the quality and reliability of the energy transmission to the traction unit. This contact depends on the design of the pantograph and contact line, the location of contact between the contact wire and the pan head, the horizontal geometry and the speed of the train [8]. This contact causes a nonlinearity in the system.

In this thesis simulations are done using the Finite Element Software Abaqus. The details of the FEM method will not be discussed. However, the dynamic equilibrium equation will be shown, since it is used to describe the contact formulation using FEM.

$$[M]\ddot{D} + [C]\dot{D} + [K]D = R^{ext} \tag{15}$$

In this chapter the theory needed to describe the interaction between the pantograph and the contact wire will be introduced. First describing nonlinearity, then contact in general, lastly the equation of motion for the contact wire when under influence of the contact force, with the motivation of showing how the contact is dependent on the contact wire movement.

3.1 Nonlinear Problems

The types of nonlinearity that arise in structural dynamics are divided into *material nonlinearity*, *geometric nonlinearity* and *contact nonlinearity*. A material nonlinearity is when the material properties are dependent of the of the state of stress or strain, as for example for plasticity. In the case of a geometric nonlinearity the deformations in the structure are so large that the equilibrium equation must be written with respect to the deformed geometry.

Contact nonlinearity are a special type of geometric nonlinearity that arise when structures interact, and contact forces has to be determined before calculating the structures behavior. For all three cases the problem becomes nonlinear because the stiffness, and in some cases also the load, as well becomes a function of displacement or deformation. Thus the principle of superposition does no longer apply. Hence, equation 15 can not be solved for D right away,

because the stiffness K and R is a function of a unknown deformation D. Thus iterations are needed to find D, and its associated R and K before solving the equilibrium equation.

The material properties are assumed linear in the catenary system. But there are a geometric nonlinearity caused by the slacking of the dropper, and a contact nonlinearity caused by the sliding contact between the contact wire and the pantograph. The geometric nonlinearity will be discussed here, and the contact problem will be discussed in next section.

As mentioned, the main difficulty with geometric nonlinear problems, is that the equilibrium equations must be written about the deformed geometry, which is unknown.

As discussed previously when a dropper is under compression, it does no longer connect the contact wire to the messenger wire. Thus the effect of the dropper is not included in the stiffness matrix, which therefore becomes a function of the deformation of the dropper. Thus the effect of that dropper is not included in the stiffness matrix. Thus the stiffness matrix becomes a function of deformation of the dropper.

Several complications arises with a nonlinear problem. It has proven difficult to find good mathematical and numerical models that describe the nonlinearity. In addition the nonlinear equations are difficult to solve, resulting in high computational cost.

3.2 The Contact Problem

Contact is a type of geometrically nonlinear problem that emerge when different structures interact by contact, separation or sliding along each other with friction. Contact can also be self contact, where different surfaces in a structure interacts. When this occur, the contact forces, gained or lost, must be calculated in order to calculate the behavior of the structure[COOK].

The contact between the contact wire and the pantograph is hard sliding contact, with no penetration in the contact surfaces. The equation for the contact force is derived in Chapter 2.2. Both the pantograph and the catenary are dynamic system that can oscillate independently. The two components have diverse masses, elasticity, damping coefficients and natural frequency, which makes the contact complicated [16]

Constraint equations must be included in the 15, for d.o.f. D in order to include the contact. The constraint equation for contact can be written in the form

$$[C]D = 0 \tag{16}$$

3.3 Solution Methods

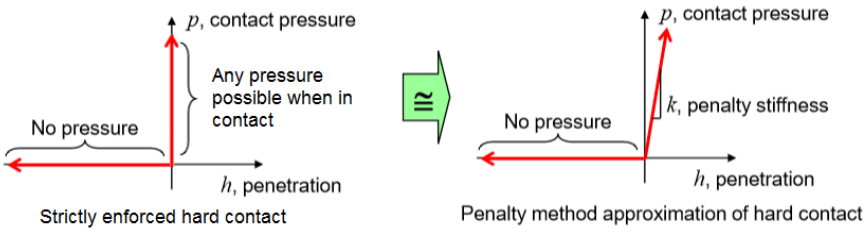

Figure 19: The penalty method [13]

There are different ways to impose the constraint equation, see Equation 16. The method for solving the contact problem will be introduced in this section. In the literature, the most frequently used methods are the penalty method and the Lagrangian method. The Lagrange method meets the contact condition exactly, while the penalty method is an approximation of the contact condition. However, the Lagrange method increase the number of unknowns in the equilibrium equation shown in Chapter 3. The penalty method gives the same number of unknowns, but can result in a set of ill-conditioned equations.

4 Frequency Domain Analysis

This chapter will give a short introduction to the spectral analysis, and some method used later in the thesis. More information on the spectral analysis can be found in [17]. The theory is based on the fact that a time signal can be thought of as a superposition of sine waves, thus they have a spectrum of components. Time signal can then be viewed as a sum of many wave trains with different frequencies. Studying the frequency domain of a signal gives valuable information, and can help analysing the signal.

4.1 The Fourier Transform

By Fourier transforming a function $F(t)$ in the time domain, to its corresponding function $C(\omega)$, the response can be analyzed in the frequency domain. The Fourier transform pair is presented in equation 17

$$F(t) = \frac{1}{2\pi}\int_{-\infty}^{\infty} \hat{C}(\omega)\mathrm{e}^{+i\omega t}\mathrm{d}x \tag{17a}$$

$$\hat{C}(\omega) = \int_{-\infty}^{\infty} F(t)\mathrm{e}^{-i\omega t}\mathrm{d}\omega \tag{17b}$$

where $\hat{C}(\omega)$ is the continous fourier transform (CFT) of the fucntion $F(t)$, defined on $-\infty < t < \infty$, $\omega = 2\pi f$ is the angular frequency, and $i = \sqrt{-1}$. The plot of $\hat{C}(\omega)$ against frequency show the amplitude of the sinus wave, against the frequency of that sinus wave. The Fourier transform of a function contains the same information as the original function. By putting $\omega = 0$ in equation 17b, it can be seen that the value of $\hat{C}(0)$ is the area under the time function [15]

Finding the Fourier transform of the signal is only possible if the function $F(t)$ is fairly simple, which is most often not the case. Thus the discrete Fourier transform (DFT) is used in stead. Whit the DFT method, the signal is viewed as a finite number of wave trains.

As seen above the CFT takes a function that is defined on $-\infty < t < \infty$ and transform it to the frequency domain. The DFT takes a signal, defined on a finite time T, and represent it by a finite number of frequencies. Since with the CFT the function is thought of to be defined on $-\infty < t < \infty$. With the DFT sees the signal as a periodic function in the time domain with a period of T. This is the main difference between the DFT and the CFT. It can also be interpreted in the way that the CFT is the DTF of a signal over an infinite period T. Thus the DFT goes towards the CFT when the sampling time goes to infinity.

The discretization in the two domains are.

$$\Delta T = \frac{T}{N} \tag{18a}$$

$$\Delta f = \frac{1}{T} \tag{18b}$$

The DFT of a signal is affected by the sampling frequency $f_s = \frac{1}{\Delta T}$. The highest detectable frequency is half of the sampling frequency. If the sampling frequency is too low, the higher

frequencies will appear as lower frequencies (its alias). In that sense the DFT is both dependent on the sampling duration and the sampling frequacy. The half of the sampling frequency is defined as the Nyquist frequency, $f_{Nyqiust} = \frac{1}{2\Delta T}$. The CFT and DFT is a good match only for frequencies under the Nyquist.

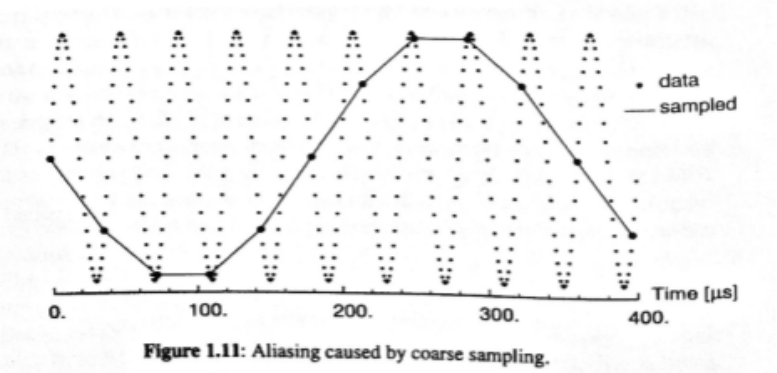

Figure 1.11: Aliasing caused by coarse sampling.

Figure 20: Aliasing [17]

Increasing the sampling frequency, i.e. increasing the Nyquist, increase the correlation between the CFT and the DFT. Using the DFT of a signal, sets the limits for the frequencies used to characterize the signal. It can be seen from equation 18b, that the discretization in the frequency domain is set by the sampling time T.

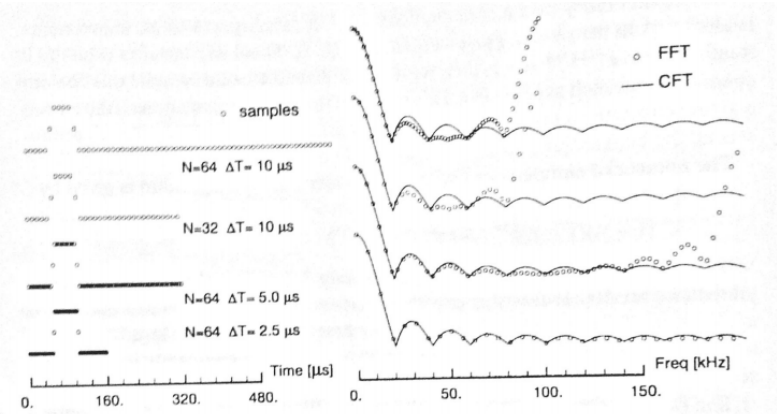

Figure 1.6: FFT transform of a rectangular pulse of width $a = 50\,\mu$s.

Figure 21: The effect the sampling time T, and the time step Δt has on the DFT [17]

An method called the fast Fourier transform FFT, have made it possible to study the DFT of a signal. Is an very effective method. The FFT is simply a technique for calculating the DFT. This algorithm have made it possible to study the frequency domain, with relatively low computational cost.

4.2 Filtering

In EN 50317 [11] there are stated that the the output from a simulation must be filtered with a cut-off frequency of 20 Hz. This is discussed, and is assumed to small in many articles. In [9] it is stated that in order to measure wear, the cut off frequency should be as high as 100 Hz. In [**?**] the effect of changing cut-off frequency from 20Hz to 80 Hz is tested. The result show a 11% increase in the standard deviation, and 36% increase in maximum values and a 19% decrease in minimum values. This show, that when looking at wear, and other local effect, the cutoff frequency must be increased.

A filter remove some frequencies in a signal, and in that way creates a smoothing effect. Low-pass filter, is a type of filter that allow signals below a given frequency to pass and stops signals above that frequency. The frequency limit is called the cut-off frequency. Chebyshev Types I filter is used in this thesis [**?**].

The Bode-Diagram for a Chebyshev Type I filter is plotted below. The sampling frequency is set to 1400 Hz, and the cut off frequency to 100 Hz.

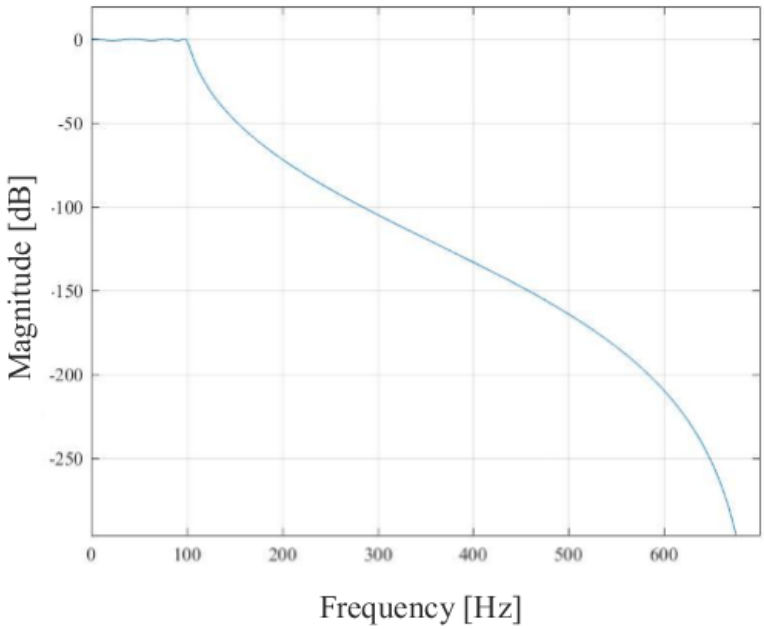

Figure 22: Magnitude response [18]

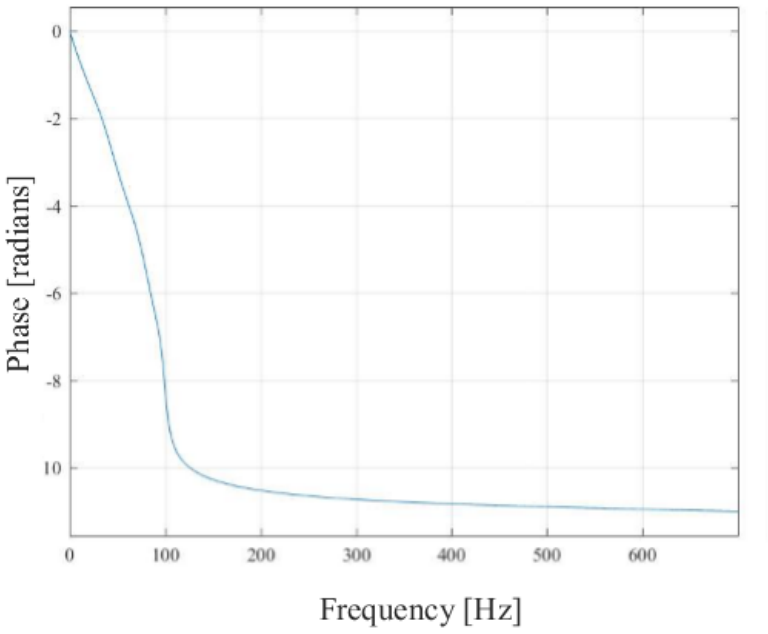

Figure 23: Phase response [18]

5 Simulations in Abaqus

In this section the simulation method used in this thesis is described. The simulations are done using a numerical model derived and validated by Petter Naavik. The simulations uses design data and field data from Fokstua wire 21, and the pantograph used is WBL88. Some modifications are done, in order to better investigate the outputs of interest.

Firstly, the design data and line geometry that is the basis of the numerical model will be presented. Secondly, the numerical model will be described. Lastly, the simulation method that is the basis for this thesis will be introduced.

5.1 Line Geometry and Design Data

The section studied in this thesis is located along the Dovre rail line, and is called: Fokstua wire 21. It is a Norwegian System 20 C1 catenary section, see Figure 24. There are between four and six droppers in each span. All of the span lengths, and number of droppers are shown in Appendix A1.

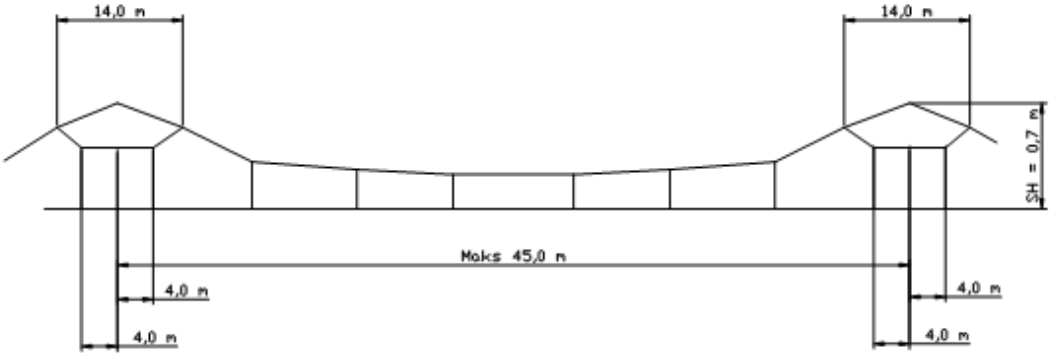

Figure 24: Standard for System 20 C1 used on Fokstua wire 21 [14]

Table 1: Key design properties of the catenary section Fokstua wire 21

Section Properties	Fokstua Wire 21
Length	1295 m
Constuciton year	2015
Catenary system	System 20 C1
Tension force in contact wire, T_{cw}	13 kN
Tension force in messenger wire, T_{mw}	13 kN
Cross-sectional area of the contact wire	120 mm^2
Cross-sectional area of the messenger wire	70 mm^2
Density of wire material	8890 kg/m^3
Stitch wire (Yes/No)	Yes
Number of spans in contact with the pantograph	28
Wave Propagation speed, c_p	435 km/h

The pantograph used is WBL88. A lumped-mass-model was provided by the manufacturer Schunk Nordiska AB. It is a method of describing a dynamic mechanical system as a series of discrete concentrated masses, that are connected trough spring and damper elements [10]. The model is described in Figure 25 and Table 2

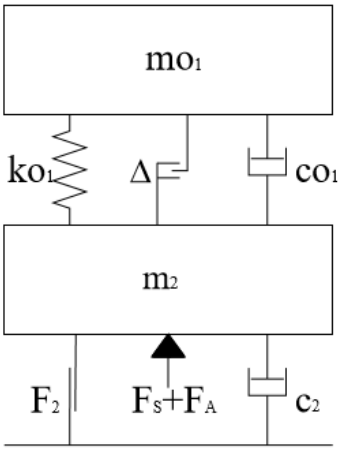

Figure 25: The lumped-mass-model for the pantograph WBL88 [8]

Table 2: WBL88 lumped-mass-model properties

	Unit	Value
mo_1	kg	6.6
m_2	kg	19.7
ko_1	N/m	4400
Δ	m	0.03
co_1	Ns/m	75.6
c_2	Ns/m	63.5
F_2	N	7
F_s	N	55
F_a	N	$0.0068 \cdot v^2$

Chapter 2.4 state a number of dynamic characteristics for a catenary section. Some are calculated in Table 3 using the values from Table 1.

Table 3: Dynamic characteristics for Fokstua wire 21

Amplification coefficient, γ	0.9988
Reflection factor, r	0.5670
Doppler factor, α	0.5677

It should be commented that the amplification factor is quite large. From 2.4 it is stated that this should be less than or equal to 1.

5.2 Numerical Model

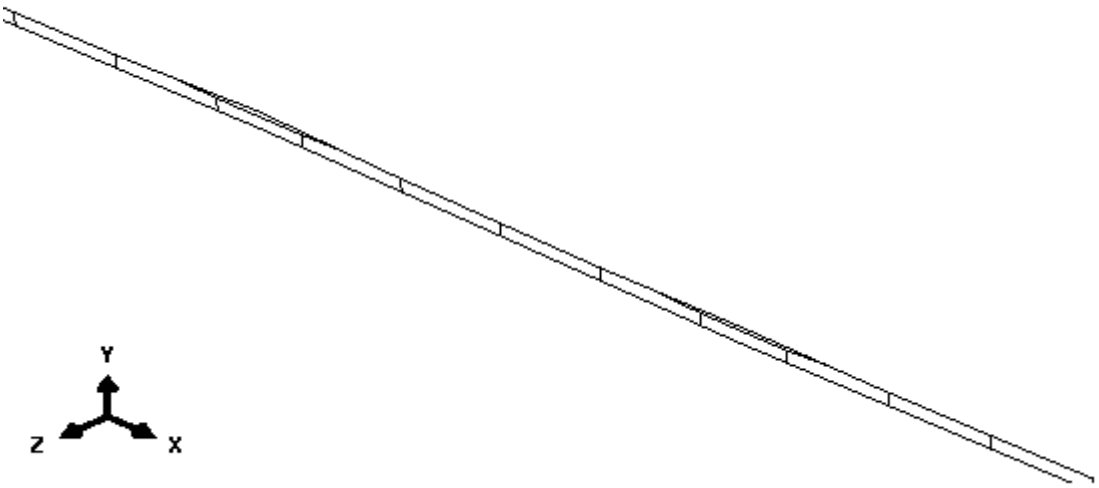

Figure 26: The catenary system in Abaqus, where x is the running direction of the train.

The numerical model used in the simulations was created by Petter Nåvik. The model is validated using field measurements. The field data were sampled according to standard. That is, with a sampling frequency of 200 Hz. This will be referred to as f_{sd}. The input is the design data from Chapter 5.1, and line geometry. A python script generates a model in Abaqus. The exact line geometry is taken from excel cell arrays, and is used in the python script. All the design parameters shown in 5.1 is included in the model

In [8] Nåvik highlights that there can be a significant difference between the the design data and the actual design, the same for the geometry. Thus the model was compared with measured geometry by using pre-sag and elasticity, which creates accurate results.

The contact wire, messenger wire, stitch wire and the dropper are modelled using three-dimensional deformable beam elements. An Timoshenko beam element was used in order to ensure a stable solution. The Euler–Bernoulli beam elements could also be used, with negligible effect on the simulated results [5]. This is the element type that is often used in simulations of catenary systems. The element length is 0.05 m.

The contact wire and messenger wire are pre-tensioned and the pre-sag of the catenary is included. The catenary section is applied tension and sag prior the dynamic analysis where the pantograph runs along the section. The Rayleigh damping coefficients estimated by Naavik from field measurements, are set to $\alpha = 0.062$ and $\beta = 6.13e^{-}06$ [5]. The forces in the stitch wires are also included model. The tension of the stitch wires has to be obtained individually in order to achieve the correct forces, this is done by an iterative step.

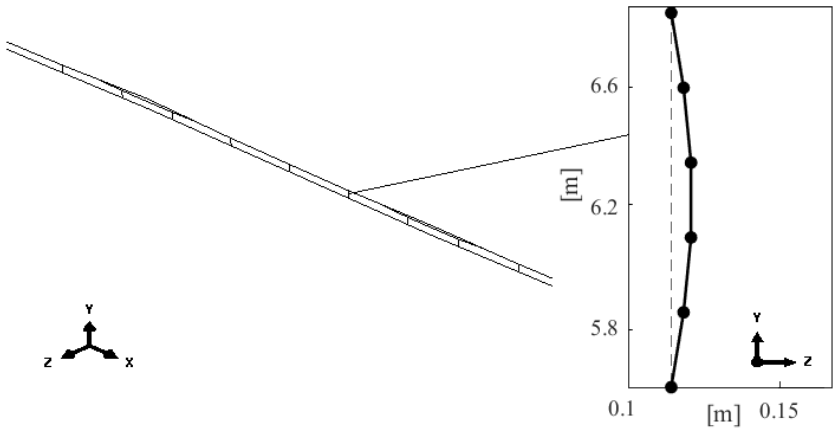

Figure 27: Formation of the dropper elements. Pre-bent to include the slacking of the dropper in the model. The dropper figure is created in Matlab, and the catenary is from Abaqus

Figure 27 illustrate how the slacking of the dropper is included in the model. The dropper is divided into five beam elements. The beam elements are arranged so that they form a half sine wave. The assumption is that when the dropper is pre-bent, it is more effected by compressive type forces.

The pre-tensioning and the pre-sagging of the catenary is the first step of the simulations. In the next step the pantograph is lifted with force $F_s + F_a$. The final step is a dynamic step where the pantograph run along the catenary section. The Hilbert Hughes Taylor Method, which is an implicit integration scheme, is used in the dynamic step. The Newton Method is used for the nonlinear equilibrium equation.

The model uses beam-to-beam contact, that allows for separation after contact occur. The contact is defined as hard contact, meaning that there is no penetration in the contact surfaces. The beam to beam contact is an generalisation of the surface to surface contact, that allows for using beam element as contact surfaces [13]. The constraint enforcement method is the Penalty method, see Chapter 3.3. And the stiffness factor K, is set to default. The default stiffness factor uses the stiffness of the underlying elements, and tries to find a balance between too low penalty stiffness, which as mentioned will result in large penetrations, and too large penalty stiffness, which can result in ill-conditioning. The interaction surfaces are the contact wire and the collector heads.

5.2.1 Pantograph Model

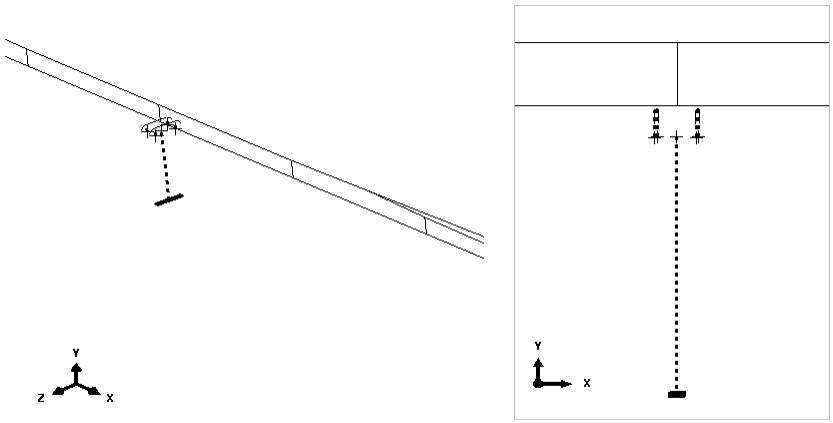

Figure 28: The catenary system and the pantograph in Abaqus, x is the running direction of the train

The lumped-mass-model described in Chapter 5.1 do not include the fact that there are two collector strips, which is the contact surface of the pantograph. Nåvik includes this in his model by dividing the top mass in Figure 25. Which leads to a more accurate description of the pantograph movement. The modified pantograph model is described in Figure 29.

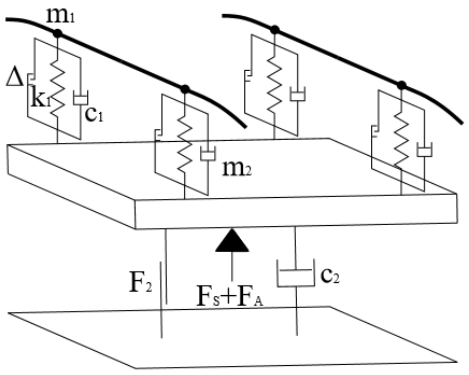

Figure 29: Improved lumped-Mass-modell [8]

The parameters in this model is derived from the original model described in Table 2 and Figure 25. Where $m_1 = mo_1/4$, $m_1 = M_1/4$, $c_1 = co_1/4$, and $k_1 = ko_1/4$.

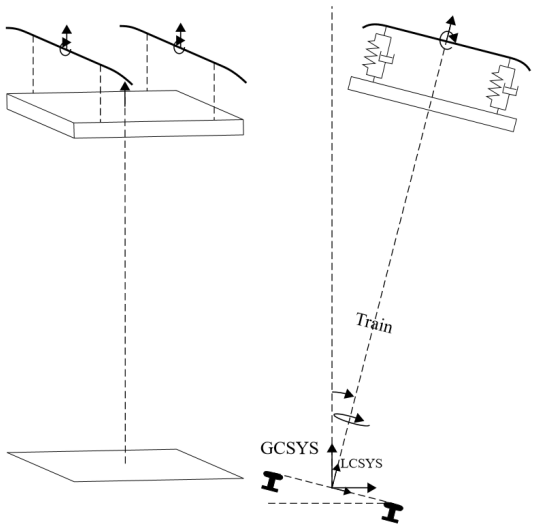

Figure 30: The DOFs in the modified pantograph model [8]

Two coordinate systems are used to describe the movement of the train. GCSYS describe the position and rotation of the base of the train, the local coordinates system LCSYS ensure that the pantograph displacements are only along the normal axis. The fact that the front collector strip experience higher contact forces than the rear one is not included in the model.

5.3 Simulation Method

EN50318 [10] define a *Simulation method* as: Any numerical method that uses a fixed set of input parameters to describe a system to calculate a set of output values representative of the dynamic behavior of this system.

The simulation method in this theses uses the numerical model derived by Naavik described in the previous chapter. In order to run multiple simulations the analysis area is reduces. Thus, the simulations in this thesis is done over two spans in the Fokstua wire 21 section already described. The alterations in the numerical model is done using Python. The simulations are preformed in Abaqus. Matlab and Python is used to analyse the results from the simulations

Firstly, the changes done in the numerical model will be described. Secondly, the effect of reducing the contact area on the computational costs are addressed.

Two separate studies are done in the thesis. First multiple simulations with different sampling frequency, studying how the response is affected by the sampling frequency. Secondly, the contact formulation is studied, by changing the penalty stiffness.

5.3.1 Changes in Numerical Model

The analytical area is reduced to span 6 and 7,see Figure 86, in the catenary section Fokstua wire 21. Tabel 4 show the span informaiton.

Table 4: WBL88 lumped-mass-model properties

Span number	Length [m]	Number of Droppers	Stitch Wire (Yes/No)
6	45,65	5	Yes
7	44,88	5	Yes

In the simulations the pantograph runs along the catenary section with constant train speed v = 120 km/h. Since the output for span number 6 and 7 are of interest the simulation start in the middle of span 5, and end at the middle of span 8. Ensuring that the output of the simulations are realistic, i.e. are not affected by responses from when the pantograph first connects to the contact wire.

The contact forces are the focus of this thesis. The contact force is measured in the intersection between the contact wire and the pantographs collector heads, and is the sum of all points of contact. The train speed is constant, thus the sampling frequency alone decide how often the contact force is measured along the span. With f_{sd} the contact force is measured every 0.167 m.

In the rest of the thesis, span 6 and 7 will be refereed to as span 1 and 2. Figure 31 show illustrate the two spans, and the notation used in this thesis. Dr_a^b refers to Dr_b in span number a.

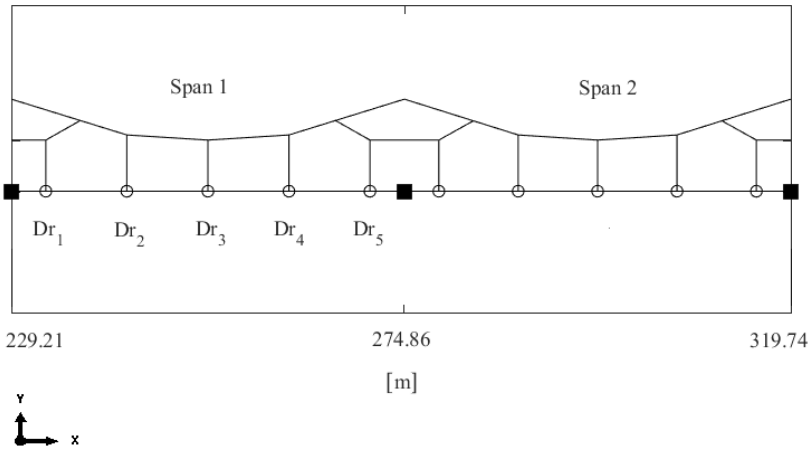

Figure 31: The two spans studied in the simulations, including the notation used. The model is derived in Matlab, and the length between the droppers and the brackets are correct. However, the section height is not scaled

According to EN50318 [10] the simulations must be able to calculate the variation of the contact forces, the wire movements and the pantograph movements when the pantograph passes along the overhead contact line model. These outputs should be filtered to exclude the frequencies outside the frequency range of interest.

5.3.2 The Contact Formulation

The simulation time is highly effected by the contact formulation. Before starting the analysis, the effect of reducing the contact area in the contact inclusion where studied. Looking at how the simulation time is effected by the contact area, by running simulations over two spans and increasing the contact surface in each simulation.

As seen the contact area is defined by two contact pairs. The first is the whole contact wire and the first pan head, and the second is the whole contact wire(28 span) and the second pan head. The simulations where done over two spans, and the contact area where increased from 5 to 20 spans.

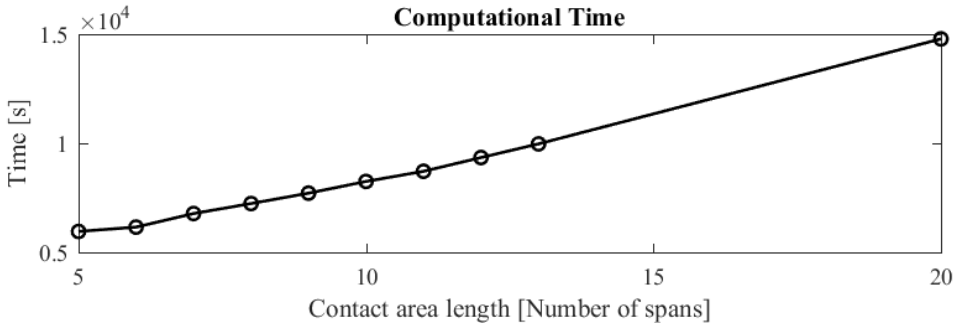

Figure 32: Computational time versus contact area

It can be seen from Figure 32 that the computational time is highly effected by the contact area. It is nearly linear and the slope k can be approximated to $k = \frac{9971-5958}{13-5} = 501.63\frac{s}{span} = 8.36\frac{min}{span}$, noted that this is for a simulation over two spans. Running the whole section, this whould be very important.

The simulations performed in this thesis, is done over two spans, so the computational time is kept relative low, approximately three hours. However, numerous simulations were performed.

5.3.3 System characteristics

The elasticity and the eigenfrequencies up to 40Hz of the catenary will be displayed in this section. The results will not be discussed in detail, but is used in the Result section.

The eigenfrequencies up to 40 Hz were calculated in Abaqus.

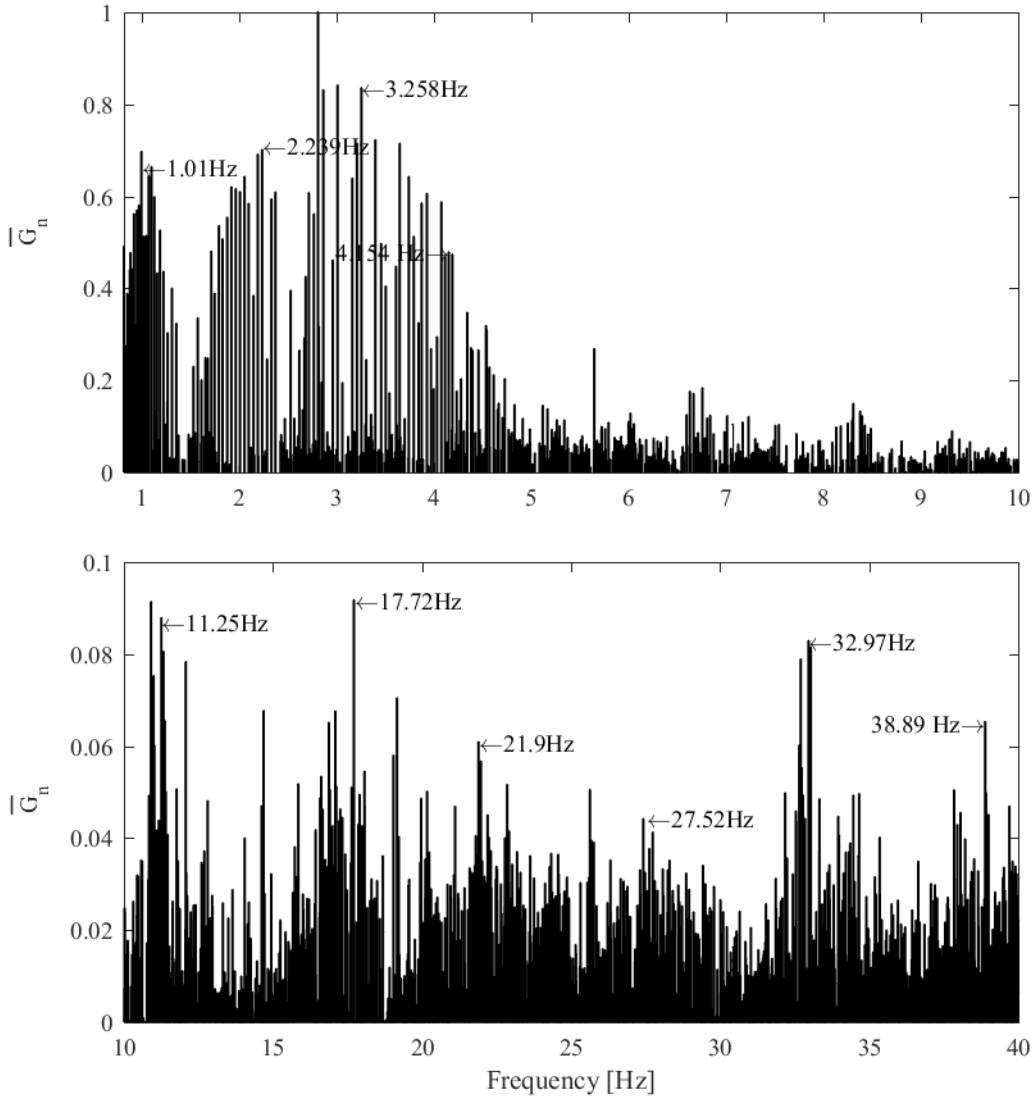

Figure 33: Eigenfrequencies in the system, $\overline{G_n}$ is the normalized general mass G_n

The elasticity were calculated by Naavik in [8].

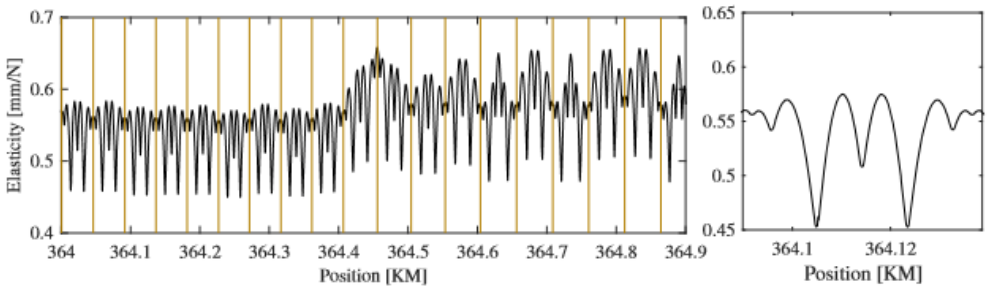

Figure 34: Elasticity in the section Fokstua Wire 21, [8].

6 Sampling Frequency Results

The contact force, together with the standard deviation or percentage of arcing and the contact wire uplift, can define the current collection quality of the system [16] Arcing occurs when the forces approach zero, or there is a loss of contact. Arcing will too some degree maintain electrical transmission, but will increase the wear of the contact wire. If the air gap is too wide, energy transmission is interrupted, i.e. loss of power to the train. As stated earlier, change in elasticity and the wave propagation is the most common cause for contact loss.

The wear of the contact wire is crucial. In addition arcing, excessively high contact forces also contribute to wear of the contact wire. This because the high forces can lead to the contact wire being lifted too high, and this would lead to unacceptable wear [16].

It is important that the model is able to show the effect of the passing of the droppers, and the brackets. The model should also be able to show the effect of the wave propagation. The movement of the contact wire highly depends on the wave propagation speed, as shown in the chapter 2.4

In [**?**] Naavik look at the effect of changing the cut off frequency from 20 Hz to 80 Hz, this has a considerable effect on the extremal values of the contact force. In [9] argues that when studying the wear the catenary system frequencies up to 100 Hz are important. This is the maximum frequency simulations done with f_{sd} are able to detect.

6.1 Contact force

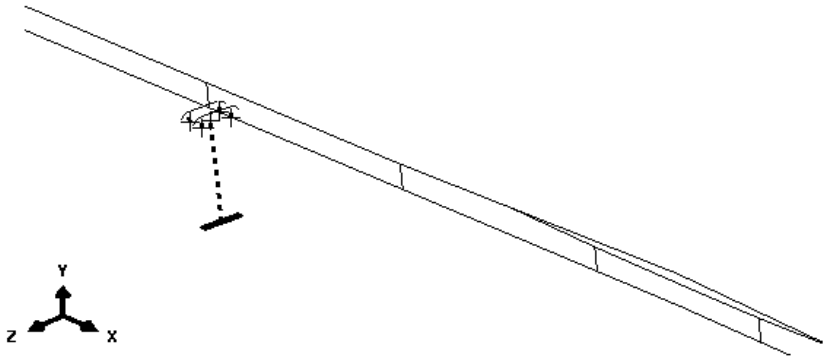

Figure 35: The catenary and the pantograph. The figure is taken from the numerical model in Abaqus

In this section, several analysis are done n order to see if a simulation with a given sampling frequency are able to measure the effect stated above. Firstly, the time domain plot of the contact force. This shows much information about the behavior of the system. It is the most suitable way to look at the dynamic behavior of the components in the system, and the interaction between them according to [16]. Secondly, the frequency content of the contact forces is examined. Identify which frequencies are important for the contact, and what should be filtered out. Thirdly, a some statistical data of the contact force are illustrated. Lastly, critical points for the contact forces in the span are located.

6.1.1 Time Domain Analysis

In this section the contact force in the time domain is plotted for the whole analytical area, and critical areas in the span are identified, the studied more closely. The contact forces where computed with sampling frequencies from 20 Hz to 1400 Hz, with a step of 20 Hz. The contact force time response from five simulations are presented in this section. The selected simulations are done with $f_s = 20, 200, 600, 1000$,and 1400 Hz. $f_s = 200$ Hz is the sampling frequencies stated as a minimum in standard EN 50318, and will be referred to as f_{sd}. The result derived with $f_s = 20$ Hz is included, even though this is critically lower than f_{sd}. This is to demonstrate that the result computed with $f_s = 20$ Hz, differ from the result computed with higher f_s and filtered at 20 Hz. Figure 36 show where the pantograph is located in the span for a given time.

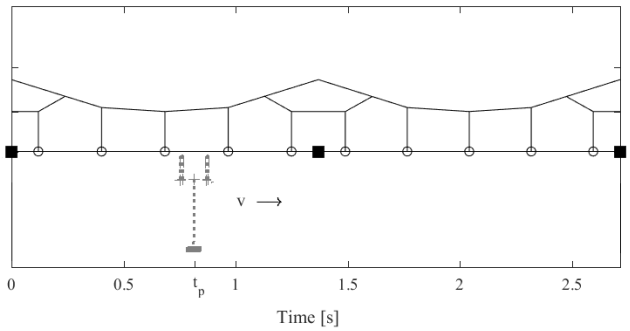

Figure 36: Pantograph position along the span at time t_p, v is the train speed. The figure derived in Matlab, and is not scaled

The elasticity of the catenary system is plotted in Figure 34, the tendency of the elasticity for span span in the catenary is shown in 37. The sudden drop in the elasticity by Dr_2 and Dr_4, suggest that the highest contact forces will be measured there. The section around the stitch wire have almost uniform elasticity, thus smaller variation in the contact force would be expected there. The maximum elasticity in the span is measured at the middle of the sections between Dr_2 and Dr_3, and Dr_3 and Dr_4, there the lowest contact forces are expected to occur.

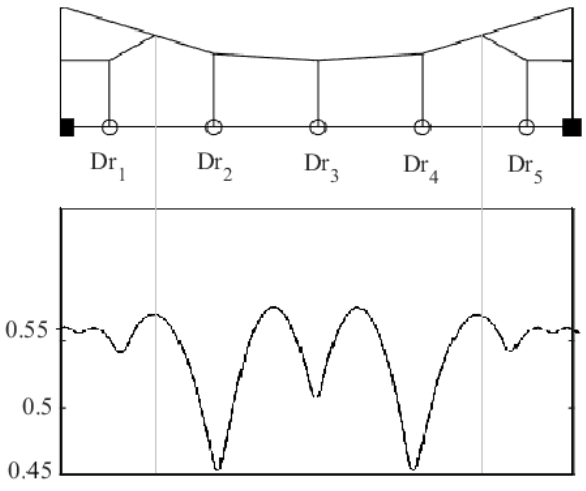

Figure 37: Elasticity variations along a span in the Catenary system. The elasticity distributions is taken from Figure 34. The grey lines illustrate where the stitch wires are connected to the messenger wire

The contact wire from figure 36 are included in the time domain plots of the contact force. For the sake of illustrating where the pantograph is located along the span at a given time, making it easier to identify critical locations in the span.

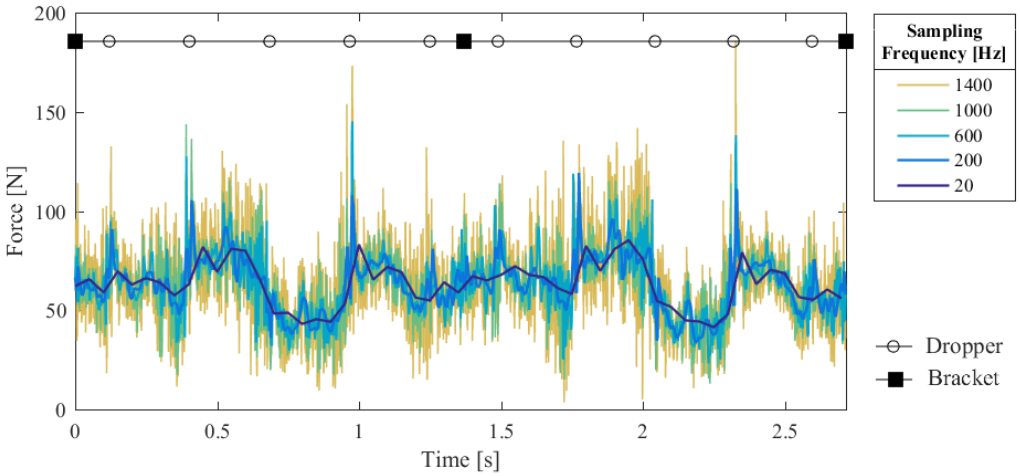

Figure 38: Contact forces in the analytical section

As expected the simulated contact forces are highly affected by the sampling frequency. The results from simulations with $f_s = 20$ Hz, are limited to the mean contact forces, and most of the dynamic effects are not included. The results measured with f_{sd}, show the most important dynamic effects in the span such as passing of the droppers.

It is apparent from Figure 38 that the largest contact force is measured at Dr_4 in the simulation with $f_s = 1400$ Hz, this can be expected from the elasticity plot. For the simulations with $f_s = 200, 600$ and 1000 Hz there are no clear maximum position for contact forces. However, there are large contact forces measured by both Dr_2 and Dr_4, also expected from Figure 38. For the simulations with $f_s = 20$Hz Figure 38 show that contact forces measured at Dr_4, correspond with the contact forces measured in the section between Dr_2 and Dr_3. This suggest that simulation done with $f_s = 20$Hz are not able to fully detect the elasticity variations along the span. All the simulations identify the smallest contact force at the section between Dr_3 and Dr_4

As stated the maximum forces is expected to occur by Dr_2 and Dr_4 in each span. However, an increase in the contact forces should be identified by all the droppers. As seen in Figure 38, there is an increase in the contact forces near all the droppers. However, the magnitude of the response is larger when f_s increase.

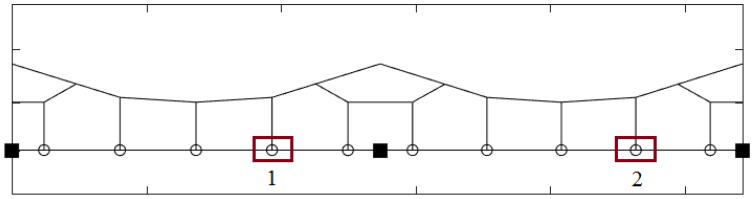

Figure 39: Critical positions in the span with regard to larger contact force.s

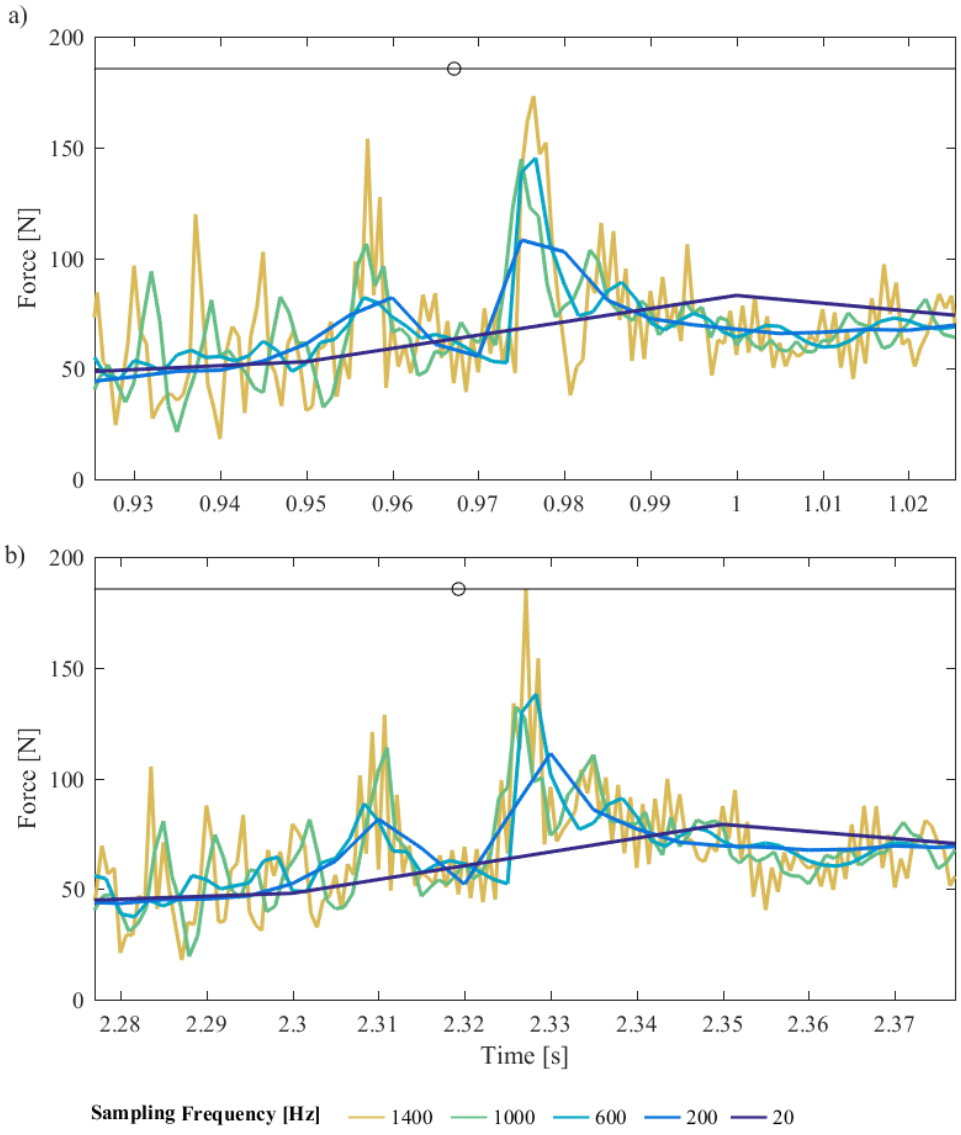

Figure 40: Contact forces measured at a) Dr_4^1 and b) Dr_4^2. The time period shown is 0.1 seconds

The sections where the maximum and minimum forces are located are studied closer, and are highlighted in Figure 39. As stated, the maximum contact forces are located by Dr_4 in each span for $f_s = 1400$ Hz. The minimum contact forces are located between Dr_3 and Dr_4 for all the simulations.

Figure 40 show that the contact forces increase when the pantograph is approaching Dr_4 in both spans, this is probably caused by the decrease in elasticity by that dropper. When the pantograph passes the dropper there is a sudden drop in the contact forces down to approximately $F_{static} =$

55 N, that is caused by the slacking of the dropper, see Chapter 2.2 and **??**. When the tension in the dropper return there is a rapid increase in the contact forces. The four simulations done with $f_s \geq 200$ Hz are able to include the effect of the slacking of the dropper. However, the magnitude of the contact forces differ. The largest difference are observed prior the passage of the dropper.

An important thing to observe from Figure 40, is that the contact forces measured with $f_s = 600$ Hz and $f_s = 1000$ Hz are closely related after the pantograph has passed the dropper. Whereas, the contact forces measured before the passage of the dropper differ a lot. There are high frequency variations in the measured contact forces from the simulations with $f_s = 1400$ and 1000 Hz, that the simulations with f_{sd} and $f_s = 600$ Hz are not able to detect. After the passage of the dropper, the contact forces measured with $f_s = 1400$ varies with frequencies of approximately 600 Hz. The cause of these frequencies can be oscillation in the dropper after the pantograph has passed. The behavior of the dropper will be evaluated in Chapter 6.3.

The plot over the analytical area in Figure 38 demonstrated that even simulations with f_s as low as 20 Hz are able represent the trend of the catenary movement. However, the simulations are not able to calculate the extremal values of the contact force correctly. This becomes more evident when considering the data in Figure 40. The local maximum for the contact forces when $f_s = 20$ occur 0.03 seconds after the pantograph has passed the dropper. Since the train speed $v = 120/3.6m/s$ this is 1 m after the passing of the dropper. When $f_s = 20Hz$ the contact force is only measured every $\Delta l = \frac{v}{f_s} = 1.67m$ along the contact wire, the chance is that it not affected by the passage of the dropper. For comparison, with $f_s = 1400$ Hz, the contact force is measured every 2.38 cm.

The peaks contact forces with $f_s = 1400$ Hz, that is not detected by the other simulations, can be caused by the small uplift in the contact wire caused by the wave propagation. The transverse wave uses approximately $\frac{1}{12000}s$ to pass a element in the contact wire, i.e. the element pass frequency for the wave propagation is 12000Hz. Sampling with a higher frequency will increase the probability of the contact force being affected by this uplift. In addition, how close to the dropper the pantograph hits the contact wire affects the contact force. Again, higher sampling frequencies increase the the probability of contact forces being measured when the pantograph is directly under the dropper.

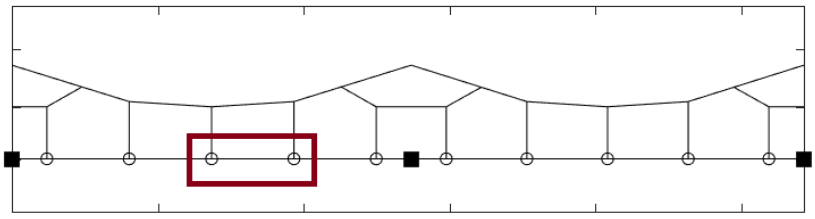

Figure 41: Critical positions in the span with regard to small contact forces

In figure **??** the contact forces from the section between Dr_3^1 and Dr_4^1 are plotted. This is the section with highest elasticities, maximum elasticity is located approximately half way between the two droppers.

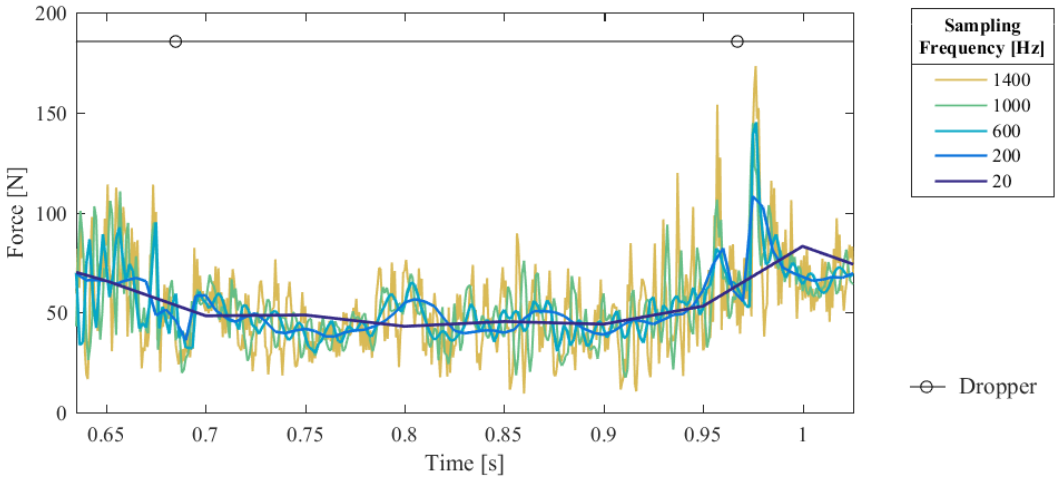

Figure 42: Contact forces measured at in the section between Dr_3^1 and Dr_4^1

Low contact forces are observed in this section when $f_s = 1400$ Hz, and the plot suggests that contact force varies with a frequency between 120 Hz to 140 Hz. This illustrates that the minimum contact forces are impacted by higher frequencies. The contact forces measured with $f_s = 1000$ Hz are able to match the extremal values for $f_s = 1400$ Hz. However for $f_s = 600$ Hz the difference is larger. However, results with $f_s = 600$ Hz matches the results with $f_s = 1000$ Hz in many sections. The difference in the result larger by Dr_4 than Dr_3. Another important result is that the simulations with f_{sd}, show no increase in the contact forces prior Dr_3^1. Suggesting that the simulations don't not include the effect of the drop in elasticity at that point.

The maximum contact forces increase with the increase of f_s, as expected. The simulations with $f_s \geq f_{sd}$ are able to detect the largest elasticity variations along the span and the passing of the dropper. However, the magnitude of the contact force increase with the increase in f_s. In the section with the lowest contact forces the simulations with f_{sd} are seemingly not sufficient.

6.1.2 Frequency Content

In this section the frequency content of contact forces are identified. The method used is the power spectral density (PSD) of the contact force estimated by the fast Fourier transform (FFT). The FFT is described in chapter 4.1. The small time period in the simulations in this thesis, T = 2.7159 s, leads to a course discretization in the frequency domain, $\Delta f = \frac{1}{T} = 0.3682Hz$. The eigenfrequencies of the catenary system, displayed in Figure 33, show that there are many closely related eigenfrequencies.

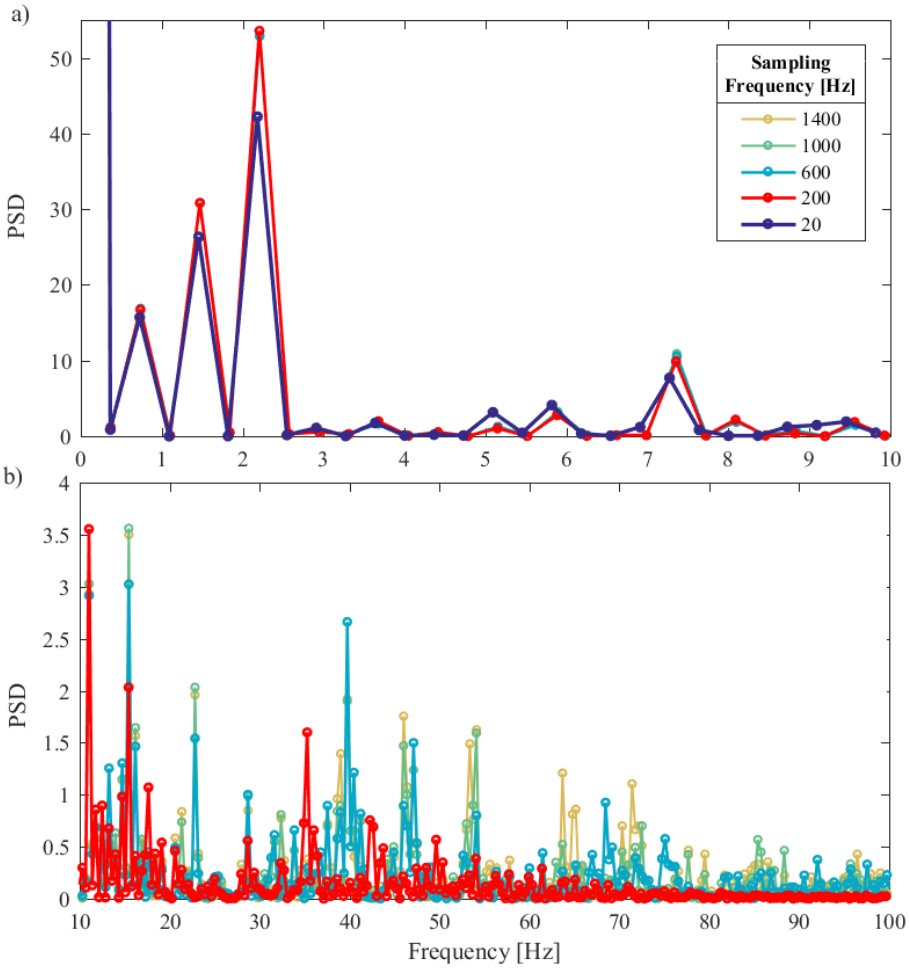

Figure 43: The FFT spectrum of the contact force, in the frequency range a) 0-10 Hz and b) 10-100 Hz. The PSD from f_{sd} = 200 Hz are highlighted in red.

This, together with the course discretization in the frequency domain makes it difficult to identify distinct eigenfrequencies that the catenary sections is most effected by. However, valuable information about simulations can be gained by analysing the PSD of the contact forces. Firstly, the frequency content up to 10 Hz will be studied. Secondly, frequency content up to 100 Hz. Lastly, the frequency content up to 200 Hz. The motivation is to identify those frequencies that are important for the contact formulation, and how the sampling frequency affects the frequency content of the simulated results.

Figure 43 a) demonstrates that the frequency content for the contact forces simulated with $f_s \geq f_{sd}$ are nearly identical for frequencies under 10 Hz . This demonstrates that if the frequency range of interest is under 10 Hz, there is no reason to increase f_s. However, looking at Figure 43 b) there are frequencies with higher powers that the results from simulations with $f_s \leq 200Hz$ do not show. The peak at 11.03 Hz can be recognize from the eigenfrequencies plotted in Figure 33

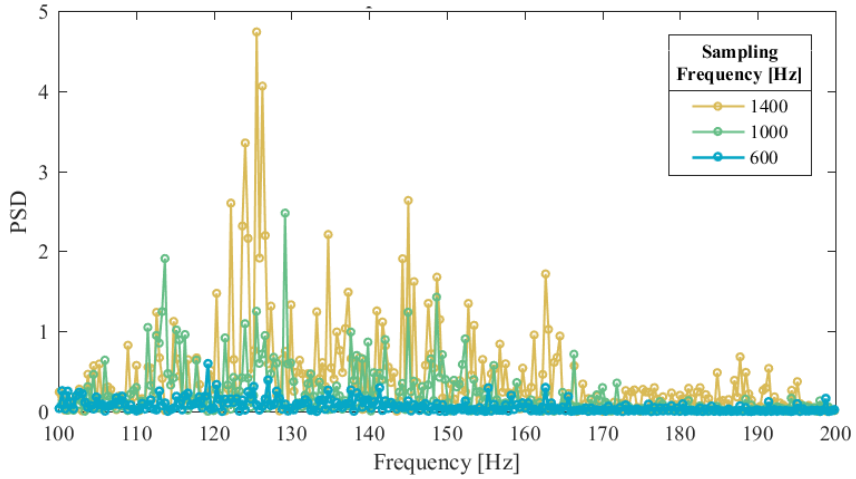

Figure 44: The FFT spectrum of the contact force, in the frequency range a) 0-10 Hz and b) 10-100 Hz.

Figure 44 demonstrates that frequencies over 100 Hz influence the contact forces sampled with $f_s \geq 600Hz$. It is not easy to detect the origin of these frequencies. The effect of filtering the sampled data with at cut-off frequency 100 Hz, and 140 Hz will be presented in Chapter 6.4, ad help identify the origin of these frequencies.

To summarise, the frequency content of the contact force measured with frequencies from 200 Hz, to 1400 are approximately the same up to 20 Hz. This is the cut-off frequency that should be used according to standards.

It was shown in the previous section, in area with low contact forces, that there are oscillations with frequencies from 120 Hz to 140 Hz that the contact force is affected by. It is also clear from figure 44 that there are frequencies over 100 Hz that are important for the contact.

6.1.3 Statistical Analysis

In this section some statistical values for the contact force are calculated. The mean, minimum, maximum and the standard deviation of the sampled contact force is presented. This is values that are important when classifying the quality of the interaction between the contact wire and the pantograph. The maximum and minimum values are, as stated earlier, important for the measurement for contact wire wear, contact loss and arching.

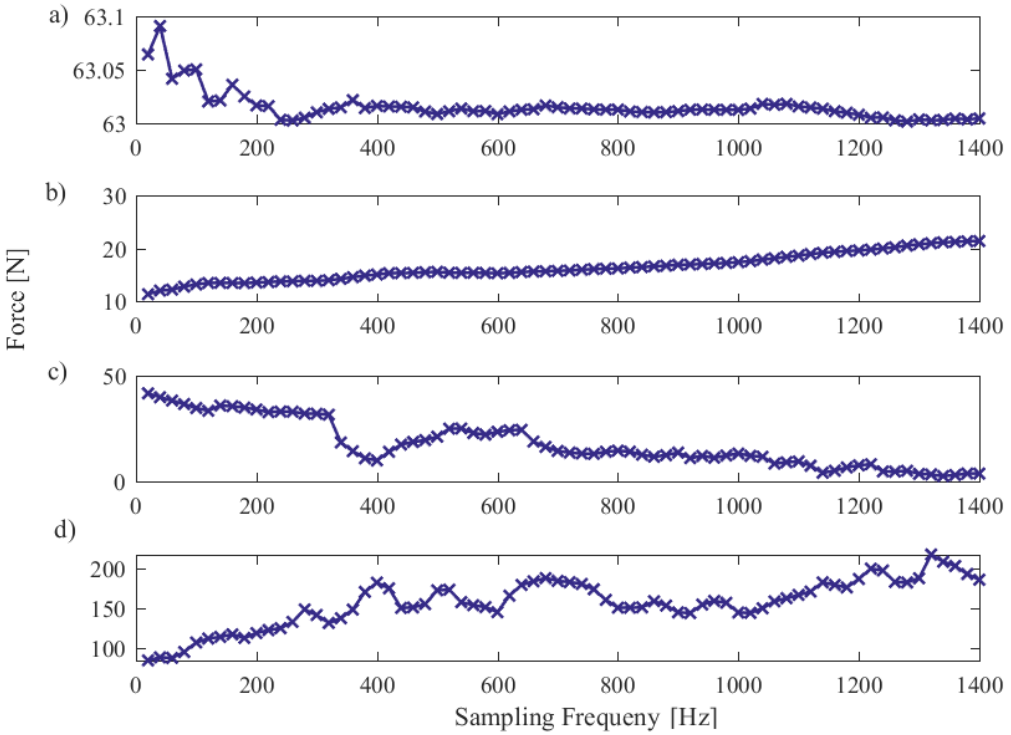

Figure 45: Statistical values of the contact force. a) mean value, b) standard deviation, c) minimum and d) maximum

As seen in Figure 45 a) the mean value of the contact force is nearly independent of the sampling frequency. The outline of this was already seen in the plotted times series of the contact force in chapter 6.1.1. However, other the statistical values highly depend on the sampling frequency. Figure 45 a) show that the sampled data with $f_s = 20Hz$ produce a good approximation of the mean response. However, when looking at the other values it is evident that the error is substantial.

The standard deviation of the contact force is used to classify the interaction between the contact wire and the pantograph. Small standard deviation of the contact force results in a smoother interaction between the contact wire and the pantograph. From figure 45 it is clear that the standard deviation increases approximately linear with the sampling frequencies. The standard

deviation of the sampled data increase with over 100 % when f_s increase from 20 to 1400 Hz, and approximately 60 % when f_s increase from 200 to 1400 Hz. The standard deviation of the field data in [**?**] are measured to 15 N. It should be stated, that these values are measured with higher train speed than used in the simulations in this thesis. The standard deviation of the sampled data are greater than or equal to 15 N, when $f_s \geq 400Hz$

Both the maximum and minimum values of the sampled data, increase and decrease respectively with the increase in f_d, as expected. The minimum of the contact force sampled with $f_s \geq 600$ decrease linearly. The maximum of the sampled data does not show the same linear effect. However, when $f_s \geq 600$ the changes in the maximum of the sampled data are small. The maximum contact force measured with $f_s = 600Hz$ is 78.38% of the maximum contact force measured with $f_s = 1400Hz$. The largest contact forces are sampled with $f_s = 1320Hz$, and there are a decrease maximum of the sampled data with higher f_s. The maximum and minimum contact forces, and their locations along the span will be discussed in further detail in 6.1.5 and 6.1.6 respectively.

6.1.4 Filtered According to Standards

The contact forces studied so far are not filtered. Chapter 6.1.2 show that there are many frequencies over 20 Hz that influences the contact force. In this section the effect of filtering the results according to the standards (with cut-off frequency 20 Hz) will be discussed, and plots of the filtered time series will be presented. The statistical data for the filtered contact forces will presented in 6.4.

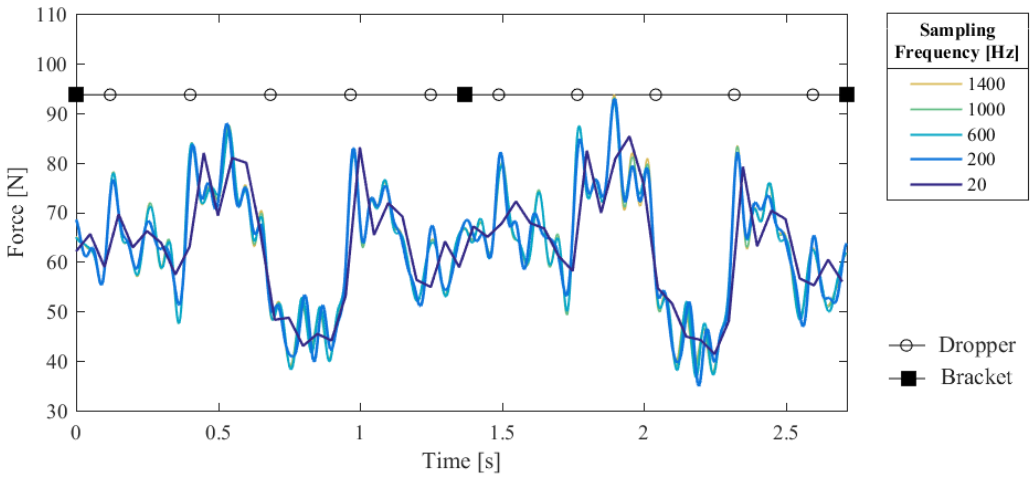

Figure 46: Contact force filtered with a cut off frequecny of 20 Hz

. The method used for filtering is the Chebyshev Type I filter which is described fully in chapter 4.2. The result demonstrate that the measured data are nearly independent of the sampling frequency, if it is filtered at 20 Hz. Some differences in the extremal values can be observed.

The filtered data show contact forces in the range of 34.93N to 92.84 N, compared to the unfiltered data where the range is 3.52N to 185.5N for the contact forces measured with $f_s = 1400N$. The location of the maximum of the measured contact forces also differ. For the unfiltered case the maximum values are measured by Dr_4 in each span, when $f_s = 1400N$, while in the filtered case the maximum values measured between Dr_2 and Dr_3. The filtered response include the discontinuity effect of the dropper. However, the effect of the slacking of the dropper is not observed.

Another important result that can be interpreted from the plot in Figure 46, is that there is a difference between the contact forces measured with $f_s = 20Hz$, and those measured with f_s and filtered down to 20 Hz. Both the extremal values, and the location of the extremal values rapidly change when the data is filtered at 20 Hz. The location of the extremal values will be studied in detail in chapter 6.1.5 and chapter 6.1.6.

6.1.5 Maximum Positions

The location of the maximum values in the span is important indications to help identify critical areas. As presented in the chapters 6.1.1, 6.1.4 and 6.1.3 the maximum contact forces and their location is highly dependent on f_s. Studying the location of the maximum contact forces can help identify if the simulations are able to detect the elasticity variations and discontinuities in the catenary section.

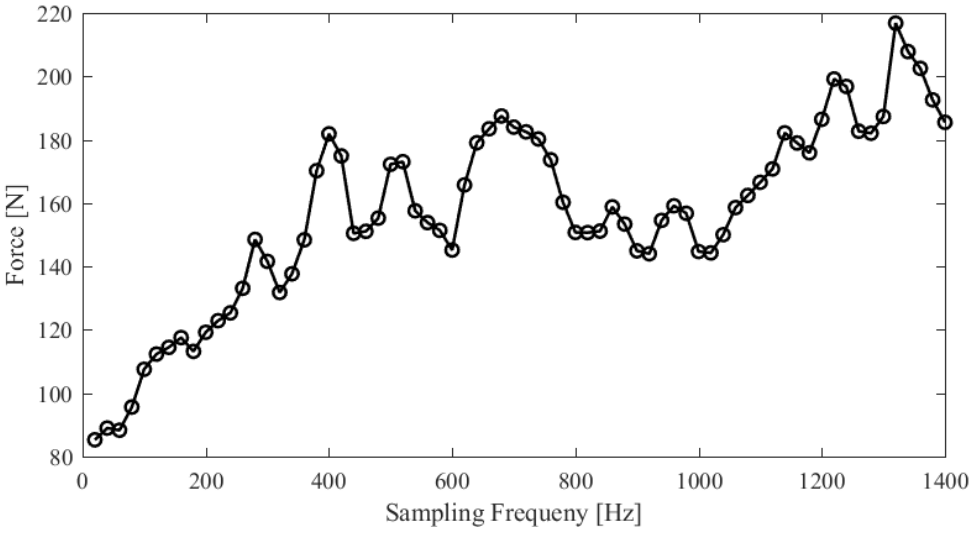

Figure 47: Maximum contact forces for $f_s \in [20Hz, 1400Hz]$

From studying the graph a nearly linear increase of the contact forces is observed up $f_s =$ 280 Hz. For sampling frequencies above 280 Hz the variations does not follow a clear pattern. Between 280 Hz and 600 Hz the variations in maximum contact forces are large. For $f_s \geq 600$ Hz, the variations are smoother. The maximum contact force from all the simulations are 219 N, and is measured with a sampling frequency of 1320 Hz. When increasing f_s over 1320 Hz, the maximum contact force decrease. With $f_s = 1400$ Hz the maximum contact force is 185 N, which is approximately the same value as with $f_s = 700$ Hz.

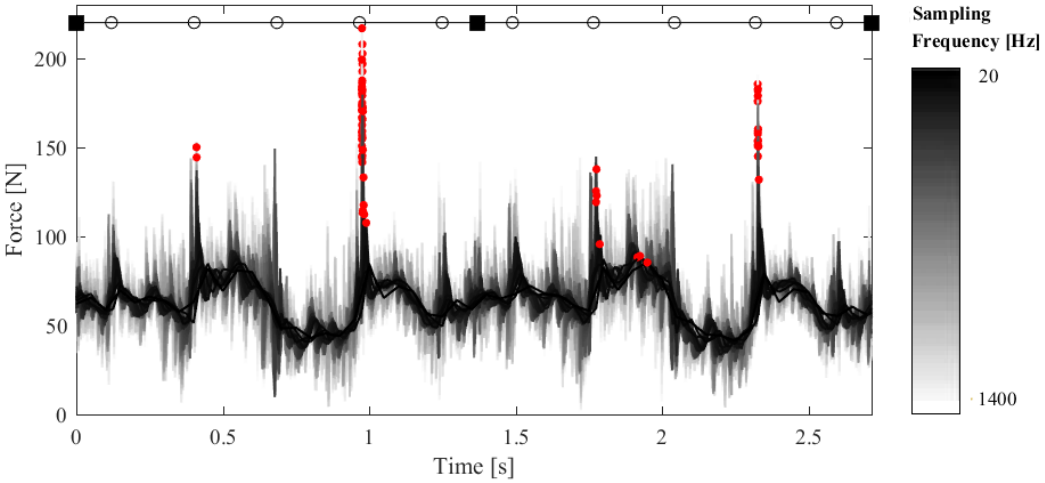

Figure 48: Contact forces for $f_s \in [20Hz, 1400Hz]$, with maximum position

In Figure 48 the time series of the contact forces for all (70) simulations are plotted, and positions where the maximum values occur are highlighted. There are five positions in the span where the maximum forces occur, by the Dr_2 and Dr_4 in each span (as expected), and in the area between the Dr_2 and Dr_3. This is for the simulations with $f_s = 20, 40$ and 60 Hz, this is also the area maximum contact forces occur when filtering according to standards, i.e. filtering the data with a cut-off frequency of 20 Hz. This was shown in Figure 6.1.4.

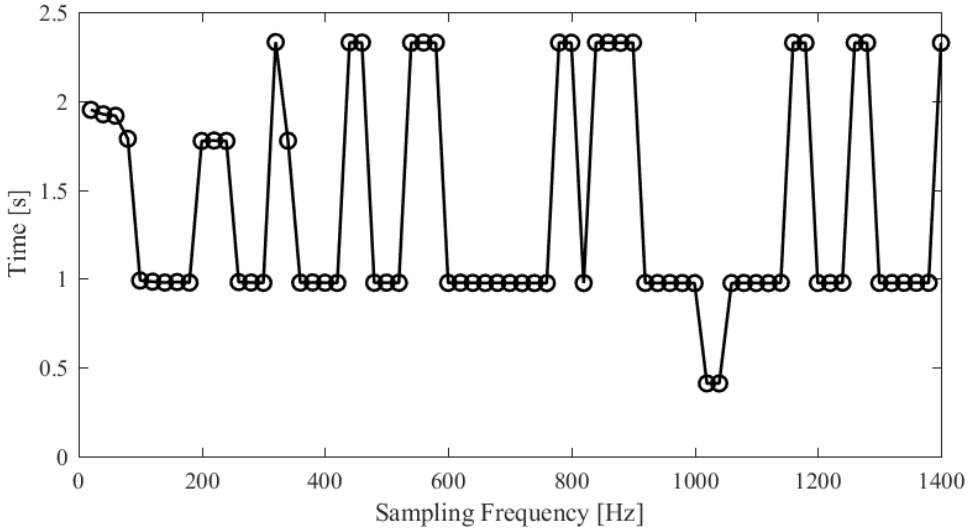

Figure 49: Maximum contact force positions for $f_s \in [20Hz, 1400Hz]$

For the simulations with f_S = 200 - 260 Hz maximum values appear by Dr_2^2. For $f_s \geq 80$ Hz, the maximum contact forces appear in the four areas that are most expected according to the elasticity in the span. 61.2 % of the maximum positions are by Dr_4^1 , 24.3% by Dr_4^2, 7.1% by is by Dr_2^2, and 2.9 is by Dr_2^1. Only 4.3 % of the maximum values appear in the area between Dr_2^2. and Dr_2^3. The majority of the maximum contact forces are measured by Dr_4^1, not Dr_4^2, this can be caused by the contact forces not having completely stabilized at this point of the simulation.

To summarize, the maximum contact forces appear by Dr_2 and Dr_4 in each span, when the simulations are done with $f_s > 80Hz$. Which is expected from the elasticity plot in the system, see Figure 37.

6.1.6 Minimum Positions

Identifying the minimum contact forces are related to the argued importance of simulating contact loss and arching in a representative manner. Figure 50 show the minimum contact forces against frequency.

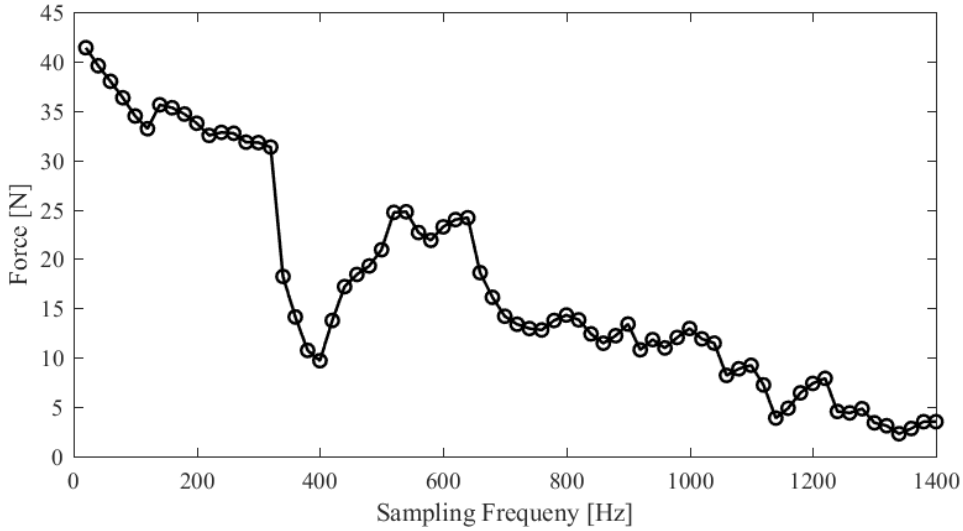

Figure 50: Maximum contact forces for $f_s \in [20Hz, 1400Hz]$

It is clear that the minimum contact forces are decreasing with increasing f_s Compared to the maximum forces plotted in Figure 47, the forces decrease in a more linear fashion, the exception is for f_s between 340 Hz and 500 Hz. Minium contact forces measured with f_s =1400 Hz is 11.43% of the minimum measured with f_{sd}. For sampling frequencies over 820 N, the minimum contact forces is under 10 N. Compared to the aerodynamic component exerted by the pantograph, which is 55 N, the contact forces are minor. In these simulations the the train speed is 120 km/h, and with an increase in this speed, contact loss could occur in the section. This need to be detected by the simulations. The location of the minimum contact forces along the span are plotted in figure 51

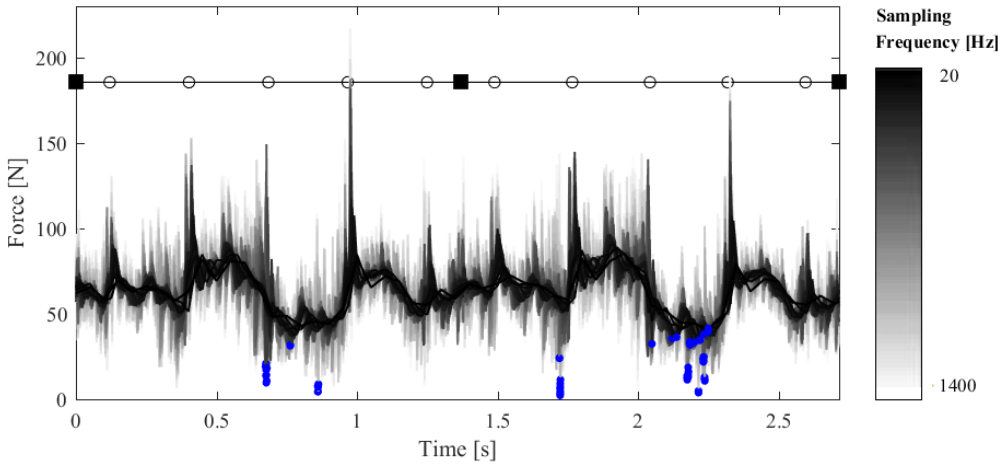

Figure 51: Contact forces for $f_s \in [20Hz, 1400Hz]$

The minimum contact forces are scattered in a more extensive manner in the span, than the maximum contact forces. Most of the minimum forces are located between Dr_3^2 and Dr_4^2. As seen elasticity plot in Figure 37, this is the section with higher elasticity. There some located in the section between Dr_3^1 and Dr_4^1. The minimum contact forces near Dr_3^1 and Dr_2^2, are located where there is a drop in the elasticity. However, this are may be caused by the slacking of the droppers, and the oscillations in the contact wire, when the pantograph is approaching the dropper. The location of the minimum forces along the span, are plotted against the sampling frequency in figure 52.

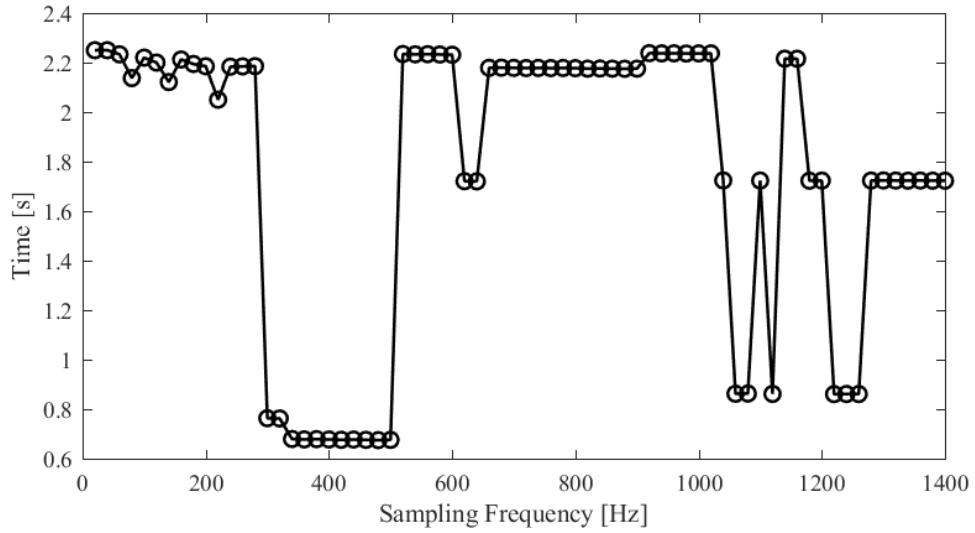

Figure 52: Minimum contact force positions for $f_s \in [20Hz, 1400Hz]$

The drop in the in the minimum contact forces in figure 50 between 340 Hz and 500 Hz are located after approximately 0.65 s in the simulations. That is around Dr_3^1, and can be caused by the variations in the elasticity, or because the simulations has not stabilized yet. The majority of the minimum contact forces are located in the area between Dr_3^2 and Dr_4^2 as already seen in 51. 57.1 % of the minimum contact forces are located in that section. While 18.6 % are located by Dr_2^2, 11.4% are located between Dr_3^1 and Dr_4^1, and 12.9% are located by Dr_3^1.

For sampling frequencies above 1260 Hz, the minimum contact forces stabilize at that position, and the change in the minimum contact forces are small. From approximately 5N at 1260 Hz to 4N at 1400 Hz. After 600 Hz, the minimum contact forces are located at three different sections. In the area between Dr_3 and Dr_4 in each span, and by Dr_2^2. It would be expected that there are small contact forces located around Dr_3 and Dr_4, when looking at the elasticity plot. However, major changes in elasticity can be observed aroundDr_2^2.

As argued in Chapter 2.4, in a catenary system the main reason for contact loss are stiffness variation, together with wave propagation.

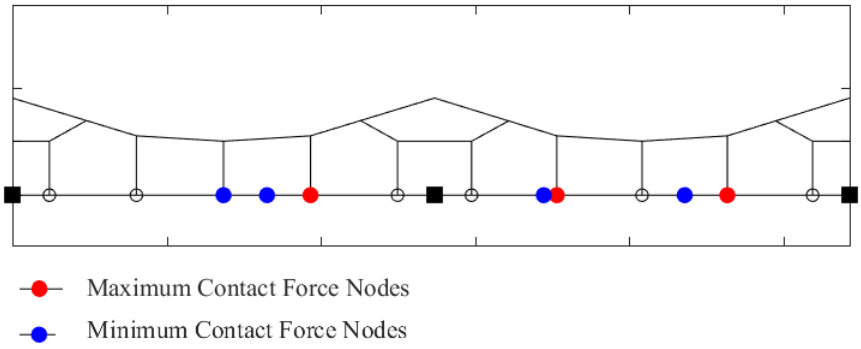

Figure 53: Critical nodes for maximum and minimum contact forces

Figure 53 summarize this Section and 6.1.5. Seven points are highlighted in the span that are critical with regard to maximum and minimum forces. Thus, these are critical points when studying wear and contact loss in a system, and are therefore of utmost importance to simulate correctly.

6.2 Contact wire

The following chapters will focus on the behavior of contact wire and the droppers in the critical points located in 6.1.5 and 6.1.6. The acceleration of the points are the main focus. The acceleration of the contact wire are closely connected to the dynamic component of the contact force, so studying this can give valuable information. In this section sampling frequencies of 200 Hz, 600 Hz, 1000 Hz and 1400 Hz will be studied. The time domain plot will be calculated, togeteher with the frequency content in form of a FFT estimate of the power spectral density.

6.2.1 Acceleration at maximum points

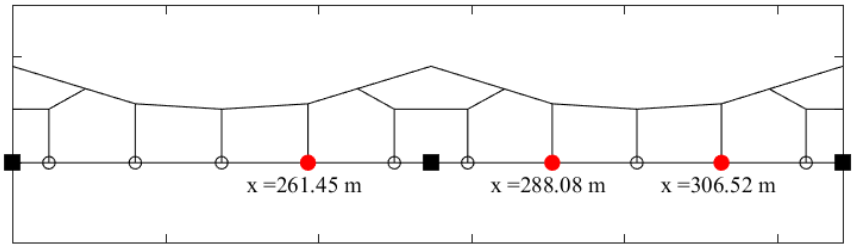

Figure 54: Points where maximum contact forces occur in the span

The point located by Dr_4^1, Figure 55 a), is the point where 7.1% of the maximum contact forces occur for the different sampling frequencies. The dotted line represent the time the mid-point of the pantograph passes the contact wire point. For the case of $f_s = 1000Hz$ and $f_s = 1400Hz$ there are oscillations that increase in amplitude when the pantograph is approaching the contact wire point. After this there is a sudden drop, that is related to the slacking of the dropper, then the tension return and there is an impulse. Figure 54 illustrate that for $f_s = 600Hz, 1000Hz$ and $1400Hz$ the response is more or less the same after the pantograph has passed. For $f_s = 200Hz$ the response only follow the mean and that there are more resemblance after the pantograph passes, than prior. Looking at the FFT plot, the frequency content is the same for all f_s up to approximately 15 Hz. The case of $f_s = 600Hz$ has the approximately the same frequency content up to 60 Hz.

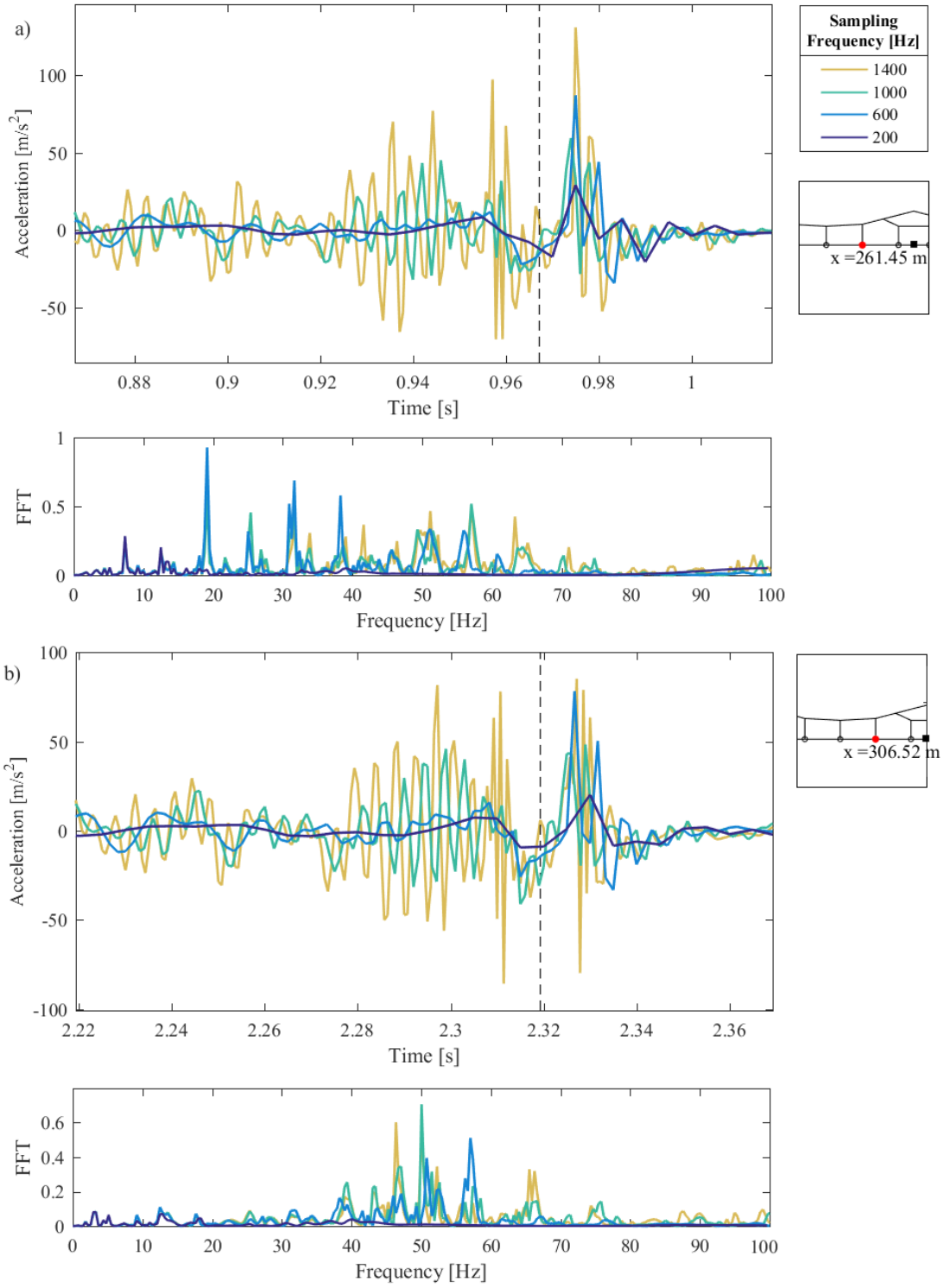

Figure 55: Critical points in the span

Looking at point Dr_4^2, Figure 55 b), where 61.2 % of the forces contact forces where located, the same effects can be seen here as for Dr_4^1, . The resemblance is better after the pantograph has passed.

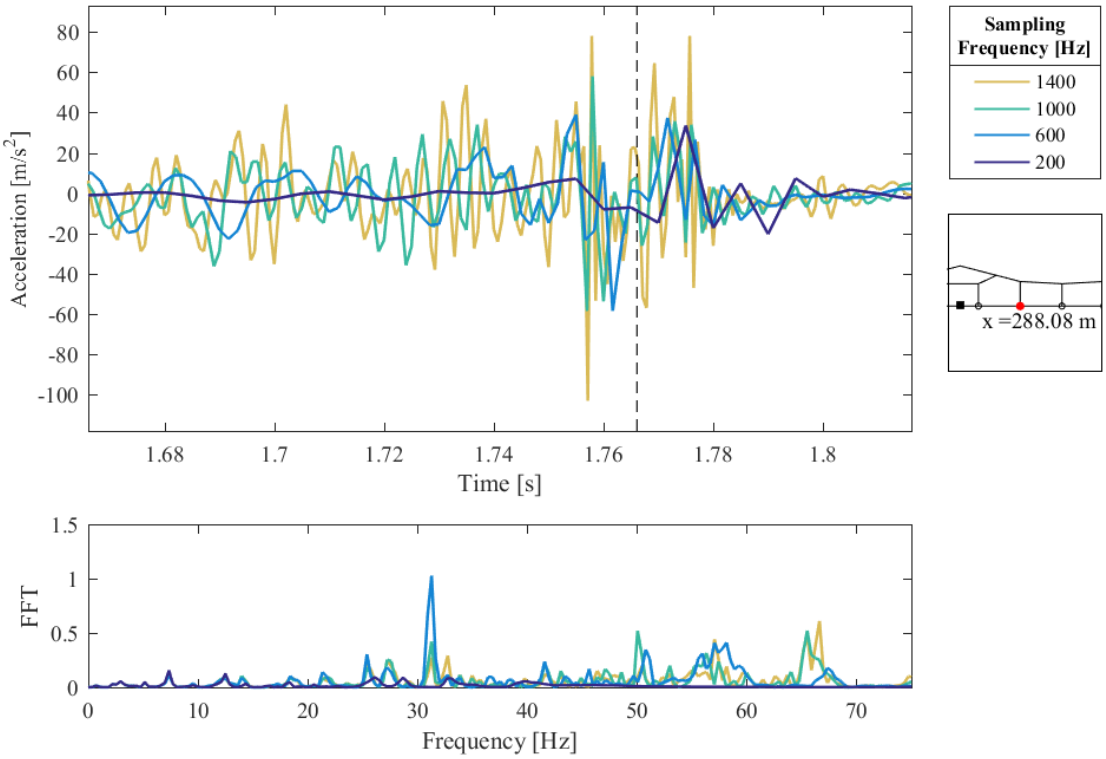

Figure 56: Critical points in the span

Looking at the contact wire point by Dr_2^2, where 24.3% of the maximum contact forces are located. The same oscillations with the increase in amplitude can be observed. Nonetheless, the simulations with $f_s = 600Hz$ better resemblance to the higher frequencies at this point. After the passage of the pantograph, the maximum values for f_{sd} are approximately the same as for higher f_s. However, prior the difference in the response is significant.

6.2.2 Acceleration at minimum points

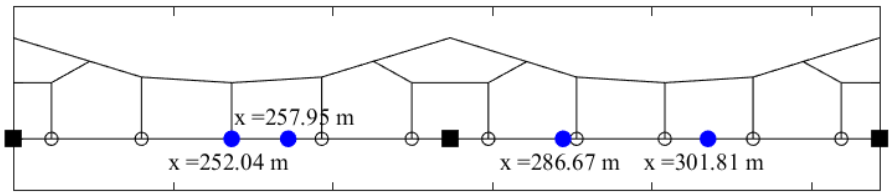

Figure 57: Critical points in the span

Figure 57 shows the critical points in the section, with regards to minimum contact forces. While four discrete points where the main location for the maximum forces, the minimum forces are located at some distinct areas between the droppers. In the area between the third and fourth dropper at each span, the minimum contact force points are located. Firstly, the point where the contact wire node is connected to a dropper ($x = 252.04m$) will be investigated. Secondly the points in section Dr_3 and Dr_4, ($x = 257.95$ and $x = 301.81$) will be studied. Lastly, the point located near Dr_2^1 (($x = 286,67m$) will be discussed.

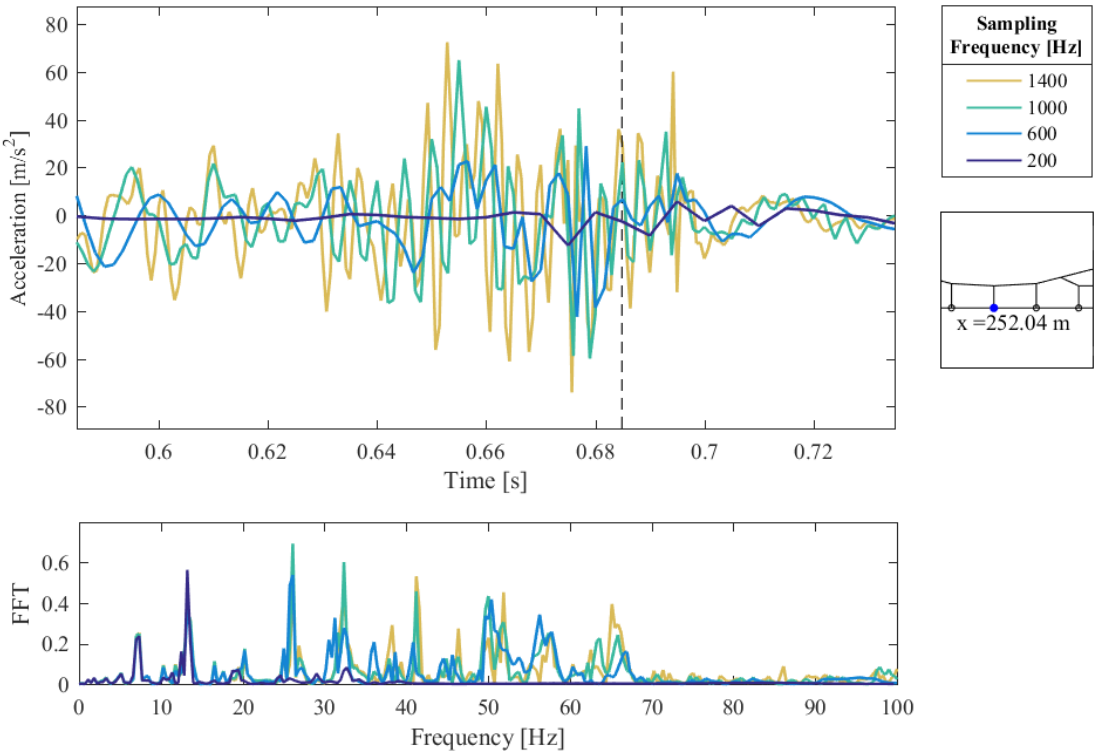

Figure 58: Critical points in the span

12.9% of the minimum contact forces measured by Dr_3^1. At this section, many of the major effects

that occurred at the points of maximum contact force, discussed in 6.2.1, can be observed. There are oscillations in the wire when the pantograph is approaching the dropper. The clear peaks before and after the pantograph has passed the point is not present in this plot. It can be seen from 38, that there are a clear decrease in the contact forces for all four sampling frequencies when the pantograph is passing that dropper, and the forces are approximately 55 N. Looks like the dropper damps the motion, does not observe any slacking of the dropper. The behavior of this dropper will be discussed in chapter **??**. The FFT show resemblance to the FFT for the Dr_4^1, which is the neighbor dropper, put the power is less.

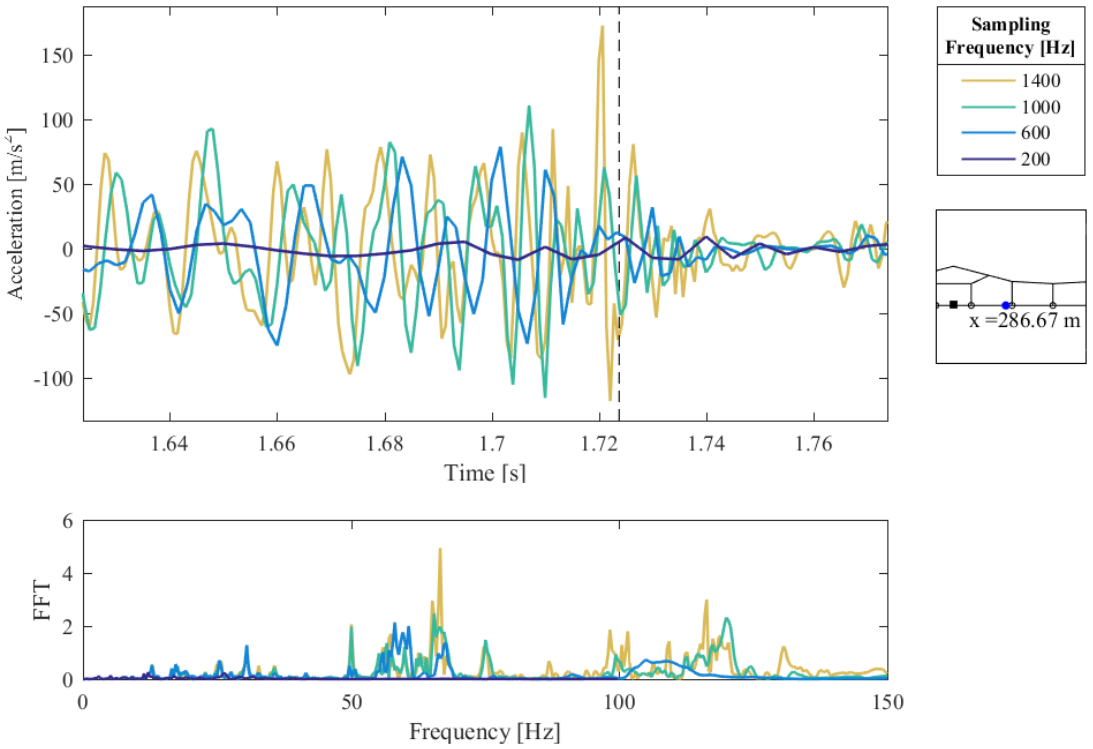

Figure 59: Critical points in the span

18.6 % of the minimum contact forces are located by Dr_2^2, the acceleration oscillates with high amplitudes, seemingly and the frequency does seemingly increase when the pantograph is approaching the point. The movement of the contact wire are similar for simulations with $f_s \geq 600Hz$ when the pantograph is further away from the point. During the passage there are larger differences. Then simulations with $f_s = 600Hz$ produces results more similar with $f_s = 200$. After the pantograph has passed the results are approximately the same in all the simulations.

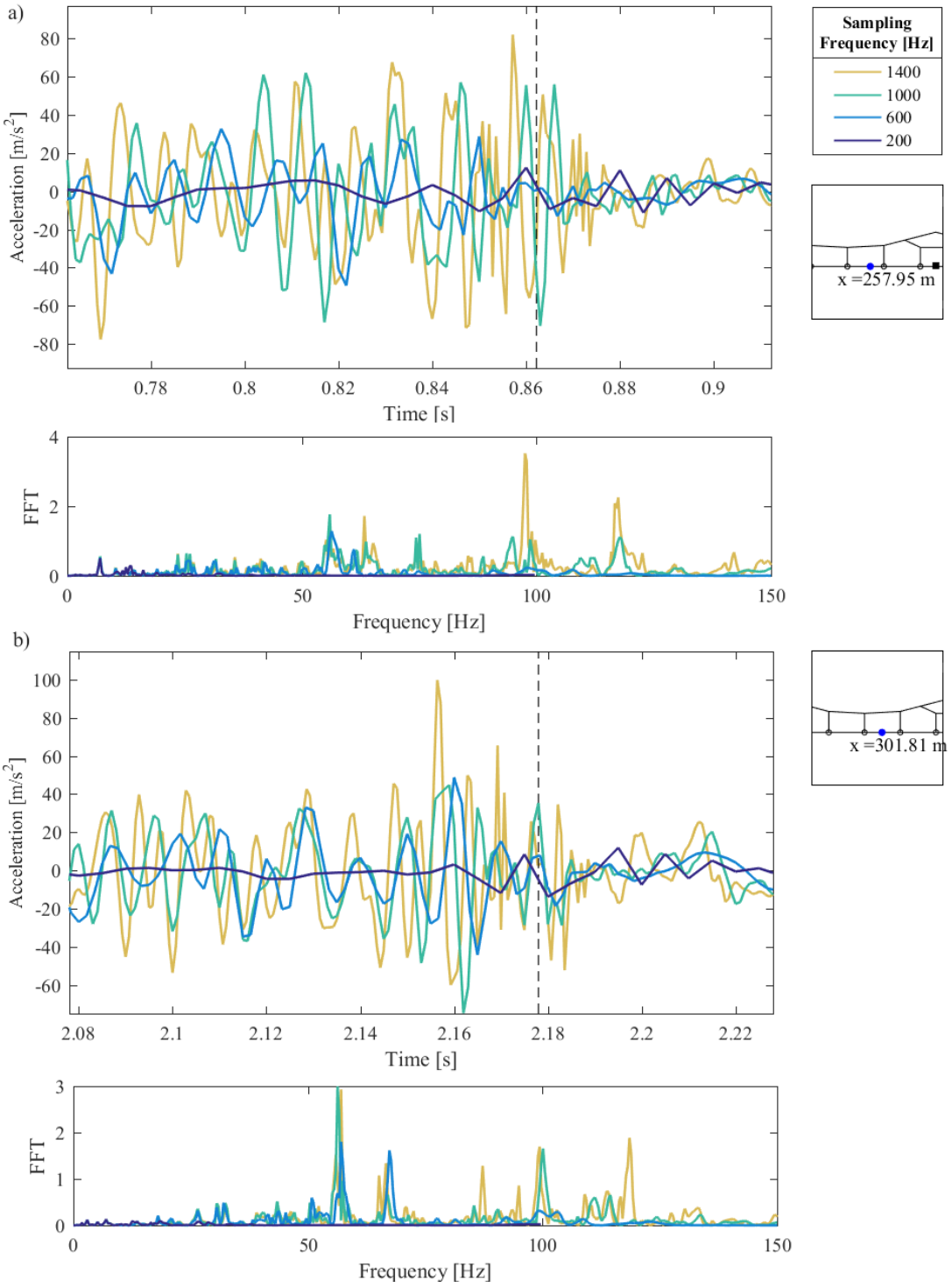

Figure 60: Critical points in the span

11.4% of the minimum contact forces are located between Dr_3^1 and Dr_4^1, Figure 60 a). The same effect of the increase in the amplitudes when the pantograph is approaching are present, but the amplitudes are higher long before the passage. The frequency content are high. A peak for 100 Hz, for $f_s = 1400Hz$. The oscillations are damped after the dropper has passed. 38 show that the mean contact forces are low, under 50 N in this area. There might be a small period of slacking that is detected for $f_s = 1400$ and $1000Hz$. Nothing is measured for the $f_s = 200Hz$ and $600Hz$.

57 % of the minimum contact forces are located in the section between Dr_3^2 and Dr_4^2, Figure 60 b). The error between the simulations results for $f_s \geq 600Hz$ are smaller here than in for $x = 257.95Hz$, between Dr_3^1 and Dr_4^1. This is further away from the simulation start point, Which can be the cause better resemblance. There is a clearer increase in the amplitude of the oscillations when the pantograph is approaching the point, for $f_s \geq 600Hz$, and there is a sudden drop after the pantograph has passed. Amplification of reflected waves. When the pantograph is moving towards an transverse wave, the amplitude of the wave can increase!

6.3 Dropper

In this section the the droppers connected to the critical points in the contact wire identified in chapter **??** will be analysed. How the dropper affects the movement of the contact wire is evaluated, furthermore if the passage of a pantograph results in slacking of the dropper. Both y and z direction are analyzed. The movement of the dropper in the z direction is important to study considering the slacking of the dropper, due to the fact that slacking of the dropper leads to deflection in the in-plane direction. The mid-point of the dropper is evaluated. Firstly the acceleration will studied, then the deflection.

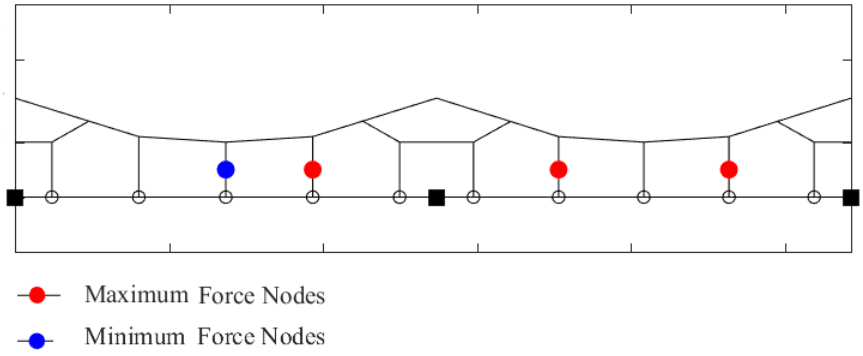

Figure 61: Droppers connected to critical points in the contact wire.

6.3.1 Acceleration

The acceleration of the mid-point of the outlined droppers are presented in this section. Firstly, the dropper exposed to lower contact forces is evaluated. Secondly, the droppers exposed to high contact forces are analysed. The time response and the frequency content are presented in the same plot. The results are from simulations with $f_s = 200Hz, 600Hz, 1000Hz$ and $1400Hz$.

Figure 62 shows the acceleration in Dr_3^1 from the simulations done with different sampling frequencies. The forces exerted on this dropper are close to the static component of the pantograph, $F_{static} = 55N$. The results from the simulations with f_{sd} differ from the results with $f_s \geq 600Hz$, for accelerations both in z and y directions.

The acceleration in z direction will be discussed first. Simulations with $f_s \geq 600Hz$ show oscillations in the dropper that the simulations with f_{sd} do not detect. The FFT plot show that the frequency content is the same up to 20 Hz. However, for frequencies over 20 Hz the difference between the results from simulation f_{sd} and the results from $f_s \geq 600Hz$ are enormous. Considering the results for $f_s \geq 600Hz$, both the time domain and the frequency domain plot show that the result with $f_s = 600Hz$ provide results that close to the results with $f_s = 1400Hz$. The acceleration increases when the pantograph is approaching the dropper, and decreases under the passage of the pantograph. There is no slacking of the dropper since the contact forces are too low. In the z direction, the results are nearly identical for the simulations with $f_s \geq 600Hz$,

both in the time ans frequency domain. The results from f_{sd} show that the acceleration in z direction increases with time after the pantograph has passed.

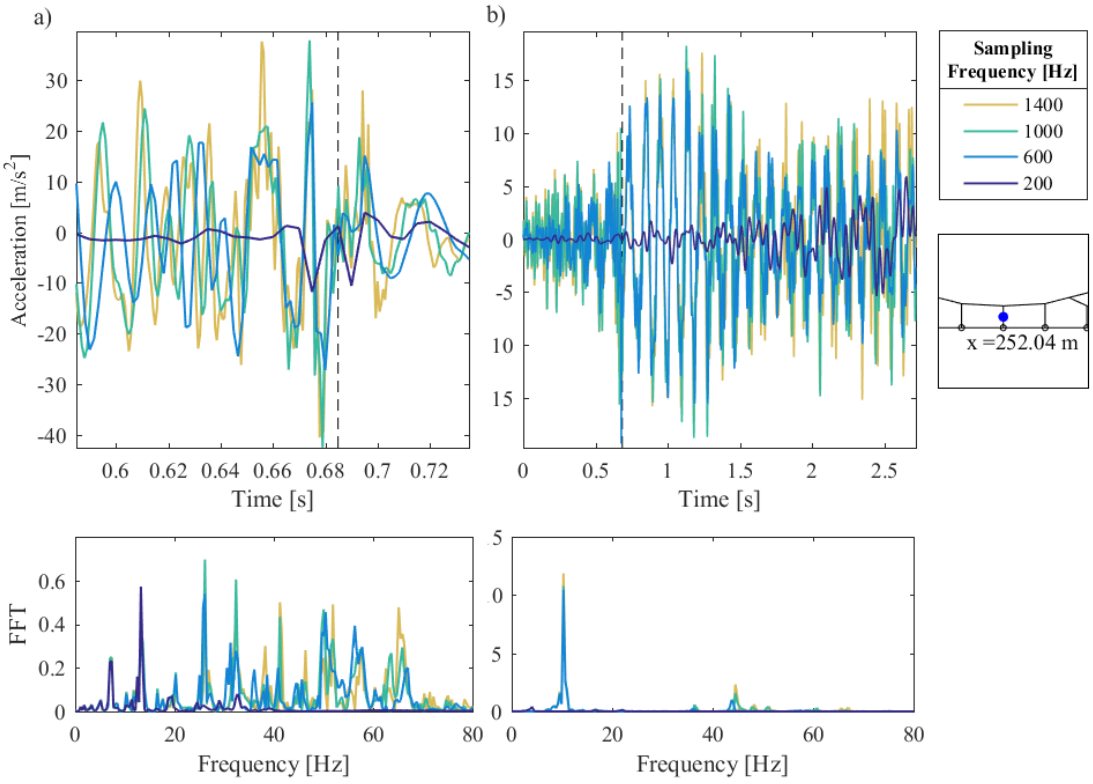

Figure 62: Acceleration of the mid point of Dr_3^1, located at $x = 252.04$ in the span. a) shows the y component and b) the y component

Figure 63 shows the result from the simulation for Dr_4^1 and Dr_4^2. These droppers experience the highest contact forces, and the results show that the force is high enough to generate a slacking of the dropper. The result from all the simulations are able to show the effect of the slacking on the dropper. However, the size of the response vary. The results from the simulations with $f_s = 600Hz$ and $f_s = 1000Hz$ are nearly identical. The FFT plot show that the frequency content is the same for the results up to 20 Hz, the same as observed for Dr_3^1. The frequency content is higher for Dr_4^2 than for Dr_4^1.

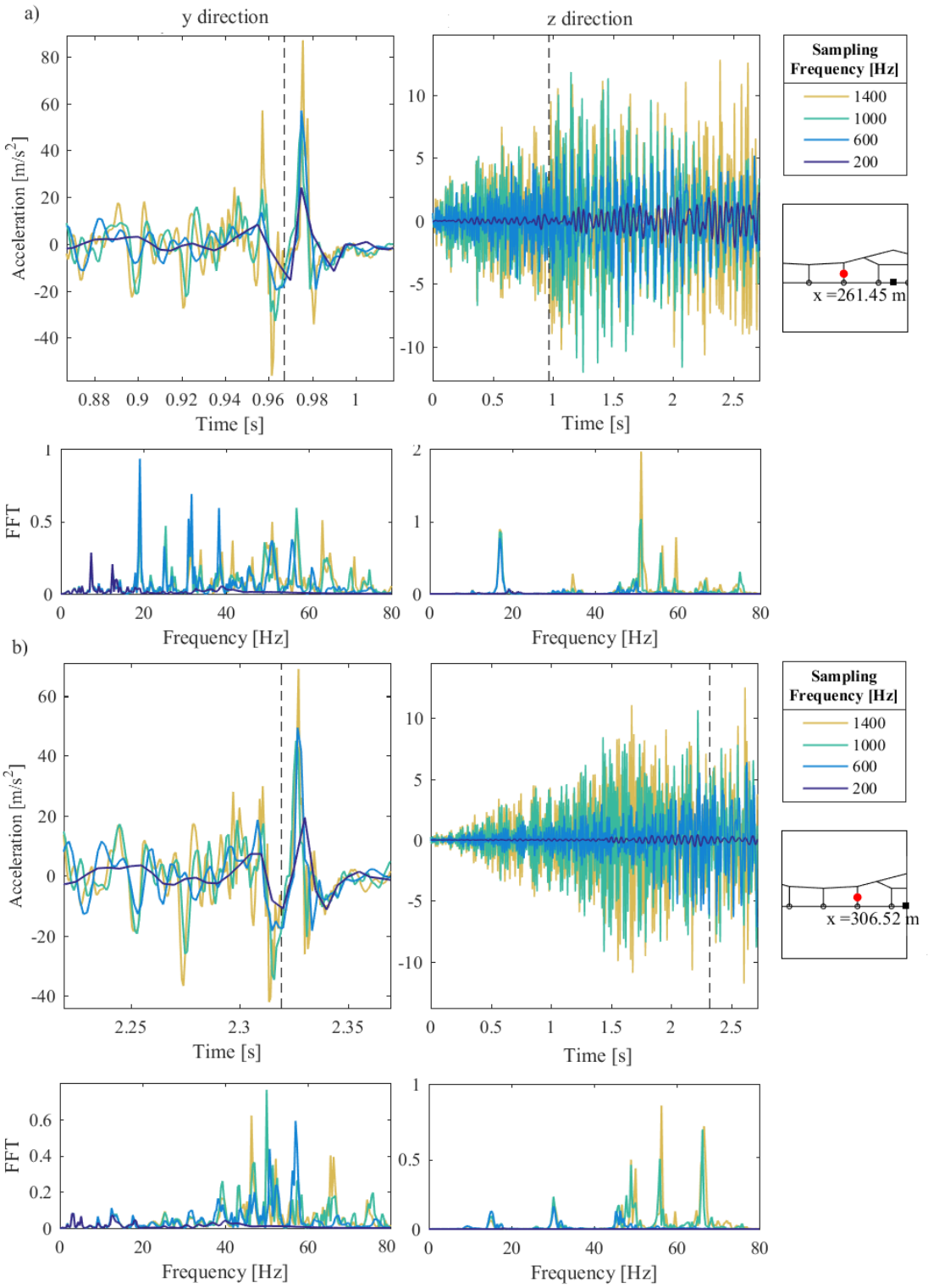

Figure 63: Acceleration of the mid point of Dr_4^1 and Dr_4^2, located at $x = 261.45$ and $x = 306.52$ in the span. a) shows the result for Dr_4^1 and b) for Dr_4^2

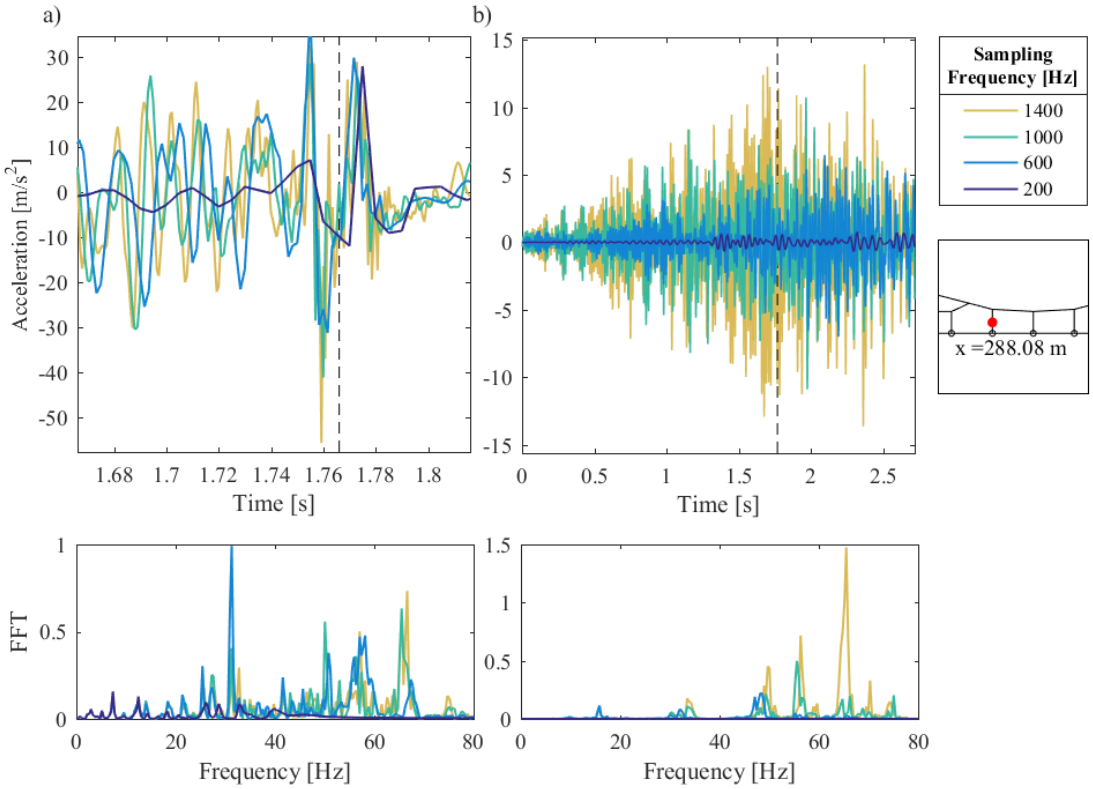

Figure 64: Acceleration of mid point of Dr_2^2, located at $x = 288.08$ in the span. a) shows the y component and b) the y component

It can be seen from the results for Dr_2^2 show that the simulation with f_{sd} the acceleration produced with higher f_s. The resemblance is higher prior the passage of the pantograph than after. The oscillations in the dropper when the pantograph is approaching the dropper is not detected by the simulations with f_{sd}. However, the simulations produce equal accelerations after the passage of the pantograph. The difference in the result from the simulations for Dr_2^2, are small compared to the result for Dr_4^1 and Dr_4^2.

To summarize, the frequency content for the results in the y direction from simulations with f_{sd} are equal to the other results up to 20 Hz. However, the results from the simulations with higher f_s suggest that there are frequencies over 20 Hz that are important for the response of the system, according to EN50318. The variations in acceleration is greater in the dropper that experiences lower contact forces, than in the dropper where the pantograph exerts high forces. The simulations with f_{sd}, are able to produce results that follow the trend of the movement of the dropper in the dropper with high forces. In the dropper that experience a contact force equal to F_s, the results from simulation with f_{sd} are not able to produce results that agree with the movement of the dropper from the simulations with $f_s \geq 600Hz$. The acceleration simulated with $f_s = 600Hz$ compare well with results with higher frequencies.

6.3.2 Deflection

In this section the deflection of the dropper in z and y direction is suited. Firstly, the deflection of dropper that experiences lowest contact forces, Dr_3^1. Secondly, the deflection of the dropper experiences that experiences highest forces , Dr_4^1 and Dr_4^2, are examined. Lastly, the deflection of Dr_{22}, that also is exposed to high contact forces. The motivation for studying the deflection of the dropper, is to show how the dropper movement is effected by the passing of the pantograph. Furthermore, decide whether the dropper is effected by the uplift of the contact wire in the section around the dropper.

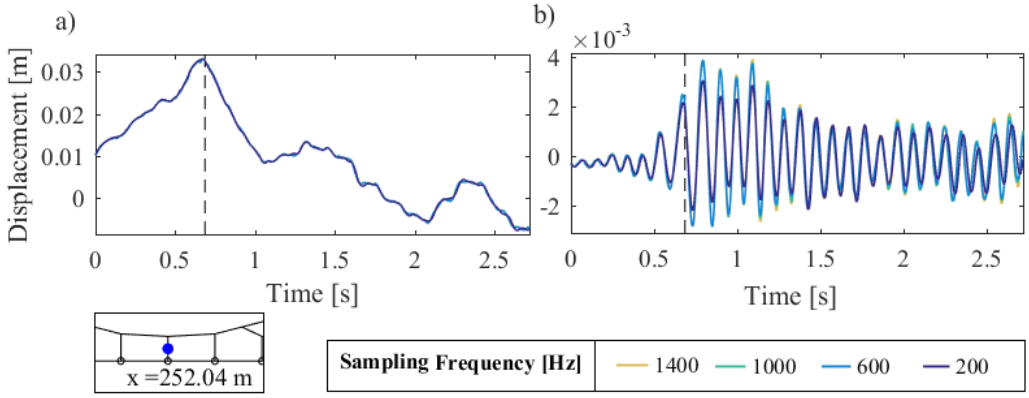

Figure 65: Deflection of the mid point of Dr_3^1, located at x = 252.04m along the catenary section. a) deflection in y direction, and b) deflection in z direction

Figure 65 a) illustrates that the dropper is lifted in y direction when the pantograph is passing the dropper. The maximum uplift of the dropper appear during the passage. Smaller increase in the uplift appear after the pantograph has passed, this is probably caused by the wave propagation in the wire. A larger uplift in the dropper occur after approximately 2.4 s in the simulations, which can be caused by the high contact wire uplift further down in the the span. The dropper oscillated in the z direction with a constant frequency, which can be recognized from 6.3.1 as one of the eigenfrequencies of the system. Figure 65 illustrate that the deflection is nearly identical in the simulations with different f_s.

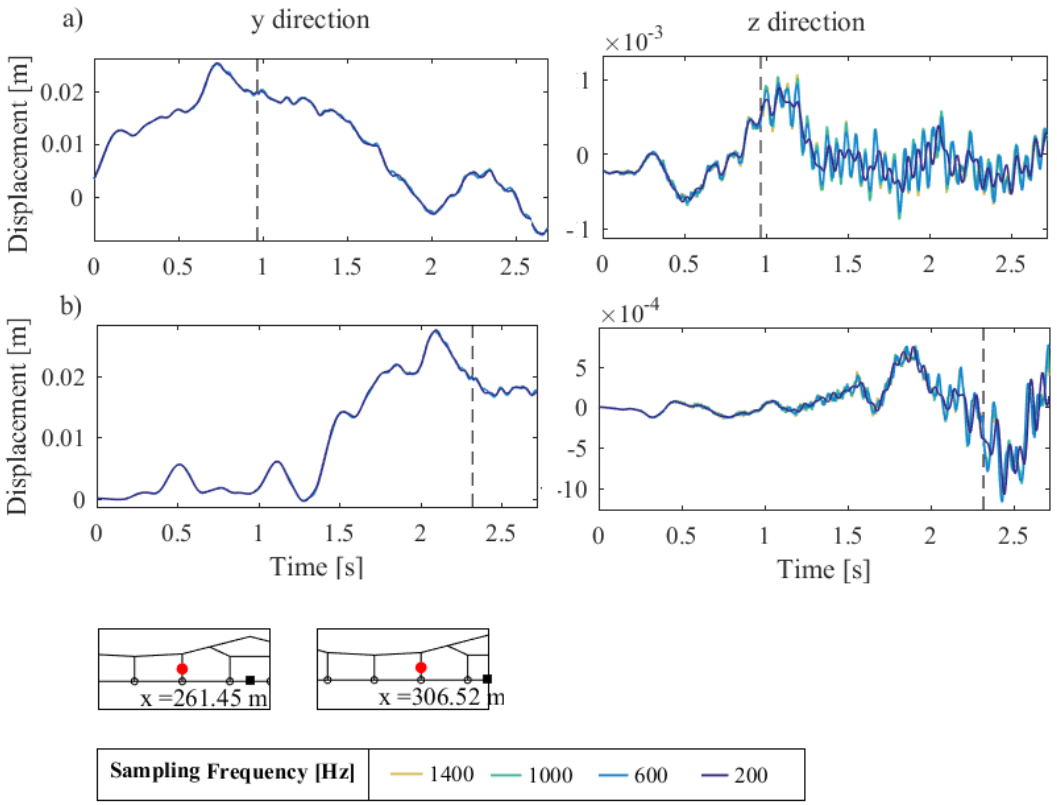

Figure 66: Deflection of the mid point of a) Dr_4^1 and b) Dr_4^2, located at x = 261.45m and x = 306.52m along the catenary section

Figure 66 show that the maximum uplift of Dr_4^1 and Dr_4^2, appear before the pantograph has passed the dropper. This is caused by the high contact wire uplift at the mid point between Dr_3 and Dr_4 in each span, where elasticity of the catenary system is highest. The passage of the pantograph only cause a small uplift in the dropper. The deflection of the dropper in z direction is affected by the movement of the wire, prior to the passage of the pantograph. The response in the z direction Dr_4^1 and Dr_4^2 are more dependent on f_s, then the response for Dr_2^2. The simulations with f_{sd} do not show as high response in z direction as the simulations done with $f_s > f_{sd}$.

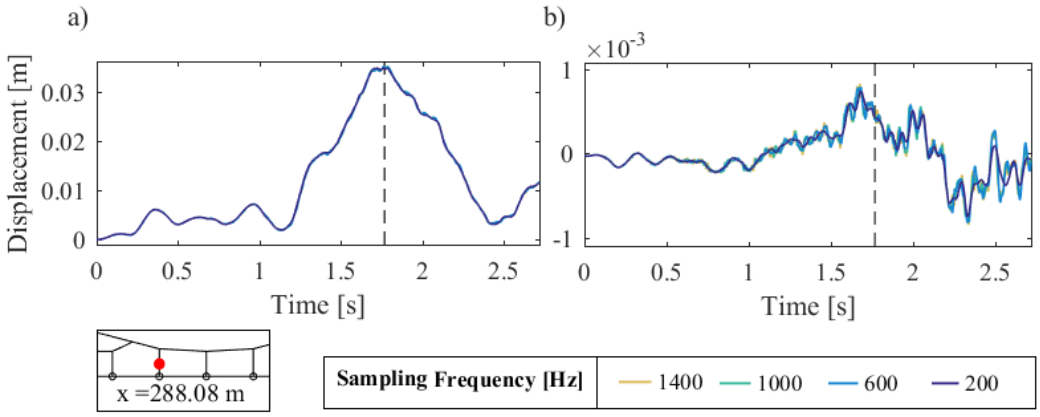

Figure 67: Deflection of the mid point of Dr_2^2, located at x = 288.08 m along the catenary section. a) deflection in y direction, and b) deflection in z direction

From figure 67 it is observed that the highest uplift of the midpoint is when the pantograph is passing the Dr_2^2. The simulations with f_{sd} produces responses in the z direction that correspond more with the results from the other simulations, at this dropper than at Dr_4 in each span.

The high contact forces measured at Dr_4 and Dr_2 in both of the spans, is related to the sudden decrease in the elasticity in the catenary. Looking at the deflection of the dropper Dr_4 in each span, it can be observed that the highest uplift in the dropper appear prior the passage of the pantograph. This uplift appear at the point when the pantograph interacts with the contact wire where the maximum elasticity of the span is located. Thus, the deflection of the contact wire is decreasing when the pantograph is passing the dropper. The difference in the simulated response in z direction is higher in the dropper that experience larger contact forces.

6.4 Cut-Off Frequency

In this section the effects of filtering the result (with cut-off frequencies 80 Hz to 200 Hz) from the simulations will be demonstrated. Firstly, the effect of phase delay of the Chebyshev filter will be illustrated, and how it is compensated for. Secondly, the statistical values of the filtered response will be reviewed. Lastly, the filtered time response of the sampled contact forces will be plotted with two different cut off frequencies.

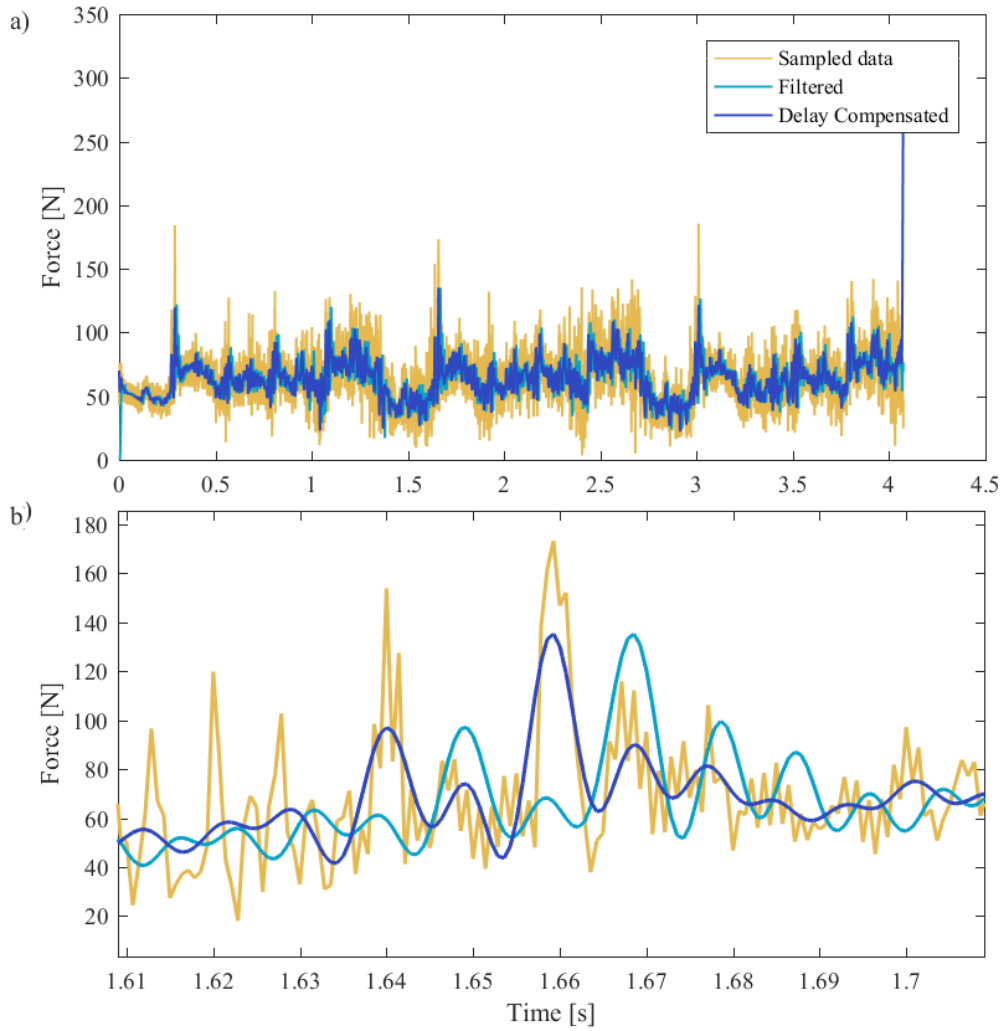

Figure 68: Contact force measured with sampling frequency of 1400 Hz, filtered with a Low Pass Chebyshev filter with Cut-Off frequency 120 Hz. a) the whole simulation section, b) the section around Dr_4^1

Figure 68 point to the fact that filtered response is delayed, this is compensated for by using the built in Matlab function filtfilt, [18]. The small peaks in the contact force is filtered out, causing an approximated decrease of 15N in the maximum contact force in Figure 68 b).

It is valuable to investigate how the filtering of the response is affecting statistical values. The same statistical values as in Chapter 6.1.3 will be calculated. Starting with the mean contact force.

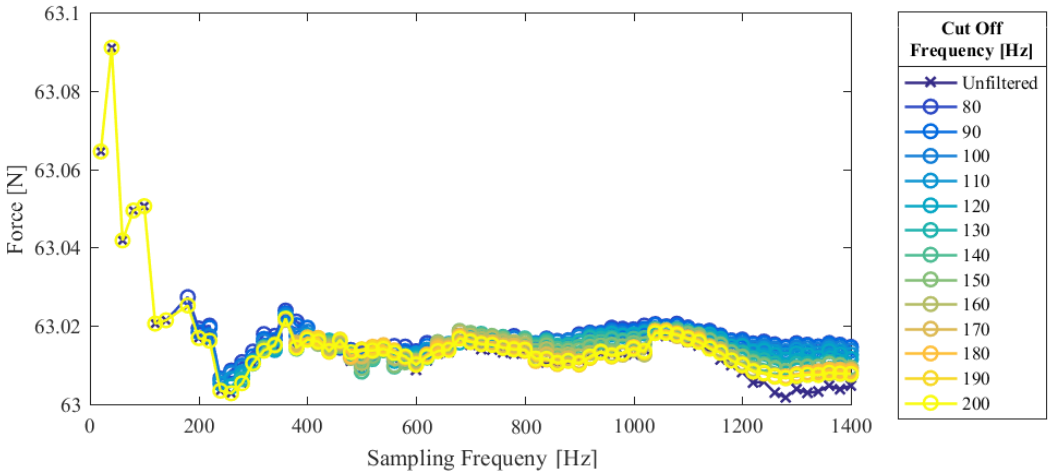

Figure 69: The mean value of the filtered and unfiltered contact forces

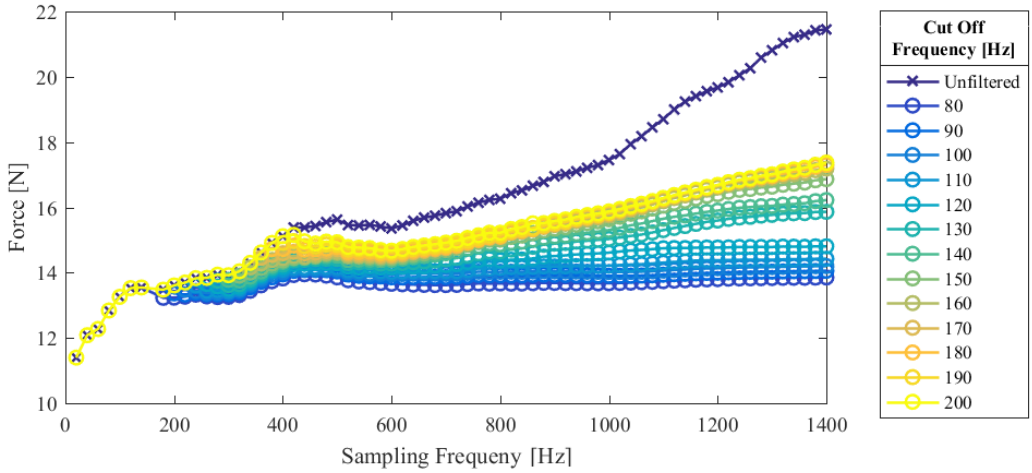

Figure 70: The standard deviation of the filtered and unfiltered contact forces

Figure 69 show that the mean value of the contact forces are not effected by the filtering frequency. This illustrate again, that if the mean response of the system is of interest, that simulations with sampling frequency as low as 20 Hz are able to produce an acceptable results.

The standard deviation of the contact force is highly dependent on which f_s used in the simulations. The unfiltered standard deviation of the calculated contact force increase approximately

linear with the increase in f_s. By looking at the data filtered with 80 Hz first. Some changes in the standard deviation can be observed up to $f_s = 600$ Hz. However, the standard deviation of the sampled contact force from simulations with $f_s > 600$ Hz is constant when the cut off frequency is 80 Hz. This can also be observed for cut off frequencies up to 120 Hz. In other words, when filtering the response with cut-off frequencies from 80 Hz to 120 Hz, there point of using f_s over 600 Hz. When the cut off frequency is over 120 Hz, the standard deviation of the sampled data increase with f_s.

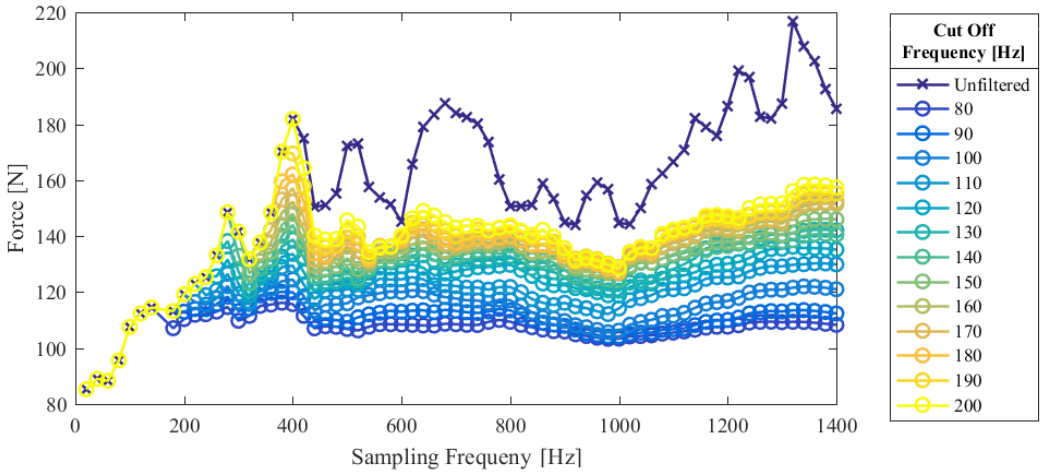

Figure 71: The maximum value of the filtered and unfiltered contact force

The maximum contact force is highly dependent of the sampling frequency. When the sampled data is filtered in the range 80 Hz to 200 Hz, it highly impacts the maximum contact force. When simulating with $f_s > 600$ Hz the contact forces from the simulations with the is more constant or less, and the maximum for these simulations are approximately 160 N. Thus, with regards to maximum contact forces, there is little to gain in accuracy by increase f_s above 600 Hz if the da is filtered in from 80 to 200 Hz. When filtering the data with cut-off frequency between 80 Hz and 90 Hz, the effect of increasing f_s in the simulation is almost gone.

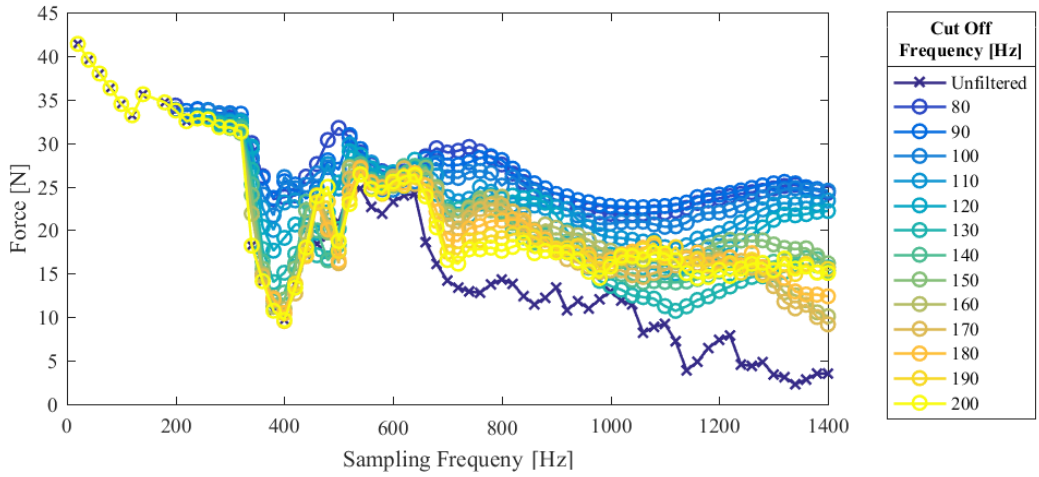

Figure 72: The minimum value of the filtered and unfiltered contact forces

For the data filtered with a cut off frequency under 120 Hz, the minimum is nearly constant when the data is sampled with $f_d > 1000$ Hz. Figure 72 suggests that the minimum contact force converges to roughly 23 N, when the cut-off frequency is under 120N. For cut-off frequencies over 120 Hz, the minimum contact force continue to decrease with the increase in sampling frequency.

To summarize, standard deviation,the maximum, and the minimum contact force simulated with f_d is highly dependent on the cut-off frequency. When filtering the data with a cut-off frequency at 80 Hz, increasing the sampling frequency over 600 Hz will not effect statistical values of the result. For the maximum and the standard deviation of the contact force, there is no difference when $f_d > 400$ Hz for the data filtered at 80 Hz. The cut-off frequency must be 120 Hz for the data to be noticeably effected by an increase of the sampling frequency. The effect of filtering with $f_s = 80$ Hz is extensively discussed by Naavik. ' Based on findings in the statistical data discussed in this section and the frequency content from the result from the simulations, it is interesting to review data filtered at 100 Hz and 140 Hz. By investigating filtered time series of the contact forces with a cut-off frequency at both 100 Hz and 140 Hz, the effects that is filtered out using 100 Hz can be identified, by comparing with the result using 140 Hz.

In the rest of this section the filtered time series of the contact forces will be presented. The contact force is filtered with cut-off frequency 100 Hz, and 140 Hz. Try to identified the the effect of the response that is filtered out with 100 Hz, that is included when filtered at 140 Hz. The time series of the contact force sampled with $f_d = 200$ Hz, 600 Hz, 1000 Hz, and 1400 Hz will be studied. For simulations with f_{sd}, a cut-off frequency of 140 Hz is too high (above Nyquist).

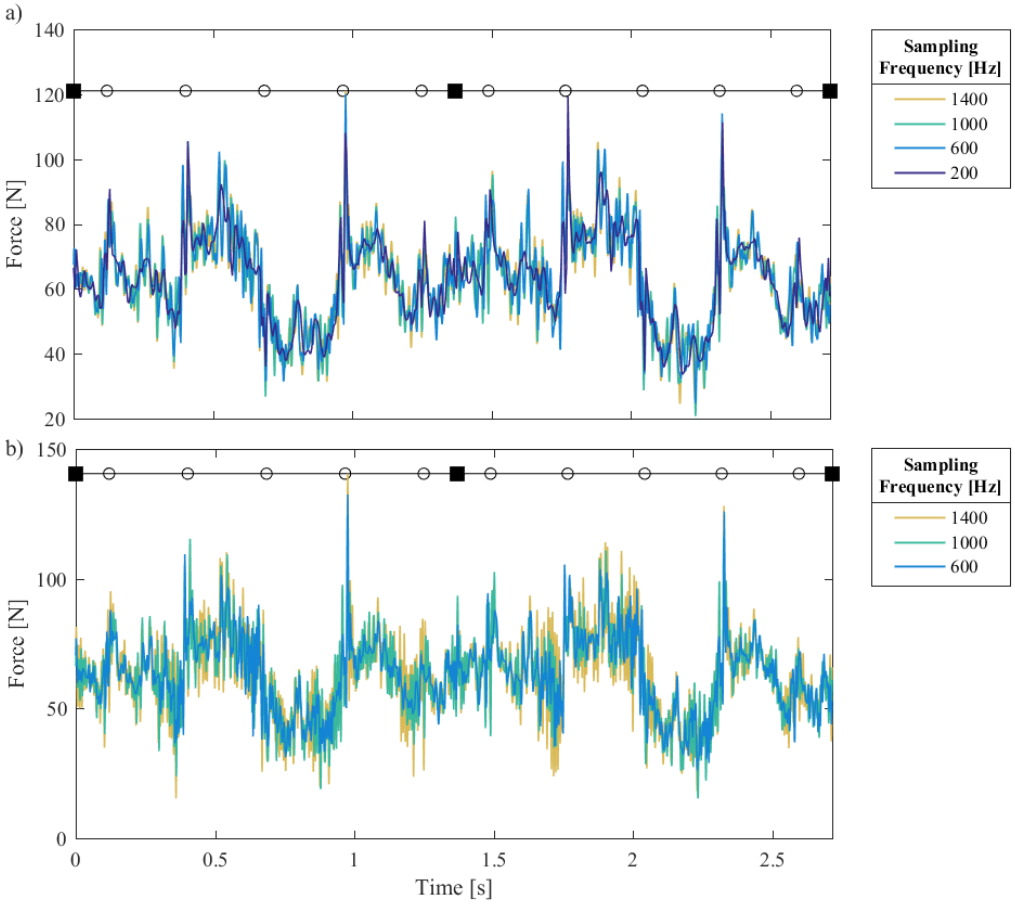

Figure 73: Contact force filtered with cut-off frequency a) 100 Hz, and b) 140 Hz. The response is plotted for the total analytical area.

The first thing to observe from 73 is that the magnitude of the contact force is smaller when the cut-off frequency is 100 Hz. Off course, the overall response is smother when the data is filtered at 100 Hz. For the contact forces sampled by Dr_2^2, high variations can be observed when the cut-off frequency is increased to 140 Hz. These variations are evident when observing the contact force at critical locations in the span.

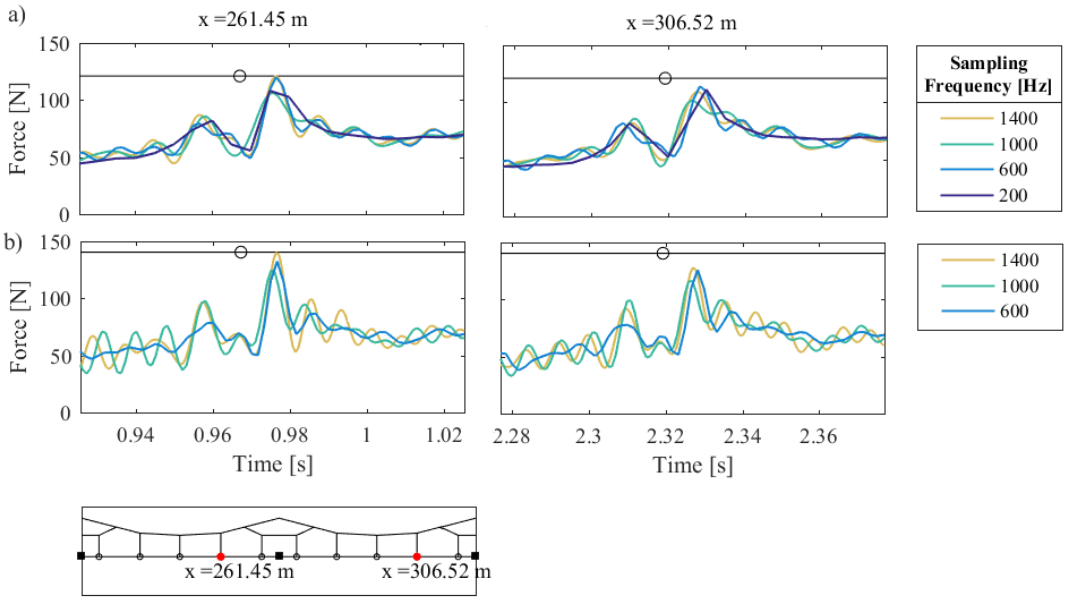

Figure 74: Contact force filtered with cut-off frequency a) 100 Hz, and b) 140 Hz. Plotted for the section around Dr_4^1 at x = 261.45 m , and Dr_4^2 at x = 306.52 m

In Figure 74 the contact forces sampled around Dr_4^1 and Dr_4^2 are illustrated. The figure demonstrates that the difference in the response increase when the sampling frequency increase. When the cut-off frequency is 100 Hz, the difference in the simulated result are negligible if $f_s \geq 600$ Hz.

When the cut-off frequency is increased to 140 Hz, the difference in the contact force from $f_s = 600$ Hz and $f_s >$600 Hz increases. However, the maximum contact force is the section same for all f_s.

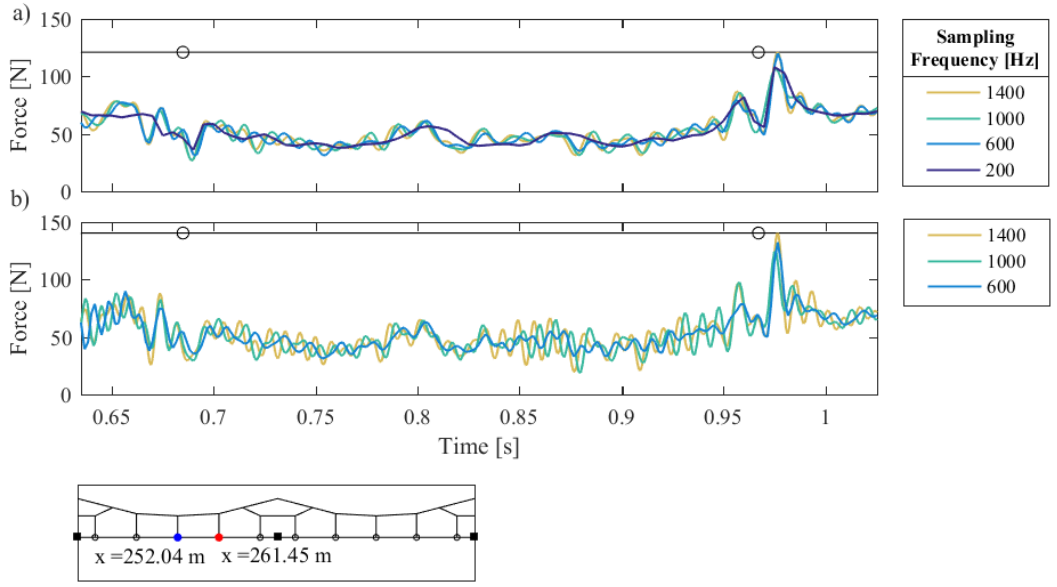

Figure 75: Contact force filtered with cut-off frequency a) 100 Hz, and b) 140 Hz. Plotted for the section between Dr_3^1 Dr_4^1

In figure 75 the contact force measured in sections with lowest contact forces are displayed. Also for this section it can be concluded that, when the results are filtered with 100 Hz, the benefits of increasing f_s are negligible. However when it is filtered with 140 Hz, the difference in the results from the simulations with $f_s \geq 600$Hz is obvious.

In conclusion, when filtering the data at 100 Hz, as suggested in by Collina [9], the benefits of increasing the sampling frequency above 600 Hz is negligible. However, when increasing the frequency range of interest to 140 Hz the effect of increasing the sampling frequency is substantial.

6.5 Computational cost

The aim for this section is to see how the increase in sampling frequency effect the computational cost.

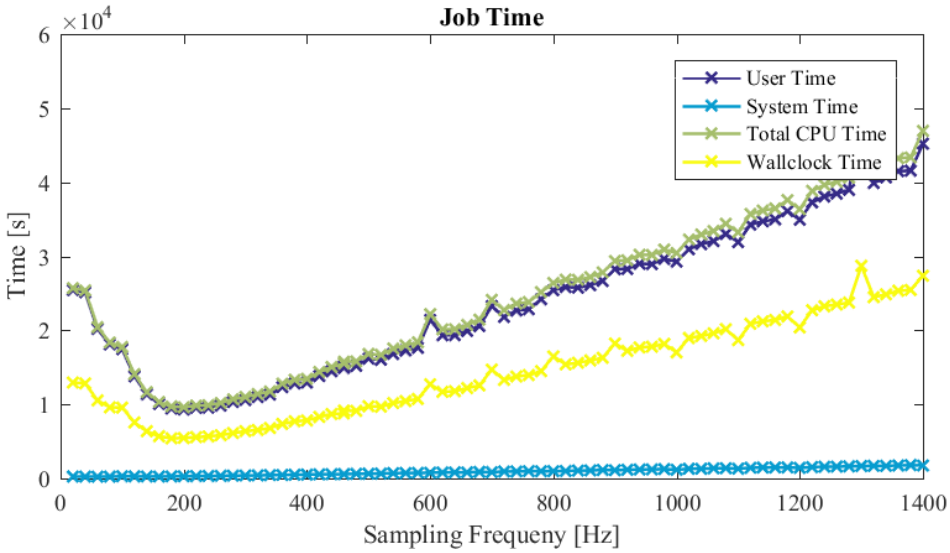

Figure 76: The simulation time for the simulaitons

The wall-clock time for the for the simulation done with a sampling frequency of 200 Hz is only 19.95% of the the wall-clock time for the simulation done with a sampling frequency of 1400 Hz. The increase in computational time is approximately linear, with the increase in sampling frequency.

The simulations are done with some time apart, and the irregularities are probably from small changes in the output written to the odb file in Abaqus. The number of output variables were the same.

The wall-clock time for 600 Hz can be estimated by the middle value of the sum of the wall-clock time for 580 Hz and 620 Hz. With this estimation the time is 40.95% of the simulation time for 1400 Hz.

7 The contact formulation Results

The numerical model derived by Naavik, uses a contact formulation that calculate penalty stiffness factor in each iteration. Making the contact as close to hard contact as possible. In standard EN50318 [10] it is stated that the penalty factor should be at least 50000 N/m. The motivation for this section is to observe the difference in the system response when changing the penalty stiffness, K, to 50000 N/m. Then, see if an increase in K, will produce similar response as for the default K.

From the Chapter **??** it was suggested that if frequencies under 100 Hz is of interest, there is no need for simulations with $f_s > 600Hz$. Thus, these results are from simulations with $f_s = 600Hz$. The time response, frequency content and the statistical values of the contact force will be used to compare the response from different K. K = 50000 N/m will be referred to as K_s

7.1 Time Domain Analysis

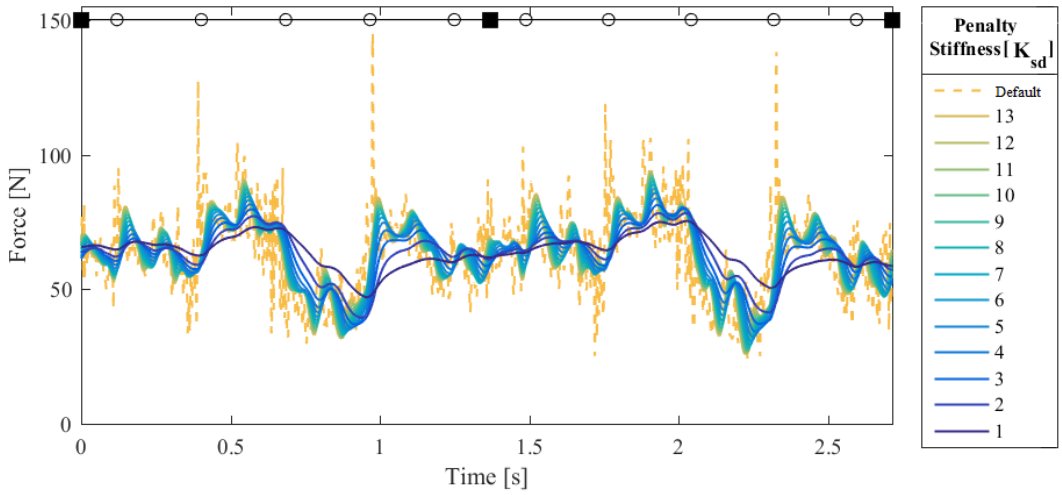

Figure 77: Time Domain Plot for linear penalty method

In figure 77, the contact force time domain is plotted for the analytical area for simulations done with K = K_{sd} to K = 13 K_{sd}. As stated, K_{sd} 50000 N is penalty stiffness that is stated as a minimum in EN50318. The result show that if the $K \leq 2K_{sd}$, the response of the simulations is not affected by the stiffness variations along the span or the passing of discontinuities, i.e. passing of droppers and brackets. When $K > 2K$, the response is affected by the most important things along the span. However, when the magnitude is small. The statistical values of the contact force will be discussed in section 8.

7.2 Frequency Content

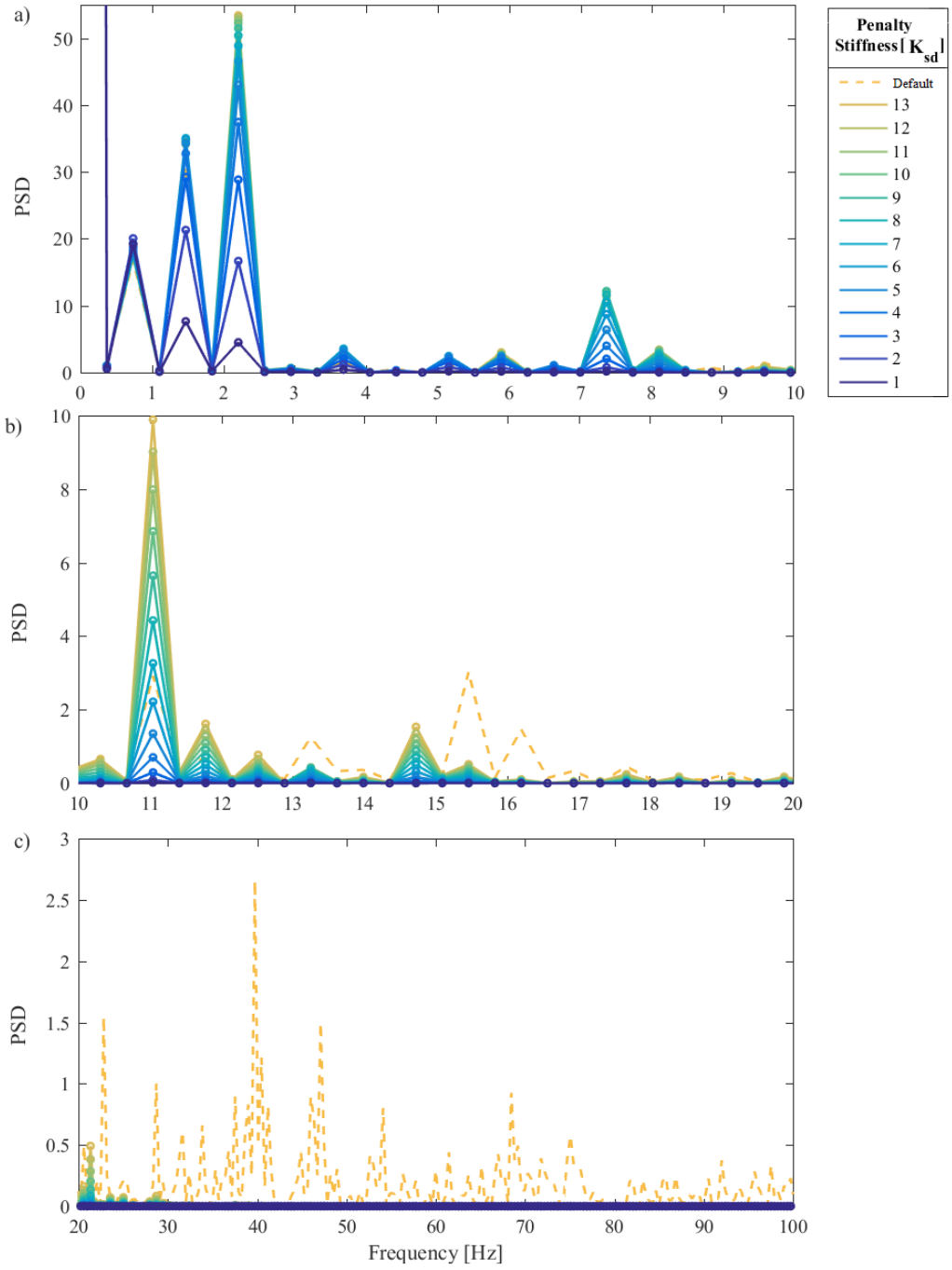

The frequency content of the contact force of the time series illustrated by the FFT spectrum. The frequency content can be recognized from Chapter 6.1.2. For $K \geq 5K$ the frequency content is the same up to 6 Hz. The distinction from the simulations done with default K increase with frequency. The contact forces the frequency content up to approximately 15 Hz is approximate the same for contact forces measured with $K = 13K_{sd}$ and $K = Default$. Suggesting that measuring with $K = 13K_{sd}$ is the same as filtering the result from simulations with default K with a cut-off filter of 15 Hz. Which, it was shown in Chapter **??** did not produce sufficient accurate result.

7.3 Statistical Analysis

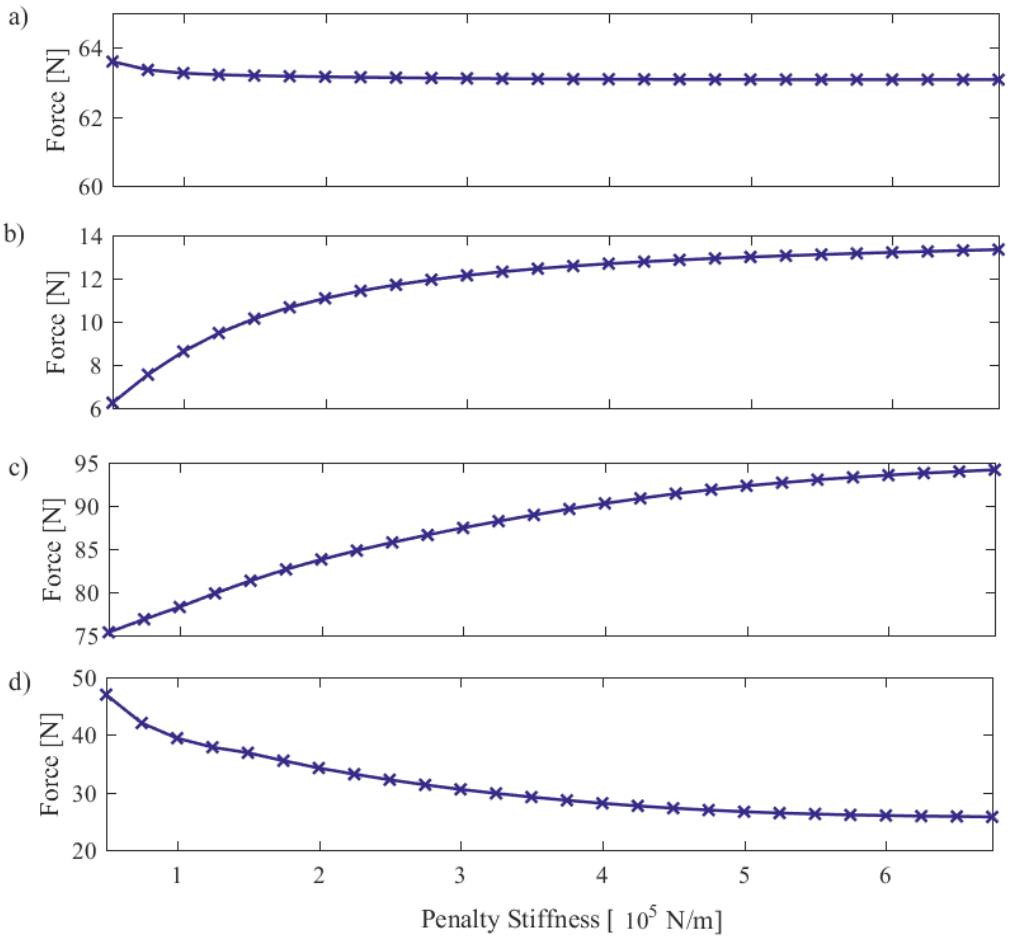

Figure 78: Statistical analysis of the contact force

Figure 78 indicates that the statistical values converge to a value after K = 500000 N/m, that is $10K_{sd}$. Compared to the statistical values of the filtered data in Chapter 6.4, it is clear that the differ a lot. Seemingly, the values converges towards the statistical values from simulations with $f_s \leq 80Hz$. The magnitude of the statistical values are small compared with those measured with default K.

8 Conclusion

This project was carried out to evaluate the dynamic response of the catenary dependency on sampling frequency. When investigating the wear of the catenary system, it is argued that a frequency range up to 100 Hz is needed, which is significantly higher than the recommended 20 Hz, stated in standard EN50318. Whether the simulations were able to detect elasticity variations along the span was studied, because of the impact this has on both contact loss and wear. In addition whether the simulations were able to detect the discontinuities and the nonlinearity the dropper introduce to the catenary section was studied.

The conclusion will address each objective individually:

How an increase in sampling frequency (i.e. decrease in time step) influences the simulations ability to...

1. *produce correct contact forces*: The minimum contact force values was more effected by the sampling frequency than the maximum contact forces. Suggesting that the sampling frequency effects the variations of the contact force in the sections with low contact forces than the sections with higher. By addressing the maximum values, can be stated that 600 Hz is enough, while for the minimum continue to decrease.
2. *detect elasticity variations along the span*: Is was observed that simulations with sampling frequencies above 80 Hz was able to detect maximum contact forces at the locations expected from the elasticity variations along the span.
3. *describe the dynamic response of the catenary*: The results suggests that the movement of the catenary is less affected by the sampling frequency after the pantograph has passed the point than prior. There were observed oscillations in the contact wire and the dropper with high frequencies pre-passage that simulations with f_{sd} did not detect. Which may imply that the simulations with f_{sd} will no be able to detect the full effect of the wave propagation prior the passage of the pantograph.

How filtering affect the dynamic response...

I *by increasing Cut-off frequency)*: It becomes clear from the filtered statistical data, that if frequency up to 100 is of interest no need to increase the sampling frequency of 600 Hz. However if frequency above at 140 the effect if increasing is clear.

II *filtering according to standard*: Filtering the data at 20 Hz, the maximum values occur in sections that is not expected. Seemingly not able detect the elasticity variations along the span. No change in the time response for different sampling frequencies when filtering the data at 20 Hz..

Based on the result presented in this thesis, a sampling frequency of 600 Hz can be recommended, if frequencies less then or equal to 100 Hz is of interest.

From the the simulations performed with the recommend frequency, it was evident from the results that a penalty stiffness factor of 50000 N/m is to small to produce correct dynamic response.

References

[1] Cho Y. Numerical simulation of the dynamic responses of railway overhead contact lines to a moving pantograph, considering a nonlinear dropper. J Sound Vib. 2008;315:433-454.

[2] Pombo J, Ambrósio J. J. Pombo and J. Ambrósio, Multiple Pantograph Interaction With Catenaries in High-Speed Trains, Journal of Computational and Nonlinear Dynamics, vol. 7, no. 4, pp. 041008–041008–7, 2012.ATO

[3] J. Pombo and P. Antunes,A Comparative Study between Two Pantographs in Multiple Pantograph High-Speed Operations, International Journal of Railway Technology, vol. 2, no. 1, pp. 83–108, 2013.

[4] Pombo J, Ambrósio J, Pereira M. Influence of the pantograph Characteristics on the Overhead Contact Quality for high speed trains. 2011

[5] P. Nåvik, A. Rønnquist, and S. Stichel,The use of dynamic response to evaluate and improve the optimization of existing soft railway catenary systems for higher speeds,Proceedings of the Institution of Mechanical Engineers, Part F: Journal of Rail and Rapid Transit, vol. 230,no. 4, pp. 1388–1396, 2015.

[6] A. Rønnquist and P. Nåvik,Dynamic assessment of existing soft catenary systems using modal analysis to explore higher train velocities: a case study of a Norwegian contact line system,Vehicle System Dynamics, vol. 53, no. 6, pp. 756–774, 2015.

[7] J. Ambrósio, J. Pombo, M. Pereira, P. Antunes, and A. Mósca, Recent Developments in Pantograph-Catenary Interaction Modelling and Analysis,International Journal of Railway Technology, vol. 1, no. 1, pp. 249–278, Apr. 2012.

[8] Nåvik, P., Dynamic behaviour of existing and new railway catenary systems under Norwegian conditions. NTNU, The Norwegian University of Science and Technology,2016.

[9] A. Collina and S. Bruni,Numerical Simulation of Pantograph-Overhead Equipment Interaction,Vehicle System Dynamics, vol. 38, no. 4, pp. 261–291, 2002.

[10] NEK EN 50318:2002 Railway applications - Current collection systems - Validation of simulation of the dynamic interaction between pantograph and overhead contact line,no. 1. p. 20, 2002.

[11] NEK EN 50317:2012 Railway applications - Current collection systems - Requirements for and validation of measurements of the dynamic interaction between pantograph and overhead contact line. 2012.

[12] EN 50119: 2009. Railway applications - fixed installations - electric traction overhead contact lines.

[13] Dassault Systèmes. ABAQUS 6.14 Theory manual. Providence, RI: Dassault Systèmes; 2014

[14] www.jernbanekompetanse.no. Mekanisk systembeskrivelse av kontaktledningsanlegg. (2011, accessed 2 October 2013).

[15] Cook D, Malkus S., Plesha E., J.Witt. Concepts and a applifications of finite element analysis. 4nd ed. John Wiley and Sons. Inc.: 2002

[16] Kiessling F. Contact lines for electric railways: planning, design, implementation, maintenance. 2nd ed. Erlangen: Publicis Publishing; 2009.

[17] Doyle, J. F., Wave Propagation in Structures: Spectral Analysis Using Fast discrete Fourier Transforms, 2nd ed. New York: Springer-Verlag New York, Inc., 1997. ISBN 0-387-94940-2.

[18] MATLAB R2014a., Filter Design and Analysis Tool. The MathWorks Inc.

A Appendix

A.1 Maximum Contact Force Location

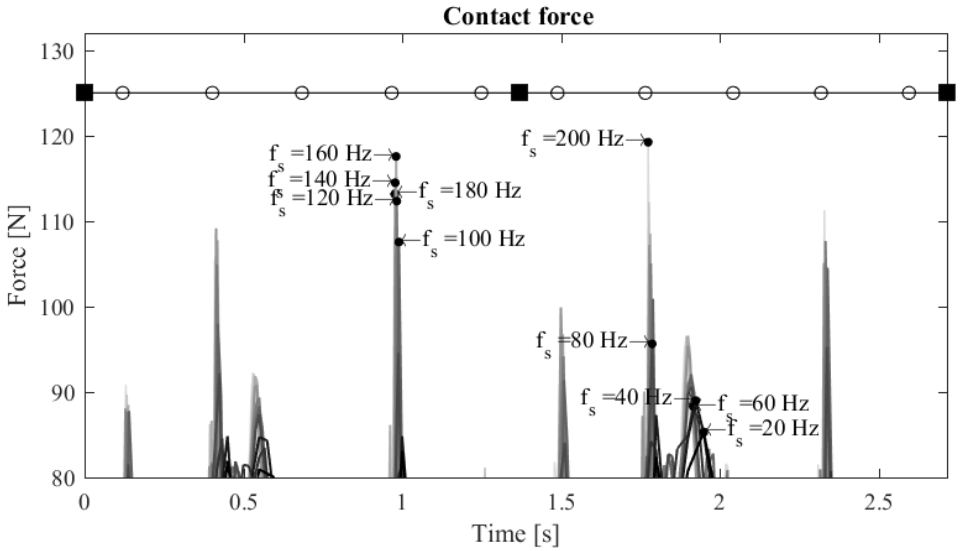

Figure 79: Position of the contact force maximum for $f_s \in [20Hz, 200Hz]$

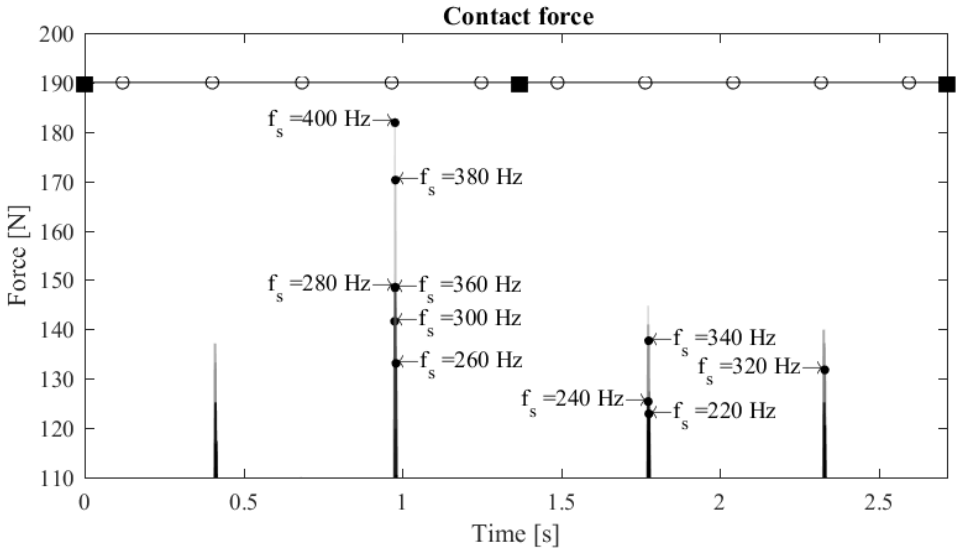

Figure 80: Position of the contact force maximum for $f_s \in [220Hz, 400Hz]$

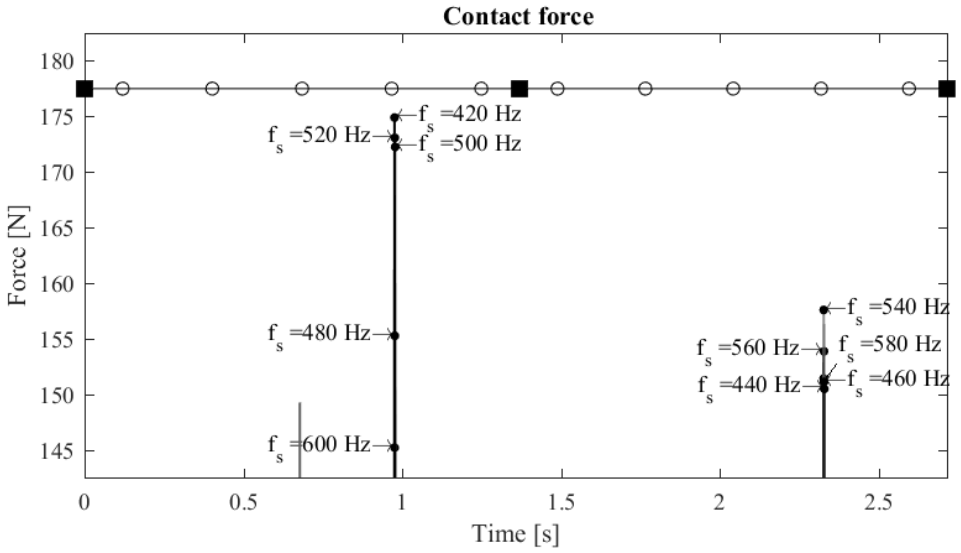

Figure 81: Position of the contact force maximum for $f_s \in [420Hz, 600Hz]$

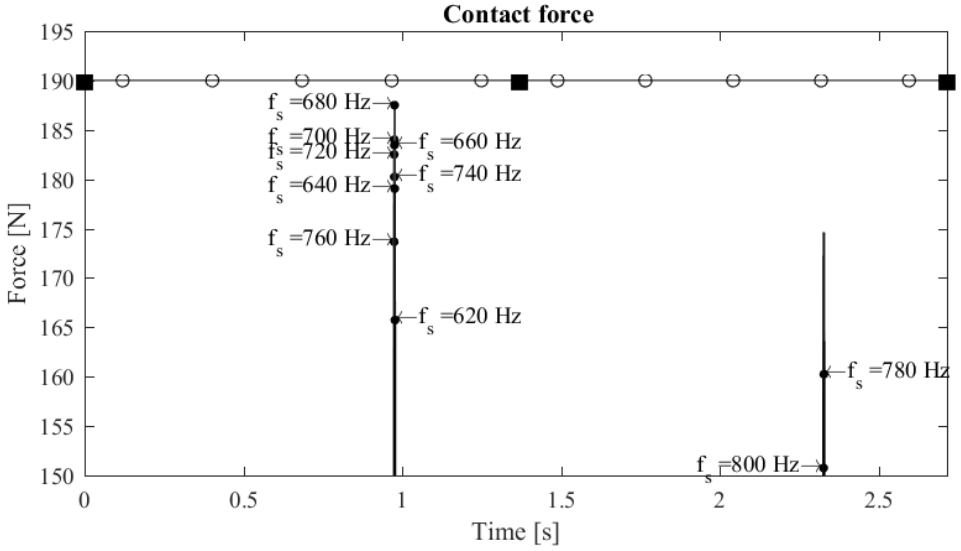

Figure 82: Position of the contact force maximum for $f_s \in [620Hz, 800Hz]$

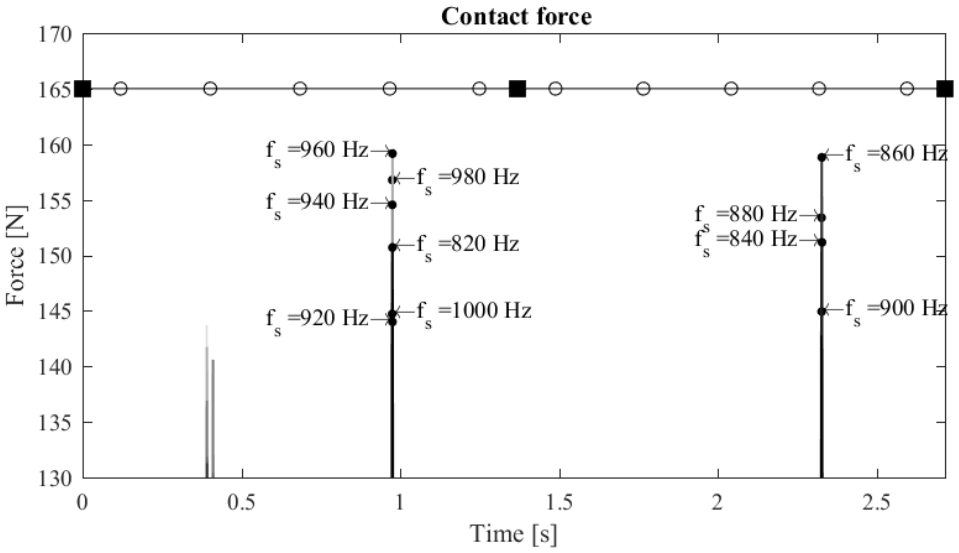

Figure 83: Position of the contact force maximum for $f_s \in [820Hz, 1000Hz]$

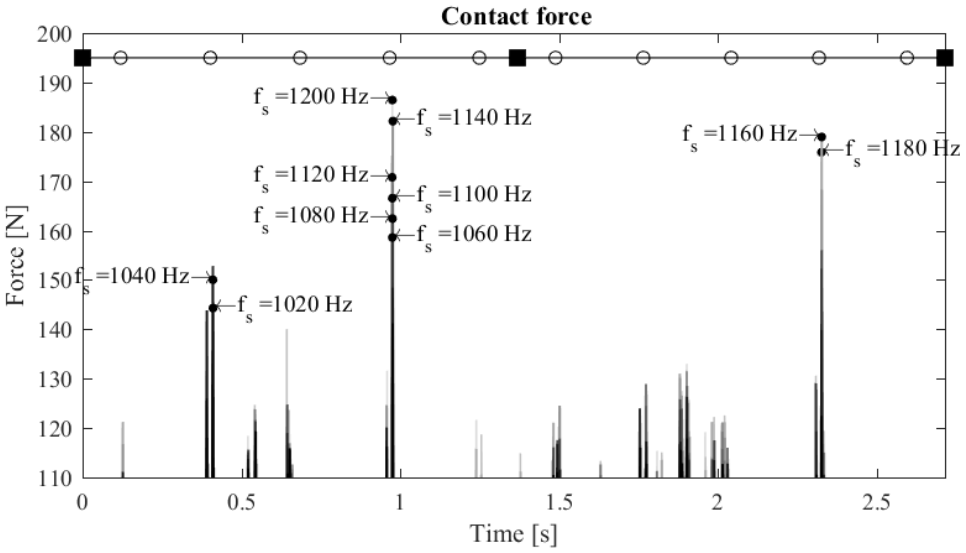

Figure 84: Position of the contact force maximum for $f_s \in [1020Hz, 1200Hz]$

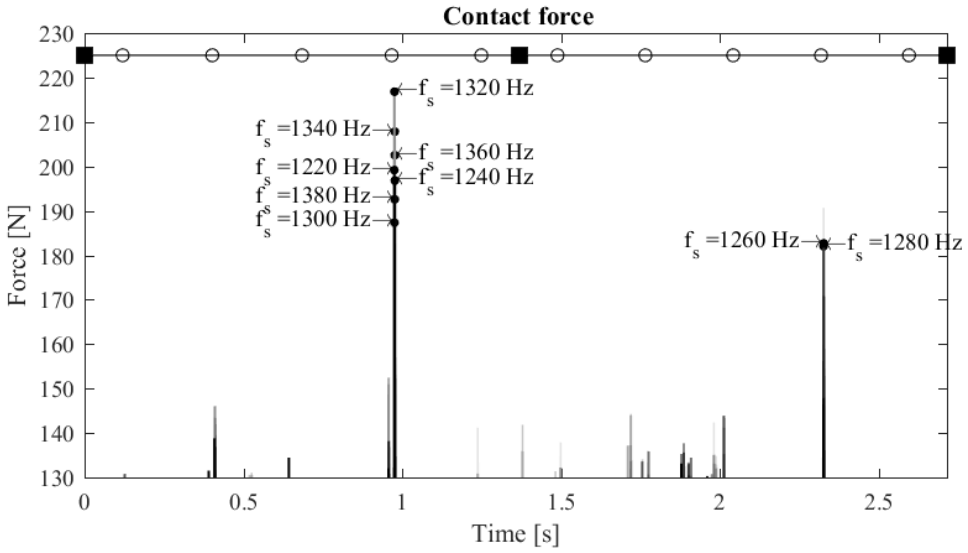

Figure 85: Position of the contact force maximum for $f_s \in [1220Hz, 1400Hz]$

A.2 Fokstua Wire 21 Geometry

Span no.	**1**	**2**	**3**	**4**	**5**	**6**	**7**	**8**	**9**	**10**	**11**	**12**	**13**	**14**
Length [m]	44.27	44.98	45	49.45	45.51	45.65	44.88	45.03	45.1	44.54	45.28	44.76	45.34	48.87
No. of droppers	2	4	5	5	5	5	5	5	5	5	5	5	5	5
Span no.	**15**	**16**	**17**	**18**	**19**	**20**	**21**	**22**	**23**	**24**	**25**	**26**	**27**	**28**
Length [m]	49.02	48.77	50.8	52.23	51.95	52.1	51.87	52	52.06	42.48	39.95	30.99	39.54	42.55
No. of droppers	5	5	5	6	5	6	5	5	6	5	4	4	4	2

Figure 86: Span lengths and number of droppers for Fokstua wire 21

A.3 Data Analysis Script

```
fontSIZE=9;
% Change default axes fonts.
set(0,'DefaultAxesFontName', 'Times New Roman')
set(0,'DefaultAxesFontSize', fontSIZE)

% Change default text fonts.
set(0,'DefaultTextFontname', 'Times New Roman')
set(0,'DefaultTextFontSize', fontSIZE)


%Output_variables = {{Symbol, Title, yaxis, xaxis}..
Output_variables = {{'CFN2',' Contact force','Force [N]','Time [s]'}; ...
                    {'CW_min_AT_y_new',' Contact wire acceleration','Acceleration [m/s^2]','
Time [s]'};...
                    {'CW_min_UT_y_new',' Contact wire displacement','Displacement [m]','Time
 [s]'};...
                    {'CW_max_AT_y_new',' Contact wire acceleration','Acceleration [m/s^2]','
Time [s]'};...
                    {'CW_max_UT_y_new',' Contact wire displacement','Displacement [m]','Time
 [s]'};...
                    {'DR_AT_y_new',' y acceleration','Acceleration [m/s^2]','Time [s]'};...
                    {'DR_AT_z_new',' z acceleration','Acceleration [m/s^2]','Time [s]'};...
                    {'DR_UT_y_new',' y displacement','Displacement [m]','Time [s]'};...
                    {'DR_UT_z_new',' z displacement','Displacement [m]','Time [s]'}};...


Output_variables_list = [1];  %2 3 4 5 6 7 8
SaHz_list =[20 40 60 80 100 200 300 400 500 600 700 800 900 1000 1100 1200 1300 1400];
SaHz = [1400 1000 600 200]; % 1300 1200 1100 1000 900 800 700 600 500 400 300 200 100 80 6
0 40 20];1400:-20:20]
LineWidth =  ones(length(SaHz),1)-0.3;

Cw_max_points = [261.45 288.08 306.52];
Cw_min_points = [252.04 257.95 286.67 301.81 ];
new_dropper_points = [252.04 261.45 288.08 306.52 ];

plots = [];%zeros((length(Output_variables))*length(SaHz),1);
Plot_number = 0;
RUN_TIME_SERIES = 0;
RUN_FREQ_ANALYSIS = 0;
NAT_FREQ =0;
PRINT = 0;
print_size =  [0 0 3 1.5];% Orginal = [0 0 6 3];
ZOOM_FFT =0;
ZOOM = 0;

FILTER = 0;
SUBPLOT = 0;
LEGEND = 0;
```

```
SPAN_INFO = 0;
ADD_MAX_VALUE =0;
ADD_MIN_VALUE =0;
ADD_POSITION =0;
color_map = colormap(parula);

if ADD_MAX_VALUE==1||ADD_MIN_VALUE ==1;
    color_map= colormap(gray(length(SaHz)));
end
color_map_2 = colormap(gray);
color = zeros(length(SaHz),3);
Figure_list = {}; %Stores names for the saved(printed) plots

%Finding maximum values and position

max_value = zeros(length(SaHz),1);
max_position = zeros(length(SaHz),1);
min_value = zeros(length(SaHz),1);
min_position = zeros(length(SaHz),1);
%Analytical area
Speed_ms = 120/3.6;
x_0 = 206.455;
Br_1 = 229.21;
Br_3 = 319.74;
tmin = (Br_1-x_0)/Speed_ms;
tmax = (Br_3-x_0)/Speed_ms;
%geometrical data
DR_geo = [233.21 242.62 252.04 261.45 270.86  278.86 288.08 297.3 306.52 315.75];
BR_geo = [229.21 274.86 319.74 ];
sim_start = 229.21;
DR_norm_time = (DR_geo-sim_start)./Speed_ms;
BR_norm_time = (BR_geo-sim_start)./Speed_ms;
DR_y = ones(1,length(DR_norm_time));
BR_y = ones(1,length(BR_norm_time));

t_dr3 = DR_norm_time(3);
t_dr4 = 0.9754;
t_dr9 = 2.327;

dt_zoom = 1/20;

tzoom_min = t_dr9-dt_zoom;
tzoom_max = t_dr9+dt_zoom;

%Natural_frequencyes
if NAT_FREQ==1
Files = {'Fokstua_wire21_Original_Frequency_Eigenfrec_max10_min0','Fokstua_wire21_Original
_Frequency_Eigenfrec_max40_min10'};
Output = {'EIGFREQ','GM','EM2','EM6'};
Names = {'Eigenfrequecncies','Generalized mass','Effective mass, y component','Effective m
ass, z rotation'};
for i =1:length(Files)
    for j= 1:length(Output)
        File = strcat(Files{i},'_',Output{j},'.txt');
        FileId = fopen(File);
        Cell = textscan(FileId,'%f');
        Vector = cell2mat(Cell);
        Out = Vector(2:2:length(Vector));
        if i==1
                if j==1
                 Eigenfreq_out = Out;
```

```
                elseif j==2
                 GM = Out;
                elseif j==3
                 Eff_y = Out;
                elseif j==4
                 Eff_rot_y = Out;
                end
        elseif i==2
                if j==1
                 Eigenfreq_out = [Eigenfreq_out;Out];
                elseif j==2
                 GM = [GM;Out];
                elseif j==3
                 Eff_y = [Eff_y;Out];
                elseif j==4
                 Eff_rot_y = [Eff_rot_y;Out];
                end
        end
    end
end
GM_norm = GM./max(GM);
Eff_y_norm = Eff_y./max(Eff_y);
Eff_rot_y_norm = Eff_rot_y./max(Eff_rot_y);
end

%zooming in FFT
fmin = 0;
fmax = 10;
fftmin = 0;
fftmax = 55;

FFT_field_min =0;
FFT_field_max = 80;
%Filtering_values

SaHz_filt = 10;

for i = 1:length(SaHz)
 delta = mod(length(color_map),length(SaHz));
 color_map = color_map(1:(size(color_map,1)-delta),:);
 color_map_2 = color_map_2(1:(size(color_map_2,1)-delta),:);
 delta2 = size(color_map,1)/length(SaHz);
 color(length(SaHz)+1-i,:) = color_map(((i-1)*delta2)+1,:);
 color_2(length(SaHz)+1-i,:) = color_map_2(((i-1)*delta2)+1,:);
end

%color(4,:) = [1 0 0];
color_filt = colormap(gray(length(SaHz)));

for i = 1:length(SaHz)
    Figure_number = 0;
    for j = Output_variables_list
```

```
        HISTORY = 0;
        File = strcat('Fokstua_wire21_Original_120kmt_WBL88_RD_SaHz_',num2str(SaHz(i)),'_O
utHz_1_',Output_variables{j}{1},'.txt');
        FileId = fopen(File);
        Cell = textscan(FileId,'%f');
        Vector = cell2mat(Cell);
```

```
        Ydata = Vector(2:2:length(Vector));
        Xdata = Vector(1:2:length(Vector));
        Ydata_0 = zeros(length(Ydata),1);
        if j==1
           Time = Vector(1:2:length(Vector));
           Frames(i) = length(Time);
        end
        a= 1:Frames(i):length(Ydata);
        % Sorting the output list
        if j>1
            for p = 1:length(Ydata)/Frames(i)
                Ydata_0(p:length(Ydata)/Frames(i):length(Ydata))= Ydata(p,1);
            end
        end
        Delta_Ydata = Ydata- Ydata_0;
        % Reducing the output values, finding start and end point
        if j==1
            dt = Xdata(3)-Xdata(2);
            for ii = 1:length(Xdata)
                if Xdata(ii)>=tmin-(dt*0.5) && Xdata(ii)<=tmin+(dt*0.5)
                    T_0 = ii;
                elseif Xdata(ii)>=tmax-(dt*0.5) && Xdata(ii)<=tmax+(dt*0.5)
                    T_end = ii;
                end
            end
        end
```

Finding the output positions

```
        Find = Xdata(1);
        pos = 1;
        for k = 2:length(Xdata)
           if Xdata(k)==Find
               break
           end
           pos = pos + 1;
        end
        Output_figures = pos;
        if pos >= length(Time)
            Output_figures=length(Xdata)/(pos);
            Output_figures_list = 1:Output_figures;
            HISTORY = 1;
        else
            Output_figures_list = 1:Output_figures;
        end
```

Plotting the output

```
    for l = Output_figures_list
% History output time series
        if HISTORY ==1;
             Delta_Ydata_node = Delta_Ydata((1+((l-1)*pos)):l*pos);
        %Output reduced to analytical region
             Delta_Ydata_Region = Delta_Ydata_node(T_0:T_end);
             Time_Region = Time(T_0:T_end);
             Time_Region = Time(T_0:T_end)-Time(T_0);

             if ADD_MAX_VALUE ==1;
```

```
                max_value(i) = max(Delta_Ydata_Region);
                position_vector = find(Delta_Ydata_Region==max(Delta_Ydata_Region));
                max_position(i) =  Time_Region(position_vector);
            elseif ADD_MIN_VALUE ==1;
                min_value(i) = min(Delta_Ydata_Region);
                position_vector = find(Delta_Ydata_Region==min(Delta_Ydata_Region));
                min_position(i) =  Time_Region(position_vector);
            end
            if SaHz(i) >= 40 %Filtering the data
                g = filter_cheby_2(SaHz(i),SaHz_filt);
                Ydata_filtered = filter(g,Delta_Ydata_node);
                Delta_Ydata_filtered = Ydata_filtered(T_0:T_end);
                [Delta_Ydata_filtered_Pwelch,freq_filtered] =  pwelch(Delta_Ydata_filtered
,[],[],[],SaHz(i));
                Ydata_filtered_phase = filtfilt(g.sosMatrix,g.ScaleValues,Delta_Ydata_node
);
                Delta_Ydata_filtered_phase =  Ydata_filtered_phase(T_0:T_end);
            else
                Delta_Ydata_filtered = Delta_Ydata_Region;
                Delta_Ydata_filtered_phase = Delta_Ydata_Region;
            end
            Figure_number = Figure_number+1;
            Plot_number = Plot_number +1;
            fig = figure(Figure_number);
            fig.PaperUnits = 'inches';
            fig.PaperPosition = print_size;
% Changing Linewidth
            if ZOOM ==1
                LineWidth(i) = LineWidth(i)+0.2;
            end
            DisplayName = strcat(num2str(SaHz(i)));
            %if FILTER ==1
             %  color = colormap(parula(15));
              % DisplayName = 'Sampled data';
            %end
            if FILTER==0
                plots(Plot_number) =  plot(Time_Region,Delta_Ydata_Region,'Color',color(i,
:),...
                   'LineWidth',LineWidth(i),'DisplayName',DisplayName);
                hold on
            end
            if ADD_MAX_VALUE ==1;
                plot(max_position(i),max_value(i),'or', 'MarkerSize',3,'MarkerFaceColor',
[1 0 0])
                if ADD_POSITION==1
                    if mod(i,2)==0 && i~=4
                        txt = strcat('\leftarrow','f_s = ',num2str(SaHz(i)),' Hz');
                        text(max_position(i),max_value(i),txt)
                    %elseif i==2
                      %  a = {'                              '};
                       %  txt = strcat('f_s = ',num2str(SaHz(i)),' Hz','\rightarrow',a);
                       % text(max_position(i),max_value(i),txt,'HorizontalAlignment','rig
ht')
                    else
                        txt = strcat('f_s = ',num2str(SaHz(i)),' Hz','\rightarrow');
                        text(max_position(i),max_value(i),txt,'HorizontalAlignment','righ
t')
                    end
                end
            elseif  ADD_MIN_VALUE ==1;
                plot(min_position(i),min_value(i),'ob', 'MarkerSize',3,'MarkerFaceColor',
```

```
[0 0 1])
            end
 % Adding the span geometry to the plot
            if SPAN_INFO ==1 && i==1
                if FILTER==1
                  Span_info_pos= max(Delta_Ydata_filtered_phase);
                elseif ADD_MAX_VALUE==1
                  Span_info_pos = 220;
                else
                  Span_info_pos = max(Delta_Ydata_Region);
                end
                plot(BR_norm_time,BR_y*Span_info_pos,'s-k','MarkerFaceColor',[0 0 0], 'Ma
rkerSize',8)
                hold on
                plot(DR_norm_time,DR_y*Span_info_pos,'-ok', 'MarkerSize',5)
            end
            if FILTER==1
               min_y= 30;
               max_y= 110;
            elseif ADD_MAX_VALUE==1 && ADD_POSITION ==1
               min_y = 80;
               max_y =132;
            else
               min_y = 0;
               max_y =230;
            end
            %axis([0 2.7159 min_y max_y])
%Adding the filtered data to the plot
            if FILTER ==1 && i~=4
                %Plot_number = Plot_number +1;
                %plots(Plot_number) =  plot(Time_Region,Delta_Ydata_filtered,'Color',colo
r(i+5,:),...
                  % 'LineWidth',LineWidth(i),'DisplayName','Filtered');
                hold on
                Plot_number = Plot_number +1;
                plots(Plot_number) =  plot(Time_Region,Delta_Ydata_filtered_phase,'Color'
,color(i,:),...
                   'LineWidth',LineWidth(i),'DisplayName','Delay Compensated');
                hold on
                xlim([0 2.7159])

            end
% Adding zoom to plot
            if ZOOM ==1 && j==1 % && i==1
                xlim([tzoom_min tzoom_max])
                %axis([tzoom-(1/20) tzoom+(1/20)   min(Delta_Ydata_Region) max(Delta_Ydat
a_Region)])
            end
            if ZOOM ==1
                title('')
                Figure_list{Figure_number} = (strcat(Output_variables{j}{1},'zoom'));
            elseif FILTER ==1
                title(strcat(Output_variables{j}{2},' Cut Off frequency',{' '},num2str(Sa
Hz_filt),' Hz'))
                Figure_list{Figure_number} = (strcat(Output_variables{j}{1},' Sampling Fr
equency',' ', num2str(SaHz(i)), 'Hz'));
            else
                Figure_list{Figure_number} = (strcat(Output_variables{j}{1},num2str(l)));
                title(strcat(Output_variables{j}{2}));
            end
            ylabel(Output_variables{j}{3})
```

```
            xlabel(Output_variables{j}{4})
            hold on
 %Frequency analysis
            if RUN_FREQ_ANALYSIS == 1;
                 Figure_number = Figure_number+1;
                 Plot_number = Plot_number +1;
                 figure(Figure_number)
                 [Delta_Ydata_FFT,freq] = fftspectra(Delta_Ydata_Region,Time(2)-Time(1));
                 [Delta_Ydata_Pwelch,freq_pwelch] = pwelch(Delta_Ydata_Region,[],[],[],Sa
Hz(i));
                 if NAT_FREQ ==1
                    plots(Plot_number) =  plot(freq,Delta_Ydata_FFT./55,'-o','Color',colo
r(i,:),'LineWidth',LineWidth(i)*0.8,'MarkerSize',3,'DisplayName',strcat(num2str(SaHz(i))))
;
                    hold on
                    stem(Eigenfreq_out,GM_norm,'LineWidth',1,'MarkerSize',3)
                   % plot(Eigenfreq_out,Eff_y_norm,'LineWidth',1.3)
                 else
                     plots(Plot_number) =  plot(freq,Delta_Ydata_FFT,'-o','Color',color(i
,:),'LineWidth',LineWidth(i),'MarkerSize',3,'DisplayName',strcat(num2str(SaHz(i))));
                     hold on
                 end
                 if j==2
                     title(strcat('FFT Spectrum ',Output_variables{j}{2},' Dropper: ', nu
m2str(l-1)))
                     Figure_list{Figure_number} = strcat('FFT Spectrum ',Output_variables
{j}{1},' Dropper ', num2str(l-1));
                 else
                     title(strcat('FFT Spectrum ',Output_variables{j}{2}))
                     Figure_list{Figure_number} = strcat('FFT Spectrum ',Output_variables
{j}{2});
                 end
                 if ZOOM_FFT ==1
                       axis([fmin fmax fftmin fftmax])
                 end
                 ylabel('FFT spectrum')
                 xlabel('Frequency [Hz]')
            end
 % Field output time series
        else % Field output time series
             %Output reduced to analytical region
             Delta_Ydata_node = Delta_Ydata(l:pos:length(Ydata));
             Delta_Ydata_Region = Delta_Ydata_node(T_0:T_end);
             Time_Region = Time(T_0:T_end)-Time(T_0);
            if j==2 || j==3
                ZOOM_vector = (Cw_min_points-sim_start)./Speed_ms;
                figure_names = round(Cw_min_points);
            elseif j==4 || j==5
                ZOOM_vector = (Cw_max_points-sim_start)./Speed_ms;
                figure_names = round(Cw_max_points);
            else
                ZOOM_vector = (new_dropper_points-sim_start)./Speed_ms;
                figure_names = round(new_dropper_points);
            end
            if SaHz(i) >= 240 %Filtering the data
                g = filter_cheby(SaHz(i));
                Delta_Ydata_filtered = filter(g,Delta_Ydata_Region);
                [Delta_Ydata_filtered_Pwelch,freq_filtered] =  pwelch(Delta_Ydata_filtered
,[],[],[],SaHz(i));
            end
                if SUBPLOT == 1;
```

```
                        figure(2)
                        if l == 1
                            position = 2;
                        elseif l==2
                            position = 6;
                        elseif l==3
                            position =5;
                        elseif l==4
                            position =1;
                        elseif l==5
                            position =4;
                        elseif l==6
                            position = 3;
                        end
                        Figure_list{2} = 'Subplot_time_Acc';
                        subplot(length(Output_figures_list)/2,2,position);
                        hold on
                        plots(Plot_number) =  plot(Time_Region,Delta_Ydata_Region,'Color',c
olor(i,:),'LineWidth',LineWidth(i),'DisplayName',strcat(num2str(SaHz(i))));
                        hold on
                         if position ==1 || position ==2
                             axis([0 4.1 -100 100])
                         elseif position ==3 || position ==4
                             axis([0 4.1 -200 200])
                         elseif position ==5 || position ==6
                             axis([0 4.1 -110 110])
                         end
                else
                    Figure_number = Figure_number+1;
                    Plot_number = Plot_number +1;
                    figure(Figure_number)
                    fig = gcf;
                    fig.PaperUnits = 'inches';
                    fig.PaperPosition = print_size;
                    plots(Plot_number) =  plot(Time_Region,Delta_Ydata_Region,'Color',colo
r(i,:),'LineWidth',LineWidth(i),'DisplayName',strcat(num2str(SaHz(i))));
                    hold on
                    if ZOOM ==1
                        xlim([ZOOM_vector(l)-0.1 ZOOM_vector(l)+0.05])
                        if i==1 &&( j==2||j==4 && SPAN_INFO ==1)
                            ylim([min(Delta_Ydata_Region)-15 max(Delta_Ydata_Region)+15])
                        elseif i==1 &&( j==6||j==7 && SPAN_INFO ==1)
                             ylim([min(Delta_Ydata_Region)-5 max(Delta_Ydata_Region)+5])
                        end
                    else
                        xlim([0 2.7159])
                    end
                     if SPAN_INFO ==1 && i==1
                         Span_info_pos = max(Delta_Ydata_Region)+0.0001;
                         if j==3 || j==5
                            plot([ZOOM_vector(l) ZOOM_vector(l)],[min(Delta_Ydata_Region)
max(Delta_Ydata_Region)+0.005],'--k')
                         elseif j==2 || j==4
                            plot([ZOOM_vector(l) ZOOM_vector(l)],[min(Delta_Ydata_Region)-
15 max(Delta_Ydata_Region)+15],'--k')
                         elseif j==6 || j==7
                            plot([ZOOM_vector(l) ZOOM_vector(l)],[min(Delta_Ydata_Region)-
2 max(Delta_Ydata_Region)+2],'--k')
                            ylim([min(Delta_Ydata_Region)-2 max(Delta_Ydata_Region)+2])
                         elseif j==8
                            plot([ZOOM_vector(l) ZOOM_vector(l)],[min(Delta_Ydata_Region)-
```

```
0.001 max(Delta_Ydata_Region)+0.001],'--k')
                            ylim([min(Delta_Ydata_Region)-0.001 max(Delta_Ydata_Region)+0.
001])
                        elseif j==9
                            plot([ZOOM_vector(l) ZOOM_vector(l)],[min(Delta_Ydata_Region)-
0.00025 max(Delta_Ydata_Region)+0.00025],'--k')
                            ylim([min(Delta_Ydata_Region)-0.00025 max(Delta_Ydata_Region)+
0.00025])
                        end

                        %plot(BR_norm_time,BR_y*Span_info_pos,'s-k','MarkerFaceColor',[0
0 0], 'MarkerSize',8)
                        %hold on
                        %plot(DR_norm_time,DR_y*Span_info_pos,'-ok', 'MarkerSize',5)
                    end
                end
            if FILTER ==1
                Plot_number = Plot_number +1;
                Delta_Ydata_filtered_phase = filtfilt(g.sosMatrix,g.ScaleValues, Delta_Yda
ta_Region);
                plots(Plot_number) =  plot(Time_Region,Delta_Ydata_filtered_phase,'Color',
color_2(i,:),'LineWidth',LineWidth(i),'DisplayName',strcat(num2str(SaHz(i))));
                hold on
                Plot_number = Plot_number +1;
                plots(Plot_number) =  plot(Time_Region,Delta_Ydata_filtered,'Color','r','L
ineWidth',LineWidth(i),'DisplayName',strcat(num2str(SaHz(i))));
                hold on
            end
        if SUBPLOT == 1;
                if j==3 || j==4
                    txt = ['Position: ' Node_name_CW{position}];
                    title(txt)
                else
                    title(strcat(' Node: ',num2str(Xdata(l))))
                end
                Figure_list{length(Output_figures_list)+3} = strcat(Output_variables{j}{1}
,'Subplot');
                if position == 3 %position == 1 ||
                    ylabel(Output_variables{j}{3})
                elseif position == 5
                    %ylabel(Output_variables{j}{3})
                    xlabel('Time [s]')
                elseif position == 6
                    xlabel('Time [s]')
                end
        else
                if j==2||j==3
                    title(strcat(Output_variables{j}{2},' x = ',num2str(Cw_min_points(l)),
'm'))
                elseif j==4||j==5
                    title(strcat(Output_variables{j}{2},' x = ',num2str(Cw_max_points(l)),
'm'))
                else
                    title(strcat(Output_variables{j}{2},' x = ',num2str(new_dropper_points
(l)),'m'))
                end
                Figure_list{Figure_number} = strcat(Output_variables{j}{1},num2str(figure_
names(l)));
                ylabel(Output_variables{j}{3})
                xlabel('Time [s]')
            end
```

```
            if RUN_FREQ_ANALYSIS == 1;
                [Delta_Ydata_FFT,freq] = fftspectra(Delta_Ydata_Region,Time(2)-Time(1)); %
 The FFT Spectrum
                [Delta_Ydata_Pwelch,freq_pwelch] =  pwelch(Delta_Ydata_Region,[],[],[],SaH
z(i)); % The power spectral density
                if SUBPLOT == 1;
                   figure(3)
                   if l == 1
                       position = 2;
                   elseif l==2
                       position = 6;
                   elseif l==3
                       position =5;
                   elseif l==4
                       position =1;
                   elseif l==5
                       position =4;
                   elseif l==6
                       position = 3;
                   end
                   subplot(length(Output_figures_list)/2,2,position);
                   hold on
                   Plot_number = Plot_number +1;
                   plots(Plot_number) =  subplot(freq,Delta_Ydata_FFT,'Color',color(i,:),'
LineWidth',LineWidth(i)+0.2 ,'DisplayName',strcat(num2str(SaHz(i))));
                       if ZOOM ==1
                           xmax = 200;
                       else
                           xmax = 800;
                       end
                       if position ==1 || position ==2
                            axis([0 xmax 0 1.2])
                        elseif position ==3 || position ==4
                            axis([0 xmax 0 5.2])
                        elseif position ==5 || position ==6
                            axis([0 xmax 0 2.2])
                       end

                else
                   Figure_number = Figure_number+1;
                   figure(Figure_number)
                   fig = gcf;
                   fig.PaperUnits = 'inches';
                   fig.PaperPosition =print_size;
                   Plot_number = Plot_number +1;
                   plots(Plot_number) =  plot(freq,Delta_Ydata_FFT,'Color',color(i,:),'Lin
eWidth',LineWidth(i)+0.2 ,'DisplayName',strcat(num2str(SaHz(i))));
                   if ZOOM_FFT ==1
                      xlim([FFT_field_min FFT_field_max])
                   end

                end
                hold on
                if FILTER ==1
                    Plot_number = Plot_number +1;
                    plots(Plot_number) =  plot(freq_filtered,Delta_Ydata_filtered_Pwelch,'
-o','Color','r','LineWidth',LineWidth(i)+0.2 ,'DisplayName',strcat('Frequency = ',num2str(
SaHz(i))));
                    hold on
                end
                if SUBPLOT == 1;
```

```
                    if j==2||j==3
                        title(strcat(Output_variables{j}{2},' x = ',num2str(Cw_min_points(
l))))
                    elseif j==4||j==5
                        title(strcat(Output_variables{j}{2},' x = ',num2str(Cw_max_points(
l)),'m'))
                    else
                        title(strcat(' Node: ',num2str(Xdata(l))))
                    end
                    Figure_list{3} = strcat('PSD ',Output_variables{j}{1},'Subplot');
                    if position == 1 || position == 3
                        ylabel('PSD')
                    elseif position == 5
                        ylabel('PSD')
                        xlabel('Frequency [Hz]')
                    elseif position == 6
                        xlabel('Frequency [Hz]')
                    end
                else
                if j==2||j==3
                    title(strcat(Output_variables{j}{2},' x = ',num2str(Cw_min_points(l)),
'm'))
                elseif j==4||j==5
                    title(strcat(Output_variables{j}{2},' x = ',num2str(Cw_max_points(l)),
'm'))
                end
                    if ZOOM_FFT ==1
                        Figure_list{Figure_number} = strcat('FFT_',Output_variables{j}{1},
num2str(figure_names(l)),'_',num2str(FFT_field_min),'_',num2str(FFT_field_max));
                    else
                        Figure_list{Figure_number} = strcat('FFT_',Output_variables{j}{1},
num2str(figure_names(l)));
                    end
                    ylabel('FFT')
                    xlabel('Frequency [Hz]')
                end
            end
        end
       end
```

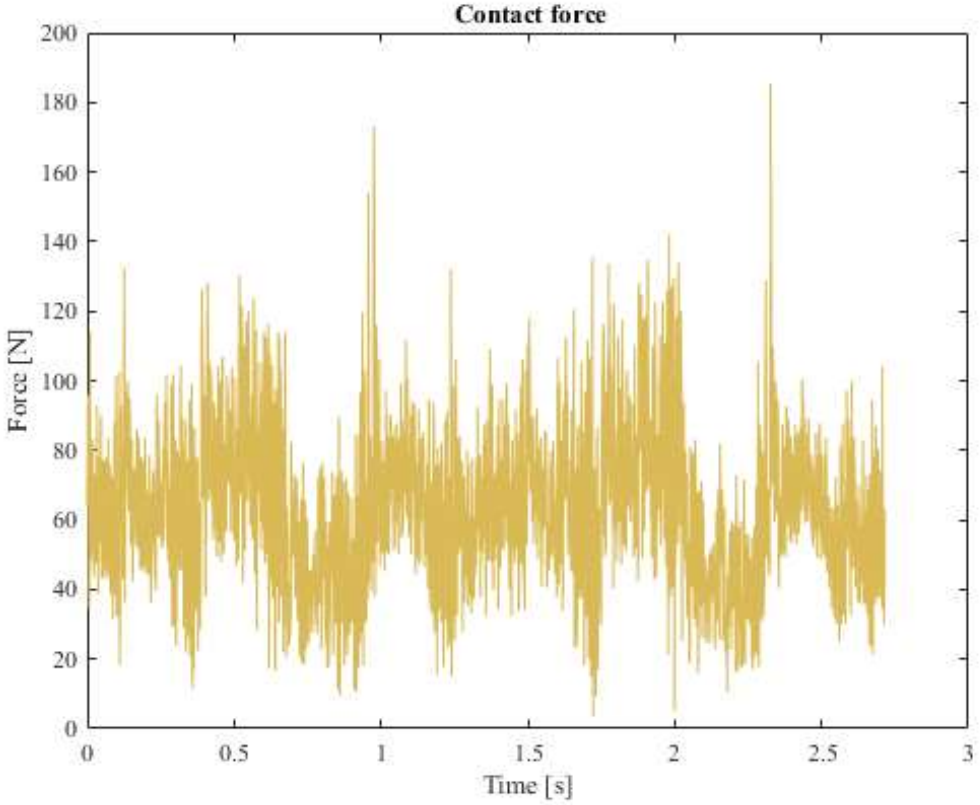
Contact force
Force [N]
Time [s]
0
20
40
60
80
100
120
140
160
180
200
0
0.5
1
1.5
2
2.5
3

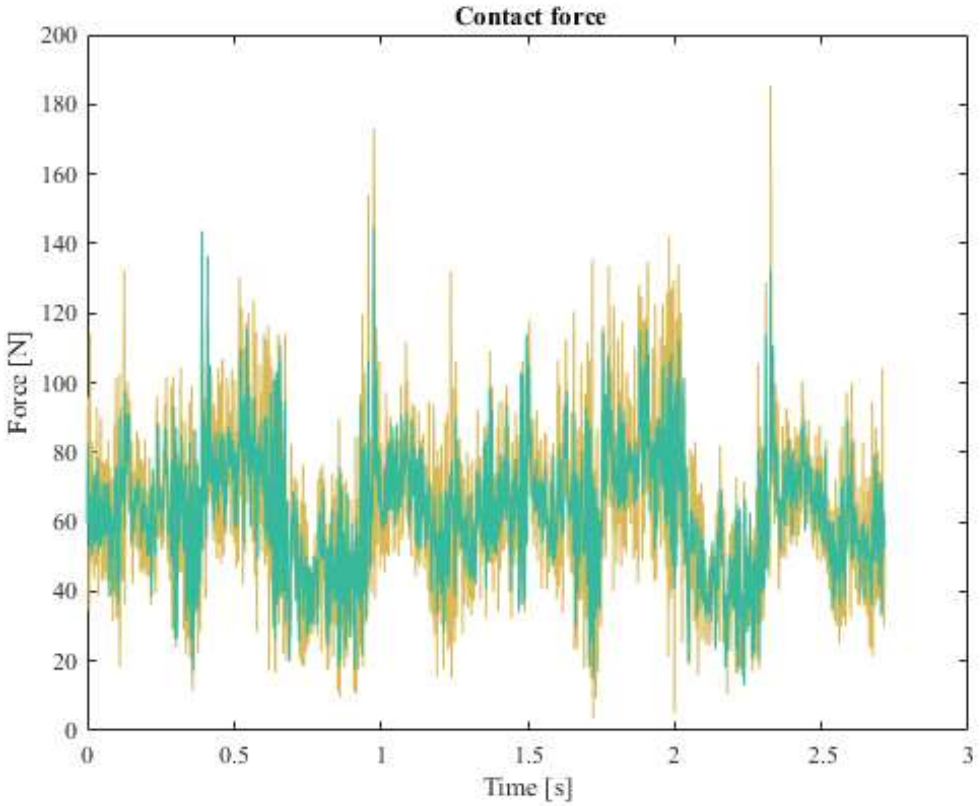
Contact force
Force [N]
Time [s]
0
20
40
60
80
100
120
140
160
180
200
0
0.5
1
1.5
2
2.5
3

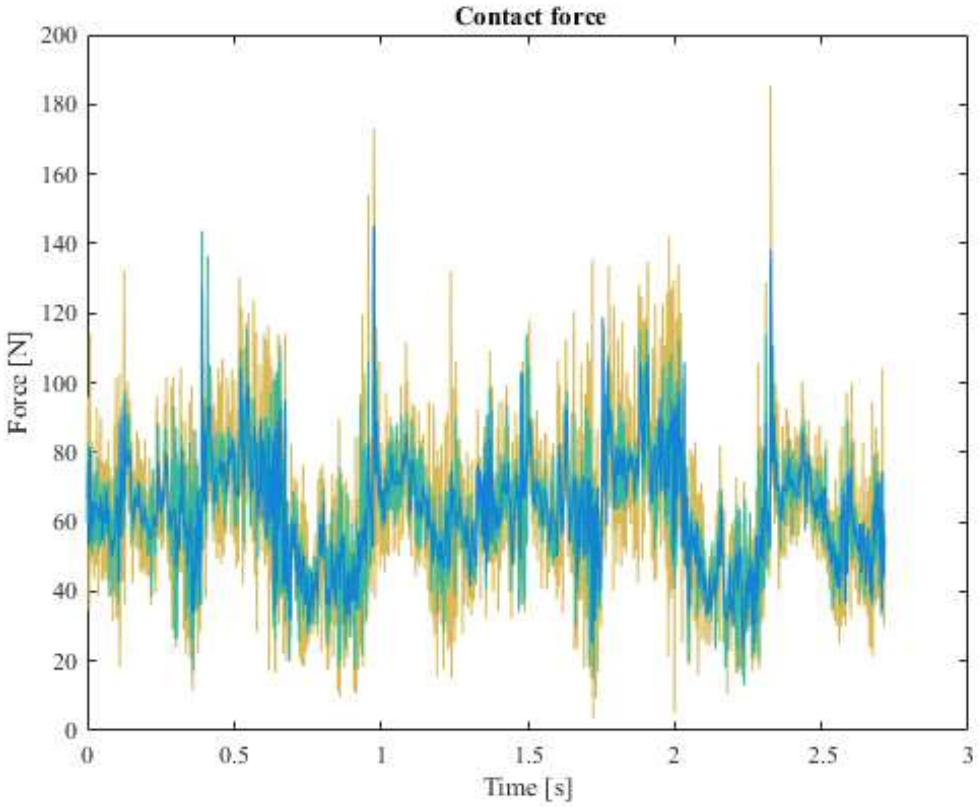

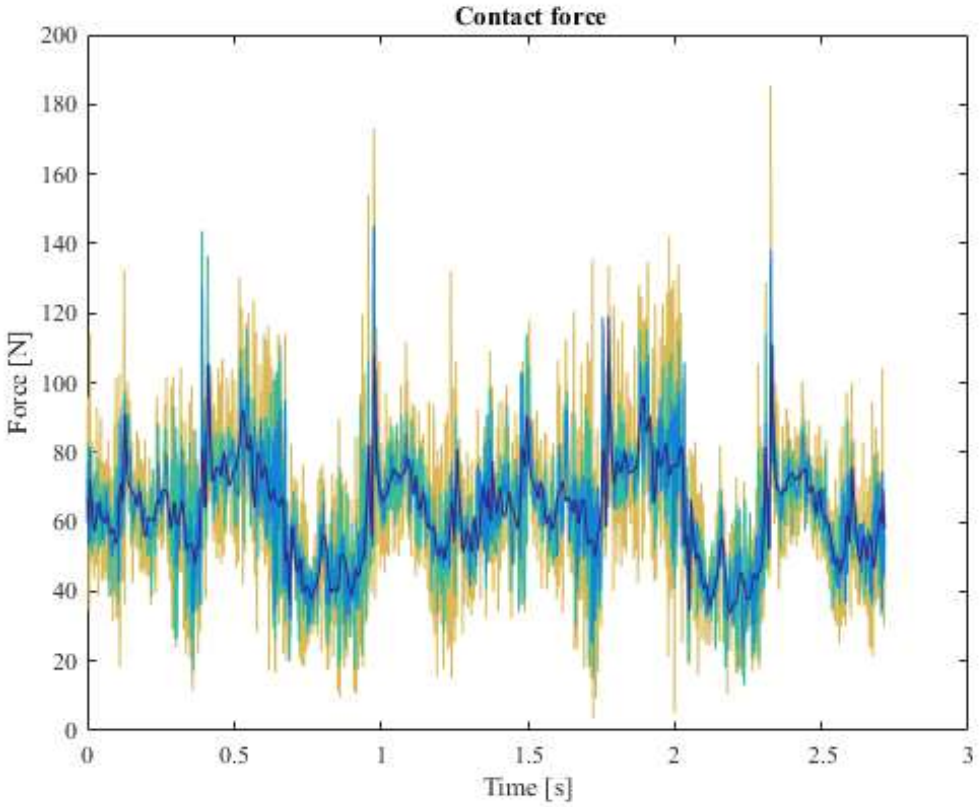


```
    end
end


if ADD_MAX_VALUE == 1 || ADD_MIN_VALUE ==1
```

```
    Figure_number = Figure_number +1;
    Plot_number = Plot_number +1;
    figure(Figure_number)
    fig = gcf;
    fig.PaperUnits = 'inches';
    fig.PaperPosition = print_size;
    if ADD_MAX_VALUE == 1
        plots(Plot_number) = plot(SaHz,max_position,'o-k','LineWidth',1.2);
        Figure_list{Figure_number} = ' Maximum CF position vs Sampling Frequency';
        title('Maximum Contact Force Position')
        ylabel('Time [s]')
    elseif ADD_MIN_VALUE ==1
        plots(Plot_number) = plot(SaHz,min_position,'o-k','LineWidth',1.2);
        Figure_list{Figure_number} = ' Minimum CF position vs Sampling Frequency';
        title('Minimum Contact Force Position')
        ylabel('Time [s]')
    end
    xlabel('Sampling Frequency [Hz]')
end

 fclose('all');

if RUN_TIME_SERIES == 1
if SUBPLOT ==1
  Delta_plot = Figure_number +length(Output_figures_list) ;
  Figure_number = Figure_number +1;
else
  Delta_plot = Figure_number ;
end
if LEGEND ==1;
for m = 1:Delta_plot
    lgd = legend(plots(m:Delta_plot:length(plots)));
    str = {'Sampling', 'Frequency [Hz]'};
    title(lgd,str)
end
end
end



for i = 1:Figure_number
    if PRINT == 1
        fig = gcf;
        fig.PaperUnits = 'inches';
        fig.PaperPosition = print_size;
        figure_print = strcat('-f',num2str(i));
        name_print =Figure_list{i};
        print(figure_print,name_print,'-dpng')
    end
end
```

Published with MATLAB® R2016a

A.4 Penalty Results with Time Step According to EN50318

```
Files_Lin = {'Fokstua_wire21_Original_120kmt_WBL88_LinPenalty_K_50000_12_11_CFN2.txt'
;'Fokstua_wire21_Original_120kmt_WBL88_LinPenalty_K_100000_14_11_CFN2.txt'...
    ;'Fokstua_wire21_Original_120kmt_WBL88_LinPenalty_K_150000_14_11_CFN2.txt';'Fokst
ua_wire21_Original_120kmt_WBL88_LinPenalty_K_200000_17_11_CFN2.txt';...
    'Fokstua_wire21_Original_120kmt_WBL88_LinPenalty_K_250000_19_11_CFN2.txt';'Fokstu
a_wire21_Original_120kmt_WBL88_LinPenalty_K_300000_06_12_CFN2.txt';...
    'Fokstua_wire21_Original_120kmt_WBL88_LinPenalty_K_350000_06_12_CFN2.txt';'Fokstu
a_wire21_Original_120kmt_WBL88_LinPenalty_K_500000_22_11_CFN2.txt';...
    'Fokstua_wire21_Original_120kmt_WBL88_LinPenalty_K_750000_05_12_CFN2.txt';'Fokstu
a_wire21_Original_120kmt_WBL88_LinPenalty_K_900000_05_12_CFN2.txt';...
    'Fokstua_wire21_Original_120kmt_WBL88_LinPenalty_K_DEFAULT_22_11_CFN2.txt'};

Files_NonLin = {'Fokstua_wire21_Original_120kmt_WBL88_NonLinPenalty_K_50000_19_11_CFN
2.txt';'Fokstua_wire21_Original_120kmt_WBL88_NonLinPenalty_K_100000_19_11_CFN2.txt'..
.
    ;'Fokstua_wire21_Original_120kmt_WBL88_NonLinPenalty_K_150000_20_11_CFN2.txt';'Fo
kstua_wire21_Original_120kmt_WBL88_NonLinPenalty_K_200000_21_11_CFN2.txt';...
    'Fokstua_wire21_Original_120kmt_WBL88_NonLinPenalty_K_250000_22_11_CFN2.txt';'Fok
stua_wire21_Original_120kmt_WBL88_NonLinPenalty_K_300000_06_12_CFN2.txt';...
    'Fokstua_wire21_Original_120kmt_WBL88_NonLinPenalty_K_350000_06_12_CFN2.txt';'Fok
stua_wire21_Original_120kmt_WBL88_NonLinPenalty_K_500000_22_11_CFN2.txt';...
    'Fokstua_wire21_Original_120kmt_WBL88_NonLinPenalty_K_750000_23_11_CFN2.txt';'Fok
stua_wire21_Original_120kmt_WBL88_NonLinPenalty_K_900000_23_11_CFN2.txt';...
    'Fokstua_wire21_Original_120kmt_WBL88_NonLinPenalty_K_DEFAULT_22_11_CFN2.txt'};

teller = 0;
teller2 = 1;
h = zeros(12,1);

m = [0.9,0,0.9];
r = [0.8,0,0.1];
g = [0,0.6,0.1];
b = [0.11,0,0.9];

color= [b;r;g;m];

color_long = zeros(length(Files_NonLin),3);

for kk = 1:2
if kk ==1
    Files = Files_Lin;
    Read_from = 51;
    Read_to = 56;
    Description = 'Linear Penalty Method';
elseif kk == 2
    Files = Files_NonLin;
    Read_from = 54;
    Read_to = 59;
    Description = 'Nonlinear Penalty Method';
end
```

```
color_map = colormap(parula);
delta = mod(size(color_map,1),length(Files));
color_map = color_map(1:(size(color_map,1)-delta),:);
delta2 = (size(color_map,1)/(length(Files)));

 for i = 1:length(Files)
    color_long(length(Files)+1-i,:) = color_map(((i-1)*delta2)+1,:);
 end

CF_mid = zeros(length(Files)-1,2);
CF_max = zeros(length(Files)-1,2);
CF_min = zeros(length(Files)-1,2);

for ii=1:length(Files)
    FileId = fopen(char(Files(ii)));
    Cell = textscan(FileId,'%f');
    Vector = cell2mat(Cell);

    if ii  == length(Files)
        K = 'DEFAULT';
    elseif ii == 1
        K = str2num(Files{ii}(Read_from:(Read_to-1)));
        time = Vector(1:2:length(Vector));
    else
        K = str2num(Files{ii}(Read_from:(Read_to)));
    end


    if ii  == length(Files) && kk ==2
        CF_default_delta = Contact_force-Vector(2:2:length(Vector));
    end

    Contact_force = Vector(2:2:length(Vector));

    if ii<length(Files)
        CF_mid(ii,2) = K;
        CF_max(ii,2) = K;
        CF_min(ii,2) = K;
        CF_mid(ii,1) = (sum(Contact_force))/length(Contact_force);
        CF_max(ii,1) = max(Contact_force);
        CF_min(ii,1) = min(Contact_force);
    end

    figure(1+teller)
    plot(time,Contact_force,'Color',color_long(ii,:),'LineWidth',1.1,'DisplayName',st
rcat('K = ',num2str(K)));
    title(Description)
    ylabel('Contact Force [N]')
    xlabel('Time [s]')
    hold on

end
legend('show')
hold off

CF_mid_def =ones(length(Files)-1,1)*(sum(Contact_force))/length(Contact_force);
CF_max_def =ones(length(Files)-1,1)* max(Contact_force);
```

```
CF_min_def =ones(length(Files)-1,1)* min(Contact_force);

color = colormap(parula(4));
%brighten(color,-0.9)

figure(2)
h(teller2)= plot(CF_mid(:,2),CF_mid(:,1),'Color',color(kk,:),'LineWidth',1.2,'Display
Name',Description);
hold on
h(teller2+1)=plot(CF_mid(:,2),CF_mid_def,'Color', color((5-kk),:),'LineStyle', '--','
LineWidth',1.1,'DisplayName',strcat(Description,' Default K'));
title('Mean Contact force')
ylabel('Contact Force [N]')
xlabel('Contact Stiffness, K [N/m]')


figure(3)
h(teller2+2)=plot(CF_max(:,2),CF_max(:,1),'Color',color(kk,:),'LineWidth',1.2,'Displa
yName',Description);
hold on
h(teller2+3)=plot(CF_max(:,2),CF_max_def,'Color', color((5-kk),:),'LineStyle', '--','
LineWidth',1.1,'DisplayName',strcat(Description,' Default K'));
title('Maximum contact force')
ylabel('Contact Force [N]')
xlabel('Contact Stiffness, K [N/m]')


figure(4)
h(teller2+4)= plot(CF_min(:,2),CF_min(:,1),'Color',color(kk,:),'LineWidth',1.2,'Displ
ayName',Description);
hold on
h(teller2+5)= plot(CF_min(:,2),CF_min_def,'Color', color((5-kk),:),'LineStyle', '--',
'LineWidth',1.1,'DisplayName',strcat(Description,' Default K'));
title('Minimum contact force')
ylabel('Contact Force [N]')
xlabel('Contact Stiffness, K [N/m]')

teller = teller + 4;
teller2 = teller2+6;
end
for i = [1,3,5] % 3 plots
legend([h(i),h(i+1),h(i+6),h(i+7)])
end

fclose('all')

%figure(6)
%plot(time,CF_default_delta)
```

```
ans =

     0
```

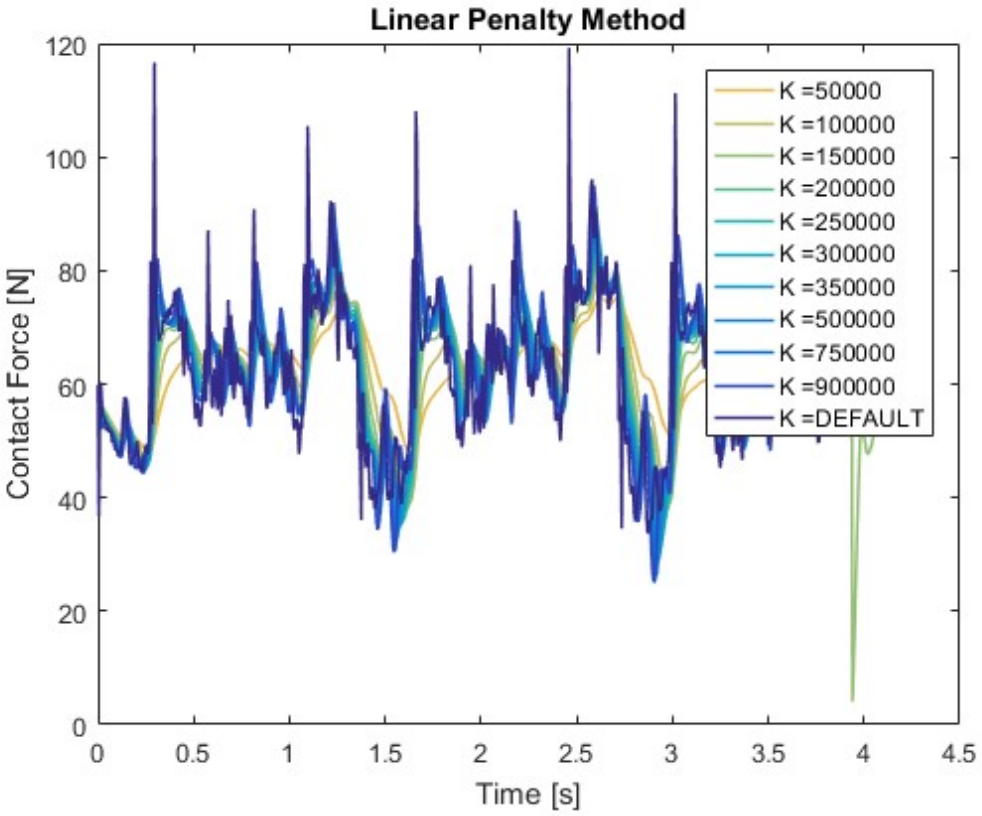
Linear Penalty Method
Contact Force [N]
Time [s]
K =50000
K =100000
K =150000
K =200000
K =250000
K =300000
K =350000
K =500000
K =750000
K =900000
K =DEFAULT

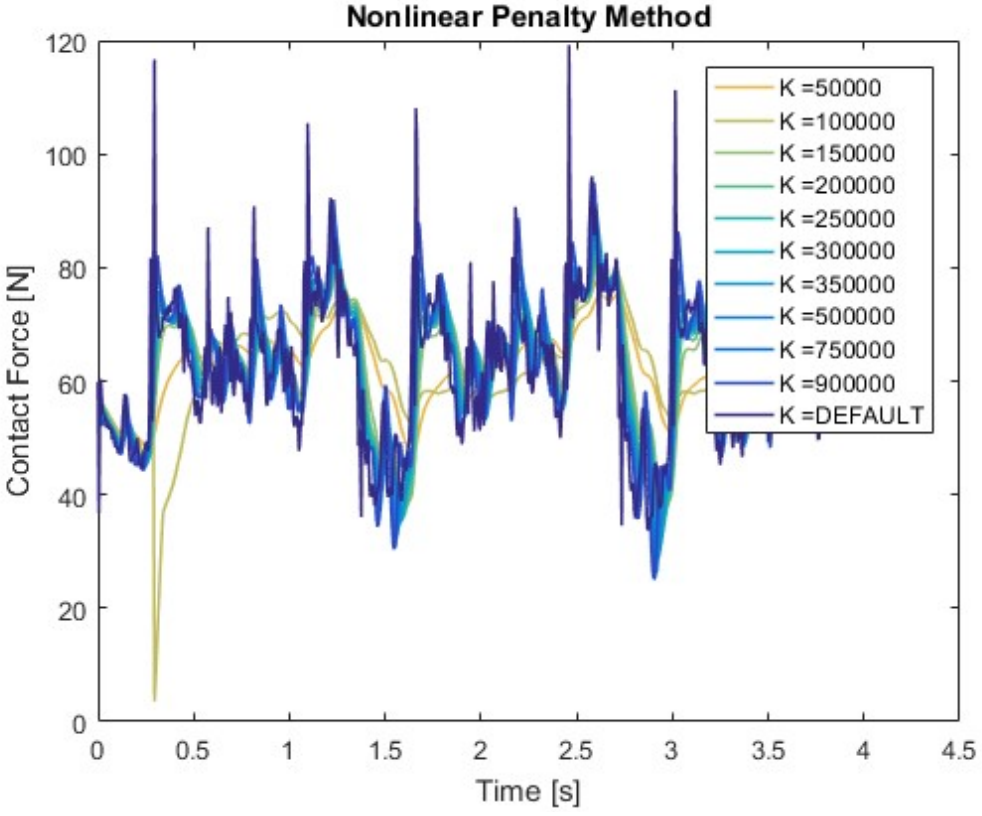
Nonlinear Penalty Method
Contact Force [N]
Time [s]
K =50000
K =100000
K =150000
K =200000
K =250000
K =300000
K =350000
K =500000
K =750000
K =900000
K =DEFAULT

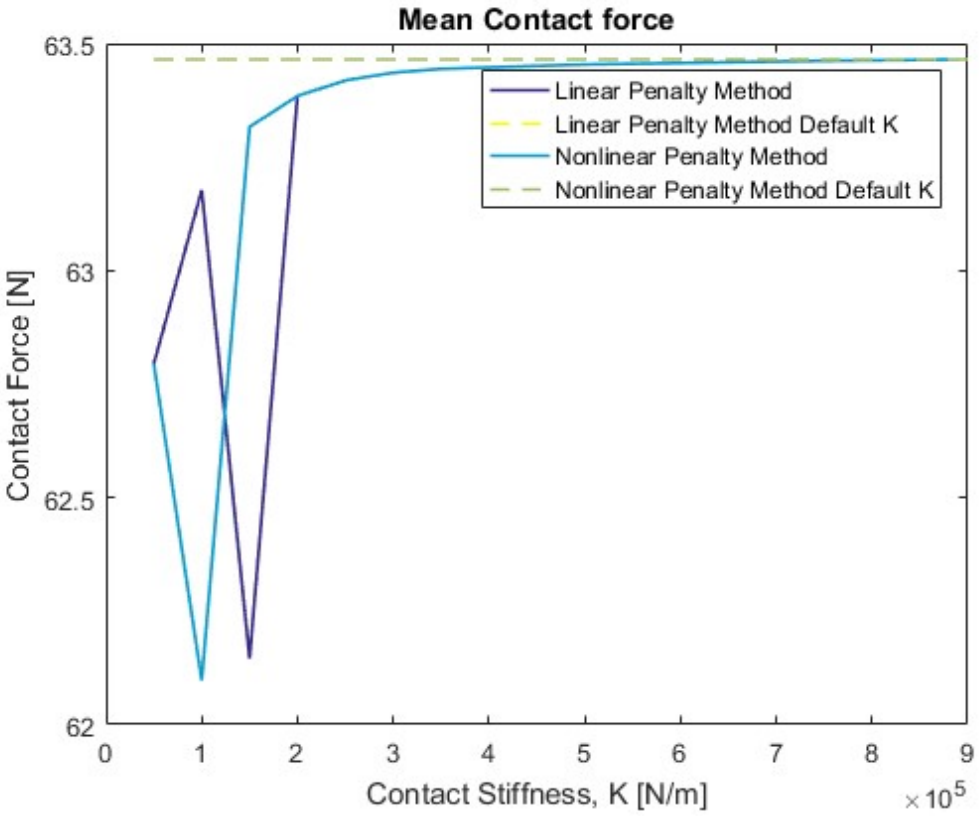
Mean Contact force
Linear Penalty Method
Linear Penalty Method Default K
Nonlinear Penalty Method
Nonlinear Penalty Method Default K
Contact Force [N]
Contact Stiffness, K [N/m]
63.5
63
62.5
62
0
1
2
3
4
5
6
7
8
9
$\times 10^5$

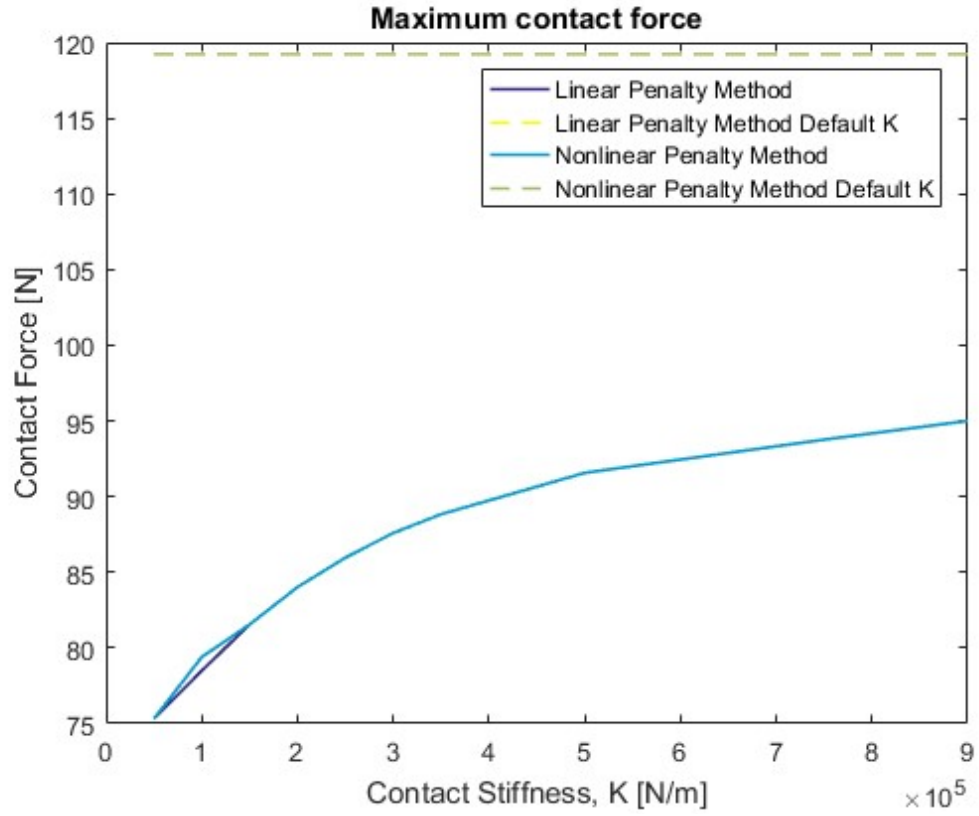
Maximum contact force
Linear Penalty Method
Linear Penalty Method Default K
Nonlinear Penalty Method
Nonlinear Penalty Method Default K
Contact Force [N]
Contact Stiffness, K [N/m]
120
115
110
105
100
95
90
85
80
75
0
1
2
3
4
5
6
7
8
9
$\times 10^5$

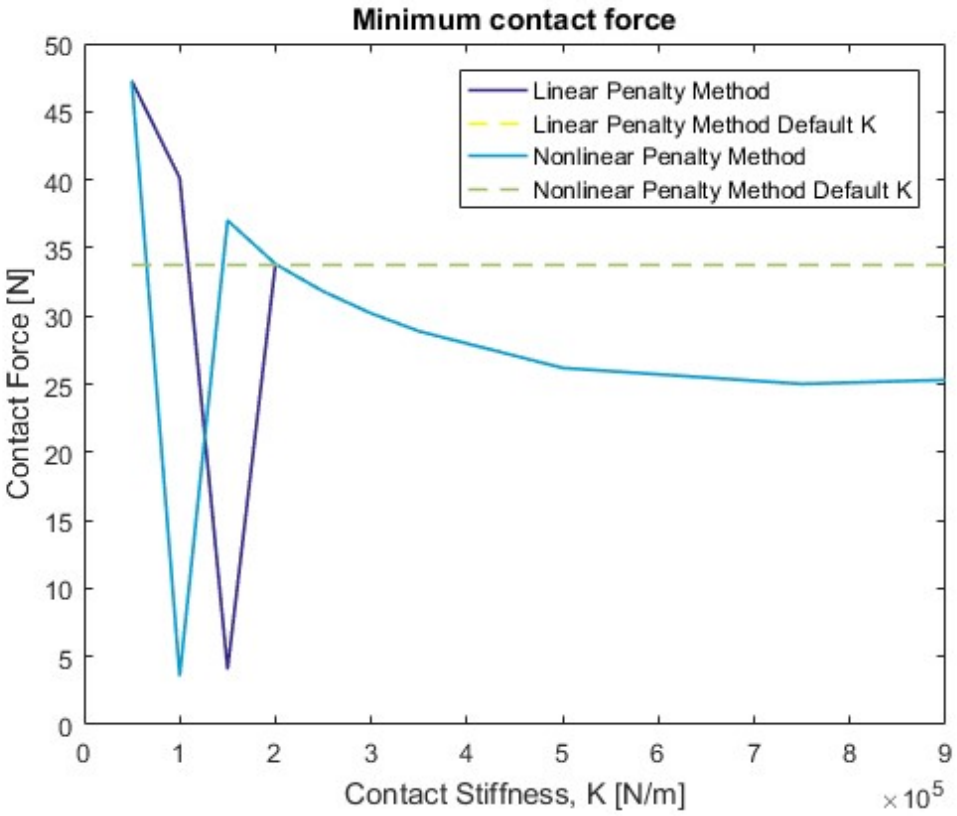

Published with MATLAB® R2016a